

Rationalizing PINK1 Transmembrane Mutations in Parkinson's Disease

by

Emmanuella Afua Frempomaa Takyi

A thesis submitted in partial fulfillment of the requirements for the degree of

Master of Science

Neuroscience

University of Alberta

© Emmanuella A. F. Takyi, 2019

ABSTRACT

PINK1 (Phosphatase-Tensin homologue (PTEN)-induced putative kinase 1) is a protein kinase heavily involved in mitochondrial health and integrity. It has multiple domains: an N-terminal mitochondrial targeting sequence, a transmembrane domain, and a kinase domain. Some mutations, located throughout the entire length of the protein, have been identified in persons diagnosed with Parkinson's disease (PD). The focus of this thesis is the transmembrane domain of PINK1, particularly PD-linked mutations in this region that have been reported to influence PARL-mediated cleavage. PARL (Presenilin-associated rhomboid-like) protease is responsible for the constitutive proteolysis of PINK1 in the inner mitochondrial membrane in healthy mitochondria. This cleavage event is key for PINK1 signaling pathways in the mitochondrion.

Cellular studies have shown defects in proteolysis of PINK1 with mutations in its TM region. Furthermore, cellular studies demonstrate redundancy in the cleavage of PINK1 by various mitochondrial proteases. A gap in knowledge exists to precisely define the effect of these mutations by *in vitro* analysis. The primary goal of this thesis is to develop a protocol for the overexpression of human PINK1, and to assess whether PD-linked mutations in PINK1 affect PARL protease-mediated cleavage.

A protocol for the expression and purification of a truncated human PINK1 (residues 70-134) was developed. PINK1 PD-linked variants were cloned and recombinantly expressed in *Escherichia coli*. Recombinant human PINK1 was purified from cell lysates via immobilized metal affinity chromatography and size exclusion chromatography.

Additionally, human PARL protease was recombinantly expressed in *Pichia pastoris* and purified resulting in a sufficient yield for downstream applications. Using a robust Fluorescence Resonance Energy Transfer (FRET)-based kinetic assay adapted in the Lemieux lab, we assessed the kinetic activity of PARL protease towards recombinantly expressed PD-linked variants of human PINK1. This work provides insight into the molecular etiology of PINK1 variants associated with PD.

PREFACE

The works published in this thesis contribute to a collaborative project within the Lemieux Lab at the University of Alberta. In chapter 4, the FRET-based kinetic assay was developed and modified for our use by Dr. Elena Arutyunova. Kinetic data was acquired and processed by Laine Lysyk. I was responsible for data interpretation within this thesis. Concluding analysis found in chapters 4 and 5 are my original work.

ACKNOWLEDGEMENTS

First and foremost, I would like to extend my gratitude to my supervisor and mentor Dr. Joanne Lemieux. Thank you for your unwavering support, guidance, and friendship throughout the past two years. Your energy, encouragement and overall confidence are both admirable and were extremely motivating. Thank you for being such an amazing role model! You have truly demonstrated your enthusiasm for science and its future through your interactions with colleagues, trainees, and students. Thank you for believing in me and for every opportunity you provided throughout the past couple years that have contributed to my growth and competence as a both a scientist and a person.

Thank you to Drs. Peter Hwang and Simonetta Sipione for participating as members of my Supervisory Committee. I genuinely appreciate your support and input in the direction and progress of my project. Your comments and suggestions throughout the program were extremely helpful and encouraging. I would also like to extend thanks to Dr. Olivier Julien for participating in my exam as an external examiner.

Thank you to the funding sources that supported my contributions to this project, particularly Parkinson Alberta and the Johnston Family Endowment Fund.

A big thanks to every member of the Lemieux lab I had the absolute pleasure of working with throughout this degree. I'd like to extend thanks especially to Dr. Elena Arutyunova, Dr. Rashmi Panigrahi, Dr. Yurong Wen, Laine Lysyk, and Raelynn Brassard. Elena and

Rashmi, two amazing scientists I had the honour of working with, both my project and I would truly have been lost without your support, guidance, and continuous input. Beyond the science, I appreciate our friendships. Laine Lysyk - the other pea in this pod, the PARL protease to my PINK1, my *lab* partner in crime - you have been my MSc/Edmonton rock. I cannot begin to imagine having experienced the last two years without you. Thank you for your friendship, your support, your consistent unfaltering positivity, and all the memories I'm sure we'll continue to laugh at for years to come. I am extremely lucky I gained a best friend in you, and I am excited to see where our journey takes us next! To all the other graduate students I had the pleasure of meeting and have the honor of calling friends, thank you.

Finally, I would like to thank all my friends and family. Your support has truly meant the world to me; you have been the wind under my sails, continuously keeping me going. I'd like to give a special thanks to my parents who inspired me to pursue this MSc. I could not ask to have better people in my corner!

TABLE OF CONTENTS

| | | |
|----------------|---|-----------|
| 1 | Introduction | 1 |
| 1.1 | Parkinson’s disease | 2 |
| 1.1.1 | Classifying PD | 4 |
| 1.1.2 | Symptoms of PD | 5 |
| 1.1.3 | Pathophysiology of PD | 7 |
| 1.2 | Genes linked to PD | 10 |
| 1.3 | Mitochondrial implications in neurodegeneration | 11 |
| 1.4 | PTEN-induced putative kinase (PINK1) | 15 |
| 1.4.1 | PINK1 domains | 15 |
| 1.4.1.1 | Kinase domain of PINK1 | 17 |
| 1.4.1.2 | N-terminal region (transmembrane domain and mitochondrial targeting sequence) of PINK1 | 19 |
| 1.4.2 | PINK1 processing by PARL protease in the inner mitochondrial membrane..... | 23 |
| 1.4.2.1 | The human mitochondrial rhomboid protease, PARL | 25 |
| 1.5 | PINK1/Parkin-mediated mitophagy | 29 |
| 1.6 | Mutations found within the transmembrane domain of PINK1 have been linked to familial forms of PD | 31 |
| 1.6.1 | Compound heterozygous mutations in <i>Pink1</i> identified in PD patients results in substitution of cysteine-92 to phenylalanine and arginine-464 to histidine in PINK1 protein | 33 |

| | | |
|-------|--|----|
| 1.6.2 | Single heterozygous mutation in <i>Pink1</i> identified in PD patients results in substitution of arginine-98 to tryptophan in PINK1 protein | 35 |
| 1.6.3 | Single heterozygous mutation in <i>Pink1</i> identified in PD patients results in substitution of isoleucine-111 to serine in PINK1 protein | 37 |
| 1.6.4 | Homozygous mutation in <i>Pink1</i> identified in PD patients results in substitution of glutamine-126 to proline in PINK1 protein | 37 |
| 1.7 | Heterologous expression of membrane proteins | 39 |
| 1.8 | Expression systems for recombinant proteins | 40 |
| 1.8.1 | The use of <i>Escherichia coli</i> as a recombinant expression system | 41 |
| 1.8.2 | The use of <i>Pichia pastoris</i> as a recombinant expression system | 43 |
| 1.9 | Thesis objective | 44 |
| 2 | Expression and Purification of His-FRET- <i>HsPINK1</i> [70-134] | 46 |
| 2.1 | Introduction | 47 |
| 2.2 | Generation of PINK1 transmembrane domain and mutations in the pBAD:His-FRET-PINK1[70-134] vector | 50 |
| 2.2.1 | Cloning PINK1 variants into pBAD:His-FRET- <i>HsPINK1</i> [70-134] vector using restriction enzymes | 52 |
| 2.2.2 | Cloning PINK1 transmembrane domain mutations into pBAD:His-FRET- <i>HsPINK1</i> [70-134] vector using site-directed mutagenesis | 57 |
| 2.3 | Transformation of <i>E. coli</i> Top 10 with pBAD:His-FRET- <i>HsPINK1</i> [70-134] | 60 |
| 2.4 | Growth of <i>E. coli</i> Top10 pBAD:His-FRET- <i>HsPINK1</i> [70-134] and expression of His- <i>HsPINK1</i> [70-134] WT and variants | 60 |
| 2.4.1 | Initial expression and purification of His-FRET- <i>HsPINK1</i> [70-134] | 61 |

| | | |
|---------|--|----|
| 2.4.2 | Expression tests to optimize growth and induction conditions | 63 |
| 2.4.2.1 | Cell lines tested for expression of His-FRET- <i>HsPINK1</i> [70-134] | 63 |
| 2.4.2.2 | Induction time and temperature study for His-FRET- <i>HsPINK1</i> [70-134] expression | 65 |
| 2.4.2.3 | Testing different concentrations of L-arabinose for induction of His-FRET- <i>HsPINK1</i> [70-134] expression | 67 |
| 2.5 | Lysing <i>E. coli</i> Top10 cells expressing His-FRET- <i>HsPINK1</i> [70-134] | 68 |
| 2.6 | Optimizing immobilized metal affinity chromatography (IMAC) parameters to increase His-FRET- <i>HsPINK1</i> [70-134] purity | 69 |
| 2.7 | Size exclusion chromatography of His-FRET- <i>HsPINK1</i> [70-134] as a final purification step | 72 |
| 2.8 | Expression and purification of His-FRET- <i>HsPINK1</i> [70-134] PD-linked variants..... | 72 |
| 2.8.1 | Expression and purification of His-FRET- <i>HsPINK1</i> [70-134] C92F | 75 |
| 2.8.2 | Expression and purification of His-FRET- <i>HsPINK1</i> [70-134] R98W | 78 |
| 2.8.3 | Expression and purification of His-FRET- <i>HsPINK1</i> [70-134] I111S | 83 |
| 2.8.4 | Expression and purification of His-FRET- <i>HsPINK1</i> [70-134] Q126P | 83 |
| 2.9 | Discussion | 86 |
| 3 | Expression and purification of GFP- <i>HsPARL</i> protease | 96 |
| 3.1 | Introduction | 97 |
| 3.2 | Screen for high GFP-PARL expressing <i>P. pastoris</i> GS115 colonies | 98 |
| 3.2.1 | Transformation of <i>P. pastoris</i> GS115 | 98 |
| 3.2.1.1 | Linearizing pPICZ α plasmid DNA for <i>P. pastoris</i> transformation | 98 |

| | | |
|---------|--|-----|
| 3.2.1.2 | Preparation of electrocompetent <i>P. pastoris</i> GS115 cells | 99 |
| 3.2.1.3 | Transformation of <i>P. pastoris</i> GS115 with pPICZ α :His-GFP-PARL | 100 |
| 3.2.2 | Transfer of successful <i>P. pastoris</i> GS115 transformants to YPDS master plates..... | 100 |
| 3.2.3 | Transfer of successful <i>P. pastoris</i> GS115 transformants from YPDS master plates to BMMY induction plates | 101 |
| 3.2.4 | Screening for high GFP-PARL expressing <i>P. pastoris</i> GS115 colonies | 101 |
| 3.3 | Growth of <i>P. pastoris</i> GS115 and expression of GFP-PARL | 103 |
| 3.4 | Purification | 103 |
| 3.4.1 | Immobilized metal affinity chromatography | 104 |
| 3.4.2 | Negative immobilized metal affinity chromatography | 106 |
| 3.5 | Discussion | 108 |
| 4 | Analysis of PD-linked PINK1 variants in FRET-based kinetic assay | 111 |
| 4.1 | FRET-based assay adapted to measure kinetic parameters of PARL protease..... | 112 |
| 4.1.1 | Recombinant His-FRET- <i>HsPINK1</i> [70-134] as a substrate of PARL protease..... | 114 |
| 4.1.2 | Internally quenched (IQ)- <i>HsPINK1</i> peptide as a substrate of PARL protease..... | 115 |
| 4.2 | Discussion | 126 |
| 5 | Conclusions | 137 |
| | References | 142 |
| | Appendix | 155 |

LIST OF TABLES

| | |
|------------------|---|
| Table 1.1 | Genetics of Parkinson's disease |
| Table 1.2 | Parkinson's disease-linked mutations found in the transmembrane region of PINK1 |
| Table 2.1 | Polymerase Chain Reaction settings for amplification of <i>HsPINK1</i> [70-134] variants |
| Table 2.2 | Restriction enzymes <i>BglII</i> and <i>KpnI</i> DNA recognition sequences |
| Table 2.3 | Forward and reverse primers designed for Site-Directed Mutagenesis of His-FRET- <i>HsPINK1</i> [70-134] PD variants |
| Table 2.4 | Polymerase Chain Reaction settings for Site-Directed Mutagenesis of His-FRET- <i>HsPINK1</i> [70-134] variants |
| Table 2.5 | <i>Escherichia coli</i> cell lines used for optimization of His-FRET- <i>HsPINK1</i> [70-134] expression |
| Table 4.1 | Peptide design of small IQ- <i>HsPINK1</i> peptides used in FRET-based kinetic assay |

LIST OF FIGURES

- Figure 1.1** Mitochondrial life cycle
- Figure 1.2** PINK1/Parkin-dependent mitophagy
- Figure 1.3** PINK1 domain architecture and location of PD-linked mutations
- Figure 1.4** X-ray crystal structure of *Tc*PINK1[150-570]
- Figure 1.5** Helical representation of the putative transmembrane domain of PINK1
- Figure 1.6** Topological cartoon of the predicted structure of PARL protease in the inner mitochondrial membrane
- Figure 1.7** Homology model of PARL protease
- Figure 1.8** PINK1 proteolysis in the inner mitochondrial membrane
- Figure 1.9** Imbalance in mitochondrial damage and damaged mitochondrion removal contributes to Parkinson's disease pathogenesis
- Figure 2.1** Fluorescence resonance energy transfer (FRET)-based kinetic assay
- Figure 2.2** Condensed pBAD:FRET vector map
- Figure 2.3** PCR amplification of *Pink1* 70-134 C92F, R98W, I111S, and Q126P dsDNA
- Figure 2.4** Relative expression of His-FRET-*Hs*PINK1[70-134] WT in different *E. coli* cell lines
- Figure 2.5** 14% SDS-PAGE gel for immobilized metal affinity chromatography purification of His-FRET-*Hs*PINK1[70-134] WT using Cobalt resin
- Figure 2.6** Size exclusion chromatogram of His-FRET-*Hs*PINK1[70-134] WT

- Figure 2.7** SDS-PAGE gel for SEC column elution fractions
- Figure 2.8** Incubation of His-FRET-*HsPINK1*[70-134] at 60 °C demonstrates recombinant PINK1 exists as a single species
- Figure 2.9** 14% SDS-PAGE gel for purification of His-FRET-*HsPINK1*[70-134] C92F
- Figure 2.10** 14% SDS-PAGE gel for purification of His-FRET-*HsPINK1*[70-134] R98W
- Figure 2.11** Induction screen for expression of His-FRET-*HsPINK1*[70-134] R98W in small-scale *E. coli* culture
- Figure 2.12** Induction screen for expression of His-FRET-*HsPINK1*[70-134] R98W in small-scale *E. coli* culture
- Figure 2.13** Induction screen for expression of His-FRET-*HsPINK1*[70-134] R98W in small-scale *E. coli* culture
- Figure 2.14** Induction screen for expression of His-FRET-*HsPINK1*[70-134] R98W in small-scale *E. coli* culture
- Figure 2.15** 14% SDS-PAGE gel for purification of His-FRET-*HsPINK1*[70-134] I111S
- Figure 2.16** 14% SDS-PAGE gel for purification of His-FRET-*HsPINK1*[70-134] Q126P
- Figure 2.17** SDS-PAGE gels of His-FRET-*HsPINK1*[70-134] before and after optimization
- Figure 2.18** Popular detergents used in membrane protein purification

- Figure 2.19** 14% SDS-PAGE gel of final purified His-FRET-*HsPINK1*[70-134] variants
- Figure 2.20** Superimposed size exclusion chromatograms of His-FRET-*HsPINK1*[70-134] WT, C92F, I111S, and Q126P
- Figure 3.1** Induction plate expression screen for GFP-PARL protease
- Figure 3.2** 14% SDS-PAGE gel for purification of GFP-PARL
- Figure 3.3** 14% SDS-PAGE gel for negative-Ni column post-TEV protease cleavage
- Figure 4.1** FRET-based kinetic assay using FRET-based PINK1 substrate
- Figure 4.2** Michaelis-Menten curves for PARL-mediated cleavage of His-FRET-*HsPINK1*[70-134] WT and PD-variants
- Figure 4.3** PARL-mediated cleavage of His-FRET-*HsPINK1*[70-134]
- Figure 4.4** Fluorophore-quencher pair concept
- Figure 4.5** FRET-based kinetic assay using IQ-peptide substrate
- Figure 4.6** PARL-mediated cleavage of different wild-type PINK1 transmembrane constructs
- Figure 4.7** Michaelis-Menten curves of PARL-mediated cleavage IQ-*HsPINK1*[97-107] WT and R98W
- Figure 4.8** PARL-mediated cleavage of IQ-*HsPINK1*[97-107] WT and R98W
- Figure 4.9** Proposed model for sub-mitochondrial localization of PINK1 variants

LIST OF ABBREVIATIONS

| | |
|--------------------|--|
| AD | autosomal dominant |
| AR | autosomal recessive |
| BCA | bicinchoninic acid |
| BMGY | buffered complex glycerol medium |
| BMMY | buffered complex methanol medium |
| CCCP | carbonyl cyanide m-chlorophenyl hydrazone |
| CL | cardiolipin |
| CMC | critical micelle concentration |
| CyPet | cyan fluorescent protein for energy transfer |
| DABCYL | 4-((4-(dimethylamino)phenyl)azo)benzoic acid |
| DBS | deep brain stimulation |
| ddH ₂ O | double distilled water |
| DDM | n-dodecyl- β -D-maltoside |
| DIABLO | Direct IAP-binding protein with low pI |
| DMSO | dimethyl sulfoxide |
| Drp1 | dynamamin-related protein 1 |
| dsDNA | double-strand DNA |
| DTT | dithiothreitol |
| <i>E. coli</i> | <i>Escherichia coli</i> |
| EDANS | 5-((2-aminoethyl)amino)naphthalene-1-sulfonic acid |
| EDTA | ethylenediaminetetraacetic acid |

| | |
|-------------------------------|--|
| EM | electron microscopy |
| EOPD | early-onset Parkinson's disease |
| FRET | Förster resonance energy transfer |
| GFP | green fluorescent protein |
| GPe | globus pallidus externa |
| GPi | globus pallidus interna |
| <i>Hs</i> | <i>Homo sapiens</i> |
| Hsp | heat shock protein |
| IMAC | immobilized metal affinity chromatography |
| IMM | inner mitochondrial membrane |
| IQ | internally quenched |
| k_{cat} | catalytic rate constant (turnover rate) |
| $k_{\text{cat}}/K_{\text{M}}$ | catalytic efficiency |
| kDa | kilo-Dalton |
| K_{M} | Michaelis-Menten constant |
| KO | knockout |
| LB | Lysogeny broth |
| L-DOPA | levodopa (dopamine precursor) |
| Mfn1,2 | Mitofusin1,2 |
| MMP | matrix metalloprotease |
| mPEMT | mouse phosphatidyl ethanolamine methyl transferase |
| MPP | matrix processing peptidase |
| MTS | mitochondrial targeting sequence |

| | |
|--------------------|---|
| OD | optical density |
| OG | n-octyl- β -D-glucopyranoside |
| OMM | outer mitochondrial membrane |
| PARL | Presenilin-associated rhomboid-like |
| PCR | polymerase chain reaction |
| PD | Parkinson's disease |
| PGAM5 | phosphoglycerate mutase family member 5 |
| <i>Ph</i> | <i>Pediculus humanus corporis</i> |
| PINK1 | phosphatase tensin homolog (PTEN)-induced putative kinase 1 |
| PMSF | phenylmethylsulfonyl fluoride |
| POPC | phosphatidylcholine |
| <i>P. pastoris</i> | <i>Pichia pastoris</i> |
| ROS | reactive oxygen species |
| SDM | site-directed mutagenesis |
| SDS-PAGE | sodium dodecyl sulfate polyacrylamide gel electrophoresis |
| SEC | size exclusion chromatography |
| Smac | second mitochondrial-derived activator of Caspases |
| SN | substantia nigra |
| SNpc | substantia nigra pars compacta |
| ssDNA | single-strand DNA |
| STN | subthalamic nucleus |
| TBS | tris buffered saline |
| <i>Tc</i> | <i>Tribolium castaneum</i> |

| | |
|----------------|---|
| TCEP | tris(2-carboxyethyl)phosphine |
| TEMED | tetramethylethylenediamine |
| TEV | tobacco etch virus |
| TIM | translocase of the inner membrane |
| T _m | melting temperature |
| TM | transmembrane |
| TMAP | transmembrane helix prediction program |
| TMD | transmembrane domain |
| TMpred | transmembrane helix prediction program |
| TOM | translocase of the outer membrane |
| TTC19 | tetratricopeptide repeat domain 19 |
| UPR | unfolded protein response |
| WT | wild-type |
| YNB | yeast nutrient broth |
| YPD | yeast extract peptone dextrose media |
| YPDS | yeast extract peptone dextrose sorbitol media |
| YPet | yellow fluorescent protein for energy transfe |

CHAPTER 1: Introduction

1 Introduction

1.1 Parkinson's disease

Parkinson's disease (PD) is the second most common neurodegenerative disorder, following Alzheimer's disease (AD) and other types of dementia. Neurodegenerative diseases are characterized by the general and progressive loss of neurons in the central nervous system (CNS). Neurons of the CNS are unable to regenerate once they are damaged or lost¹. Neurodegenerative diseases such as Parkinson's disease, Huntington's disease, and Alzheimer's disease contribute to a family of pathologies characterized by neuronal degeneration. In PD, there is a specific loss of dopaminergic neurons in the substantia nigra pars compacta (SNpc) region of the brain. The SNpc serves as an output to the basal ganglia circuit supplying the striatum with dopamine². This nigrostriatal pathway acts as a regulatory mechanism for the resulting activity propagated by the basal ganglia circuit. In PD, the nigrostriatal projections that fine tune basal ganglia-mediated movement are disrupted by loss of the dopaminergic neurons. Dopaminergic neurons are a primary source of dopamine in the central nervous system, and provide both the brain and the spinal cord with the appropriate innervation for various functions. One essential function of dopaminergic neurons in the SNpc, though indirect, is motor control³. Direct electrical excitation of the SNpc does not result in movement, however lesions made in the SNpc of animal models demonstrate disruption of fine motor control.

The 4 cardinal symptoms recognized in PD patients are resting tremor, rigidity, postural instability, and bradykinesia⁴. Currently, the primary treatment for early stage PD is blood-brain barrier-penetrable levodopa, or L-DOPA, a dopamine precursor, as dopamine itself is unable to cross the blood-brain barrier⁵⁻⁸. In 1961, Birkmayer *et al.* reported small dose administration of L-DOPA resulted in symptomatic relief in 20 PD patients. Further studies revealed larger doses of L-DOPA resulted in increased benefits⁷. Once in the brain, exogenous levodopa is converted to dopamine, by decarboxylation, which stimulates dopaminergic receptors compensating for depleted dopamine in the striatum. Unfortunately, administration of L-DOPA in PD patients simply provides symptomatic relief. As a result, the L-DOPA dose requires modification with disease progression due to shortening of the therapeutic window⁹. Another treatment option for PD is deep brain stimulation (DBS). DBS is a treatment course reserved for more progressed forms of PD. DBS requires surgical implantation of electrodes. As a PD treatment, the electrodes are traditionally targeted to either the subthalamic nucleus (STN) or the globus pallidus internus (GPi)¹⁰. These treatments also result in symptomatic relief. There are no approved disease mechanism-based treatments available, primarily due to the lack of understanding the very complex, multifaceted disease etiology.

1.1.1 Classifying PD

The motor impairments that characterize PD are called parkinsonism. Parkinsonism is not exclusive to PD and is a clinical syndrome found in other disorders. A combination of bradykinesia, the slowness of movement, with any one of the three other cardinal signs: tremor, rigidity, and postural instability, qualifies for the parkinsonism designation¹¹. There are a number of identifiable causes of parkinsonism, including infections, environmental toxins, and adverse effects of drugs¹²⁻¹⁴. Parkinsonism caused by these factors is often reversible, for example valproate-induced parkinsonism cessation upon the discontinued administration of valproate in epilepsy patients¹⁵⁻¹⁷. Oftentimes, if a cause is not identified the condition is then classified as idiopathic parkinsonism. Many disorders presenting with parkinsonism also present with non-PD symptoms and these are classified as atypical parkinsonism or 'Parkinson plus' disorders. These include corticobasal degeneration¹⁸, supranuclear palsy¹⁹, and Lewy body dementia²⁰. Though no specific test exists for the diagnosis of PD, a diagnosis is made based on symptoms and medical history. A patient presenting with a combination of 2 out of the 4 cardinal symptoms is likely to receive a PD diagnosis²¹.

Parkinson's disease can also be referred to as a synucleinopathy²². Alpha-synucleinopathies are characterized by the abnormal accumulation of alpha-synuclein protein aggregates in the brain²². Alpha-synuclein is a presynaptic protein that is well-expressed in the brain²³. The interaction of alpha-synuclein with

phospholipids has been demonstrated²⁴ though its primary function is not well characterized in the healthy brain. In a PD brain protein aggregates, called Lewy bodies, are made of highly insoluble alpha-synuclein. Interestingly, mutations in the alpha-synuclein coding gene, *SNCA*, have been identified in PD patients presenting inherited forms²⁵. The extent to which and the exact mechanism of how alpha-synuclein is involved in PD pathogenesis is not clear. Despite this, evidence of disease propagation by introduction of this aggregated protein demonstrates the toxic function attributed to dysregulation of alpha-synuclein in PD as well as in other synucleinopathies^{26,27}.

The progression of PD can be described in five stages. The first, stage I, is characterized by symptoms affecting one side of the body. During stage II, both sides of the body are affected whereas posture remains unaffected. Stage III introduces a mild imbalance during standing or walking, though the patient remains independent. In stage IV the patient requires help as instability during standing or walking is disabling. Finally, in stage V there is a severe debilitation, the disease is fully developed, and the patient is restricted to a bed or chair²⁸.

1.1.2 Symptoms of PD

There are four cardinal motor symptoms in PD: tremor, rigidity, akinesia or bradykinesia, and postural instability²⁹. These hallmark motor impairments are most recognizable and often form the clinical basis of a PD diagnosis²⁹. Tremor,

typically of the extremities, occurs at rest in a rhythmic manner³⁰. Initially its presentation is usually unilateral, affecting a hand, an arm, a foot, or a leg³¹. Notably, in PD, tremor is present at rest and disappears with movement³². As a result, resting tremor is not debilitating or interfering significantly with daily activities, particularly in the initial stages of the disease. Rigidity is characterized by an increase in resistance through movement of a limb²⁹. Particularly present in the limbs, neck, or trunk, rigidity can cause postural changes, difficulties with fine movements, a fixed 'mask-like' facial expression, pain, fatigue, and other motor dysfunction^{33,34}. Akinesia, or bradykinesia, are terms used to describe the impairment of voluntary movement, or the slowness of movement, respectively. Postural instability typically presents in later stages of PD, occurring after the onset of the other motor symptoms²⁹. Neuropathological-clinical regression analysis suggests that initial motor signs in PD occurs upon loss of 30% of neurons in the substantia nigra³⁵⁻³⁷. Slightly contrasting reports of motor impairment presentation upon 50% loss of dopaminergic neurons in the substantia nigra^{38,39}. Regardless, significant neuronal loss in the substantia nigra is required before these hallmark motor symptoms begin to occur.

In addition to the well-appreciated motor symptoms, PD is associated with non-motor dysfunctions. In 1817, James Parkinson highlighted non-motor symptoms such as sleep dysregulation, dysautonomia, in addition to cognitive and neuropsychiatric disorders⁴⁰. PD patients often present with a broad spectrum of non-motor symptoms such as: apathy, depression, sleep disturbances, pain,

hyposmia, and cognitive dysfunction⁴¹. The importance, severity, and quality of life implications of these symptoms have continuously been overlooked by physicians⁴². Developments in the understanding and expansion of brain regions studied in the field of Parkinson's disease has emphasized the loss of other cell types in the PD brain. Arguably, most interesting discovery of these non-motor symptoms is that they often present prior to manifestation of the motor symptoms^{41,43}. Degeneration of other neuronal types precedes the degeneration of the dopaminergic neuron population in the substantia nigra and may represent a potential clinical biomarker of the premotor phase of PD.

1.1.3 Pathophysiology of PD

The hallmark pathological characteristics of PD are dopaminergic neuronal death in the substantia nigra pars compacta region of the basal ganglia and the presence of alpha-synuclein-containing Lewy bodies⁴⁴. Dopaminergic neurons projecting to the striatum are responsible for movement modulation. There are two main pathways of the basal ganglia. The direct pathway that results in the increase of wanted muscle movements, and the indirect pathway that results in inhibiting unwanted muscle movement in times of rest. The direct pathway begins with excitatory input from the motor cortex to the striatum signalling the initiation of the neural cascade to initiate movement. These excitatory neurons synapse onto inhibitory neurons projecting from the striatum to the globus pallidus internal (GPi) thereby inhibiting the GPi. The GPi is responsible for keeping the activity of the thalamus low,

therefore when the GPi is inhibited the thalamus experiences an increase in activity - sending excitatory messages to the motor cortex. All the while, the substantia nigra (SN) and the subthalamic nucleus (STN) are working in the background to fine-tune this process of cortex activation. The STN has excitatory projections into the SN, exciting the activity of the nigrostriatal projections. Dopaminergic neurons projecting from the substantia nigra to the striatum synapse onto inhibitory neurons expressing D1 receptors projecting into the GPi. Upon an increased activation of the substantia nigra releasing dopamine, there is an increase in the inhibition of the GPi. This allows a greater activation of the thalamus. The SN has inhibitory projections to the STN, which inhibits the STN from exciting the SN in a negative feedback regulatory mechanism. A decrease in the SN activity results in a decrease of the SN contribution to activity of the thalamus.

Conversely, the goal of the basal ganglia indirect pathway is to prevent initiation of unwanted muscle movements from competing with voluntary movements⁴⁵. Similar to the direct pathway, the indirect pathway begins at the excitatory innervation from the motor cortex to the striatum. This excitation results in the inhibition of the globus pallidus external (GPe) via inhibitory projections from the striatum. The GPe has inhibitory neurons that project to the STN, though inhibition of the GPe decreases the inhibitory signal from the GPe to the STN. The STN excitatory neurons that project to the GPi are then activated, activating the inhibitory action of the GPi to the thalamus. With increased inhibition of the thalamus, the excitatory signal from the thalamus to the cortex is decreased, thereby reducing talk to the muscle

cortex, decreasing muscle movement. Again, similarly to the basal ganglia direct pathway there is ongoing input from the SN modulating the activity of this pathway. Dopaminergic neurons from the SN project onto inhibitory neurons in the striatum that send projections to the GPe. Binding of dopamine to the D2 receptors on these inhibitory striatal neurons decreases their activity. This allows increased activity of the GPe, allowing STN inhibition mediated by the GPe. This results in decreased excitation of the GPi, thereby decreasing the inhibition of the thalamus. In this pathway, the nigrostriatal projections act as a modulator for the inhibition of muscle movement. Together, the nigrostriatal projections and the direct and indirect basal ganglia circuitries allow for fine-tuning of the signalling between the thalamus and the motor cortex. Overall, dopamine released in the striatum by the SN dopaminergic neurons promotes activation of the motor cortex and thereby motor activity. Depletion of dopamine results in hypokinesia as a reduction of motor cortex output⁴⁶. In addition to the renowned motor circuit, there are a number of major pathways connecting other regions of the brain with the basal ganglia: oculo-motor, associative, limbic, and orbitofrontal circuits, each representing the primary projection area of each basal ganglia associating circuit⁴⁶. In PD, all of these circuits are affected and explain many of the “non-traditional” symptoms experienced by patients.

The cause of neuronal death in PD is still unknown. Many theories focus on the accumulation of alpha-synuclein present in Lewy bodies. The appearance of Lewy bodies usually begins in brain regions outside of the basal ganglia before the

presentation of motor symptoms⁴⁷. It is unknown if Lewy body formation is a protective mechanism as a result of impending neuronal dysfunction or a result of diseased neurons producing insoluble protein contributing to disease pathogenesis. If the former, there must be another mechanism that leads to cell death. Other cell death mechanism can be attributed to dysfunction in mitochondria, proteasomal activity, and lysosomal activity⁴⁸. Interestingly, several links have been made between both mitochondrial dysfunction and PD^{49,50}. Cell death as a result of mitochondrial dysfunction may be related to Lewy body aggregation, oxidative stress, or a number of other dysregulated processes - though the interplay between these various mechanisms and their link to PD pathogenesis does not appear to be linear and is not fully understood.

1.2 Genes linked to PD

Though the majority of PD cases are idiopathic, familial forms, both autosomal recessive and dominant, have been identified and well studied. Idiopathic forms of PD are most common. In general, the cause of idiopathic PD is unknown, though there are symptoms and biomarkers that aid in the diagnoses^{51,52}. Conversely, some cases of PD are hereditary where mutations in specific PD-linked genes lead to an inherited form of the disease⁵³. Genetic forms of PD often present with an early age of onset. The early-onset designation is given in a patient under the age 50⁵⁴. Regardless of age of onset, the disease manifests differently among patients⁵⁵. Besides personal and social motivations, the ability to distinguish early-onset PD

from late-onset PD is important as physicians may tailor treatment based on age of onset. Though disease progression varies between patients, it is not atypical that progression may be slower in early-onset PD⁵⁶. This phenomenon has been suggested to be due to the relatively higher neuroplasticity in the young brain⁵⁷, influencing disease treatment options and accompanied side effects experienced^{58,59}. Those with a familial form of early-onset PD often carry mutations in genes linked to PD (**Table 1.1**). The identification of genes linked to Parkinson's disease has increased the general understanding of the disease pathology. There are many genes that when mutated have effects similar or identical to sporadic forms of PD. These familial forms, upon deeper investigation, may provide pivotal information about the pathogenesis of PD.

1.3 Mitochondrial implications in neurodegeneration

Neuronal degeneration in the CNS leads to subsequent loss of neuronal network integrity, driving a progressive loss of motor and cognitive function⁶⁰. Despite major differences in pathophysiology of the wide variety of neurodegenerative diseases, one major commonality between them is the presence of dysfunctional mitochondria⁶¹⁻⁶⁴.

There are several factors that influence mitochondrial life cycle such as environment and stress. Although traditionally depicted as static structures, mitochondria are highly dynamic organelles, undergoing an ongoing cycle of fission

Table 1.1. Genetics of Parkinson’s disease. Condensed list of PD-linked gene loci and their corresponding gene products. Pattern of inheritance is included in the table as well as the reported population affected. Boxed in red is the gene locus for *Pink1*. Mutations found in these genes result in an autosomal recessive inherited form of PD. EOPD = early-onset PD; AD = autosomal dominant; AR = autosomal recessive.

| | Gene | Gene product | Disease presentation | Inheritance |
|---------------|---------------|--|-----------------------------|--------------------|
| <i>PARK1</i> | <i>SNCA</i> | α -synuclein | EOPD | AD |
| <i>PARK2</i> | <i>PRKN</i> | Parkin | EOPD | AR |
| <i>PARK4</i> | <i>SNCA</i> | α -synuclein | EOPD | AD |
| <i>PARK5</i> | <i>UCHL1</i> | Ubiquitin C-terminal hydrolase L1 (UCHL1) | Classical PD | AD |
| <i>PARK6</i> | <i>PINK1</i> | PINK1 | EOPD | AR |
| <i>PARK7</i> | <i>DJ-1</i> | Protein deglycase DJ-1 | EOPD | AR |
| <i>PARK8</i> | <i>LRRK2</i> | Leucine-rich repeat kinase 2 (LRRK2) | Classical PD | AD |
| <i>PARK13</i> | <i>HTRA2</i> | HTRA2/Omi protease | Classical PD | AD or risk factor |
| <i>PARK18</i> | <i>EIF4G1</i> | Eukaryotic translation initiation factor 4 gamma 1 (EIF-4G1) | Classical PD | AD |

and fusion (**Figure 1.1**). This mechanism is key to maintaining mitochondrial functioning and health. The regulation of fission is primarily governed by dynamin-related protein 1 (Drp1)⁶⁵. Drp1 deficient neurons demonstrate a strongly interconnected mitochondrial network, this is due to the disruption in mitochondrial fission machinery⁶⁶. Alternately, the knockout of either Mitofusin 1 or 2 (Mfn1, Mfn2) in mice results in midgestational death linked to fusion defects⁶⁷, thus, emphasizing the role of Mfn1 and Mfn2 in the process of fusion. Primarily thought of as “the powerhouse of the cell”, mitochondria execute functions needed for cellular fitness and survival. Neurons are high-energy demanding cells; therefore the need for efficient functionality is imperative.

When mitochondria age or become damaged they undergo mitophagy – the selective autophagy, or removal, of a mitochondrion^{68,69}. Fission and fusion act as quality control mechanisms for the mitochondrial network, allowing for necessary clearance of defective mitochondria⁷⁰⁻⁷³. The process of mitophagy is also an essential quality control mechanism that serves to protect the integrity of the mitochondrial network⁷⁴. Several pathways result in mitophagy; including PTEN-induced putative kinase 1 (PINK1)/Parkin-dependent and PINK1/Parkin-independent pathways. Both pathways rely on protein regulators to flag specific mitochondria for degradation and thereby drive the process of mitophagy. PINK1/Parkin-dependent mitophagy is discernibly dependent on the activity of PINK1 and the E3 ubiquitin ligase, Parkin. PINK1/Parkin-independent mitophagy is regulated by other factors. These factors may include: cardiolipin – a unique lipid,

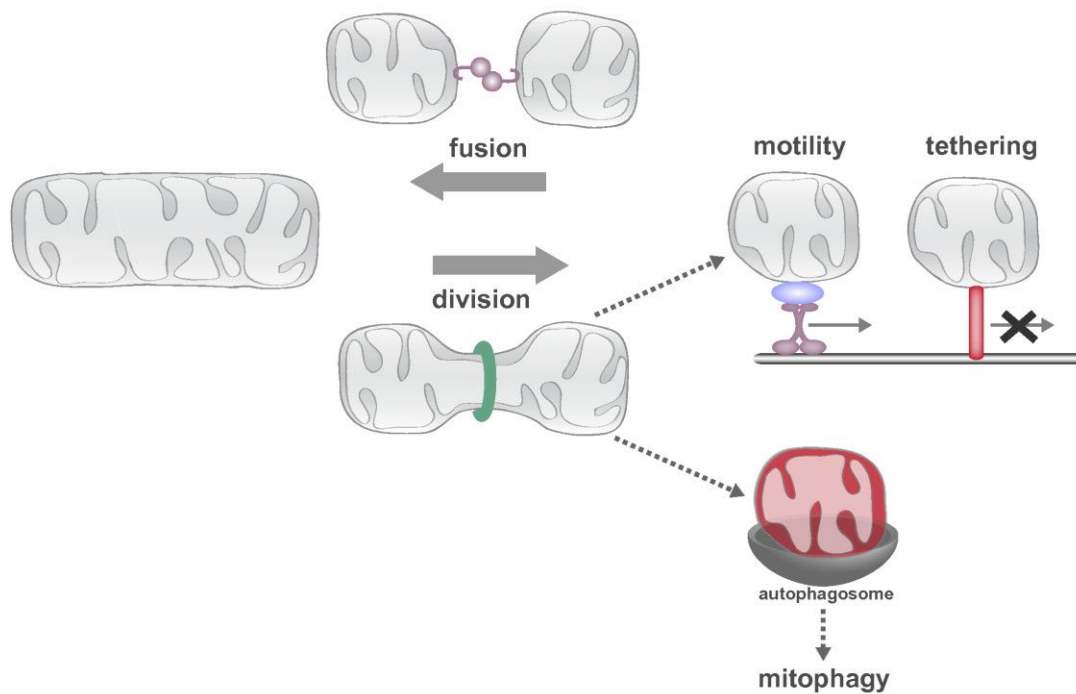


Figure 1.1. Mitochondrial life cycle. Multiple factors influence the dynamics of the mitochondrial network in a cell. Following biogenesis, mitochondria undergo fission and fusion as a means to preserve the integrity of the network. Damaged or injured portions of a mitochondrion may form buds and be isolated from the main mitochondrial network by means of fission – undergoing autophagic turnover. Conversely, as a means of local repair mitochondria may undergo fusion – promoting network stability. If damage is extensive, mitochondrial autophagy (mitophagy) is induced. In the case where repair, mitophagy, or replacement is insufficient cell death is initiated. (Adapted **with permission** from: Lackner, L. L. (2014) Shaping the dynamic mitochondrial network. *BMC Bio* 12:35.)

important in mitochondrial bioenergetics and cellular processes^{43,44}, the mitochondrial associated BCL2 Interacting Protein 3 Like (BNIP3L) protein⁴⁵, or the proautophagic Activating Molecule in Beclin 1 Regulated Autophagy (AMBRA1) protein⁷⁵; all of which result in flagging a mitochondrion for recognition and degradation by autophagosomes⁷⁶. Effectual mitophagy relies on the engulfment of damaged mitochondria without entirely disrupting the mitochondrial network⁷⁷. Defects in mitophagy have been observed and deemed important in both the onset and progression of various neurodegenerative diseases such as AD, HD, and ALS^{77,78}.

1.4 PTEN-induced putative kinase (PINK1)

PINK1 is a mitochondrial serine/threonine-protein kinase encoded by the *PINK1* gene at the PARK6 locus. Its name stems from its initial identification in a screen for proteins upregulated by Phosphatase and Tensin homologue (PTEN) overexpression⁷⁹. The primary function of PINK1 is its involvement in mitochondrial quality control. Through identification of damaged mitochondria by cellular stress signals, PINK1 flags individual mitochondria for controlled degradation⁵¹ (**Figure 1.2**).

1.4.1 PINK1 domains

PINK1 has a multi-domain organization within its sequence structure^{80,81}. It begins with a mitochondrial targeting sequence that targets the protein to the

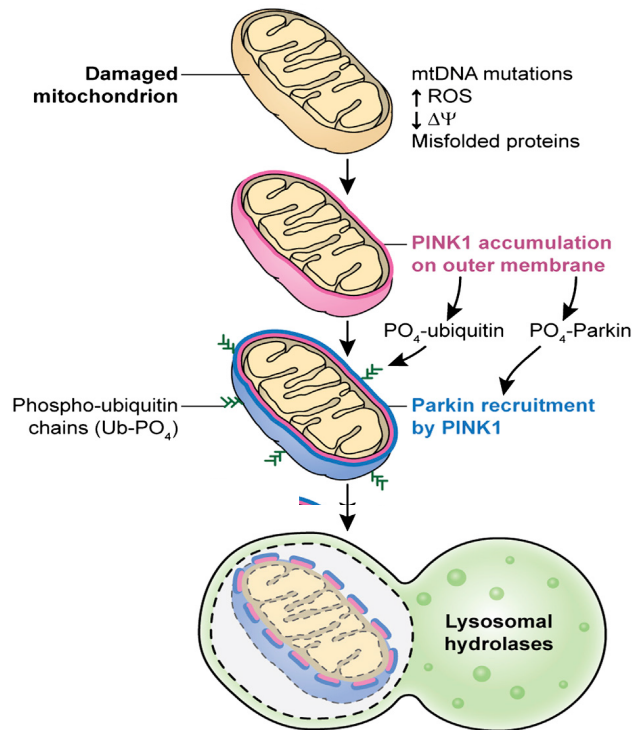


Figure 1.2. PINK1/Parkin-dependent mitophagy. There are several stressors that will result in mitochondrial damage. Mutations in mitochondrial DNA, increased population of reactive oxygen species, dismantled membrane potential, or an increase in or accumulation of misfolded proteins. As a signal of stress, dissipation of the membrane potential impairs the ability of PINK1 to complete import into the inner mitochondrial membrane. This results in an accumulation of PINK1 on the outer mitochondrial membrane, which dimerizes, autophosphorylates itself, then recruits Parkin and ubiquitin to the mitochondrion to be phosphorylated by PINK1. Phospho-Parkin and -ubiquitin flag the mitochondrion for degradation by formation and engulfment of an autophagosome. (Adapted **with permission** from: Pickrell, A. M., Youle, R. J. (2015) The roles of PINK1, parkin and mitochondrial fidelity in Parkinson's disease. *Neuron* 85(2): 257-73.)

mitochondrion, a transmembrane domain whose boundaries have not yet been established, and a large soluble kinase domain^{81,82} – responsible for its phosphorylation and recruitment activities (**Figure 1.3**). Despite advancements in the knowledge of the structure and function of PINK1 kinase domain^{81,82}, little study has been directed toward the structure of the TM region⁸³.

1.4.1.1 Kinase domain of PINK1

Protein phosphorylation plays a role in the regulation of many cellular processes. The human kinome refers to a complete set of protein kinases encoded in the human genome, which corresponds to 1.7% of human genes^{80,84-87}. Kinases are a group of proteins that act as phosphorylating agents towards specific substrates and have been isolated and identified as therapeutic targets for a plethora of human diseases and disorders⁸⁴⁻⁸⁷. Kinases themselves are regulated by phosphorylation, sometimes by themselves, a process termed as autophosphorylation. PINK1 is one human protein kinase that participates in autophosphorylation as a mechanism of activity regulation⁸⁸.

The kinase domain of human PINK1 (*HsPINK1*) spans from residues 156 to 510, where there is a remaining 71 amino acid polypeptide chain that corresponds to a C-terminal extension region. The structures of the kinase domain of *Pediculus humanus corporis* PINK1 (*PhPINK1*[143-575]) in complex with ubiquitin and *Tribolium castaneum* PINK1 (*TcPINK1*[150-570]) have been solved by X-ray

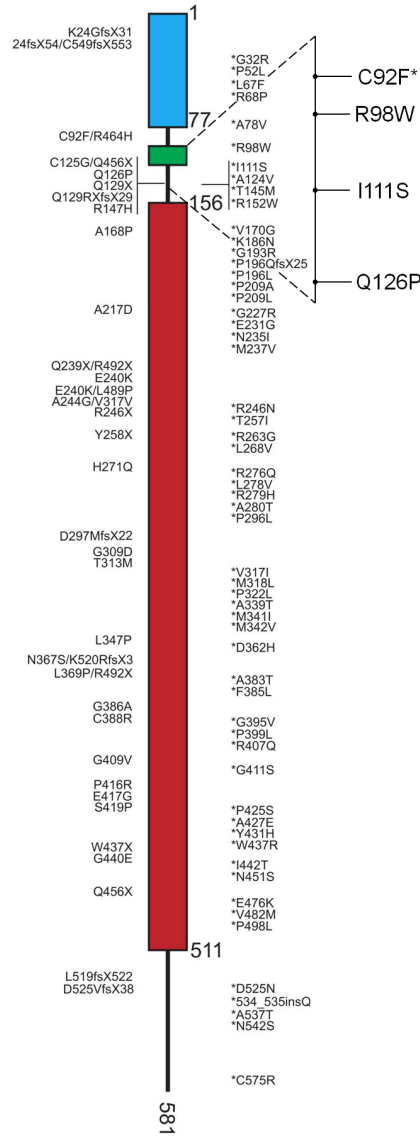


Figure 1.3. PINK1 domain architecture and location of PD-linked mutations. Mutations found in patients span the entire length of the PARK6 gene, resulting in several different PINK1 variants. The mitochondrial targeting sequence is colored in blue; the transmembrane domain is colored in green; and the kinase domain in red. (Adapted **with permission** from: Pickrell, A. M., Youle, R. J. (2015) The roles of PINK1, parkin and mitochondrial fidelity in Parkinson's disease. *Neuron* 85(2): 257-73.)

crystallography to 3.1 and 2.7 angstroms (Å), respectively^{81,82} (**Figure 1.4**). Sequence conservation of PINK1 across different species including *P. humanus corporis* and *T. castaneum* suggests that structural and functional insights into any of these models may prove beneficial to gaining a deeper understanding of the structure of human PINK1 and how *HsPINK1* functions.

1.4.1.2 N-terminal region (transmembrane domain and mitochondrial targeting sequence) of PINK1

Unlike the kinase domain of PINK1, the transmembrane domain is not entirely characterized. Several groups have demonstrated that the first 34 amino acid residues of PINK1 encode the mitochondrial targeting sequence. By appending the PINK1[1-34] to a reporter protein such as green fluorescent protein (GFP), researchers showed that these PINK1[1-34]-reporter fusion constructs localized to the mitochondrial matrix⁸⁹⁻⁹¹. The N-terminus and transmembrane regions of PINK1 are important to study because the translocation and multiple key cleavage events are important for mitochondrial signaling. Domain boundaries of the protein have not been identified, though putative boundaries have been reported from various groups mainly identified from topology predictions, that propose the TM to be within residues 89-111^{90,92-94}. Interestingly, deletion of amino acid residues 91 to 117 in PINK1 resulted in localization to the inner mitochondrial membrane fraction when transfected in human neuroblastoma SH-SY5Y cells⁹⁵. Carbonyl cyanide-m-chlorophenyl hydrazine (CCCP) treatment of HeLa cells expressing PINK1 with

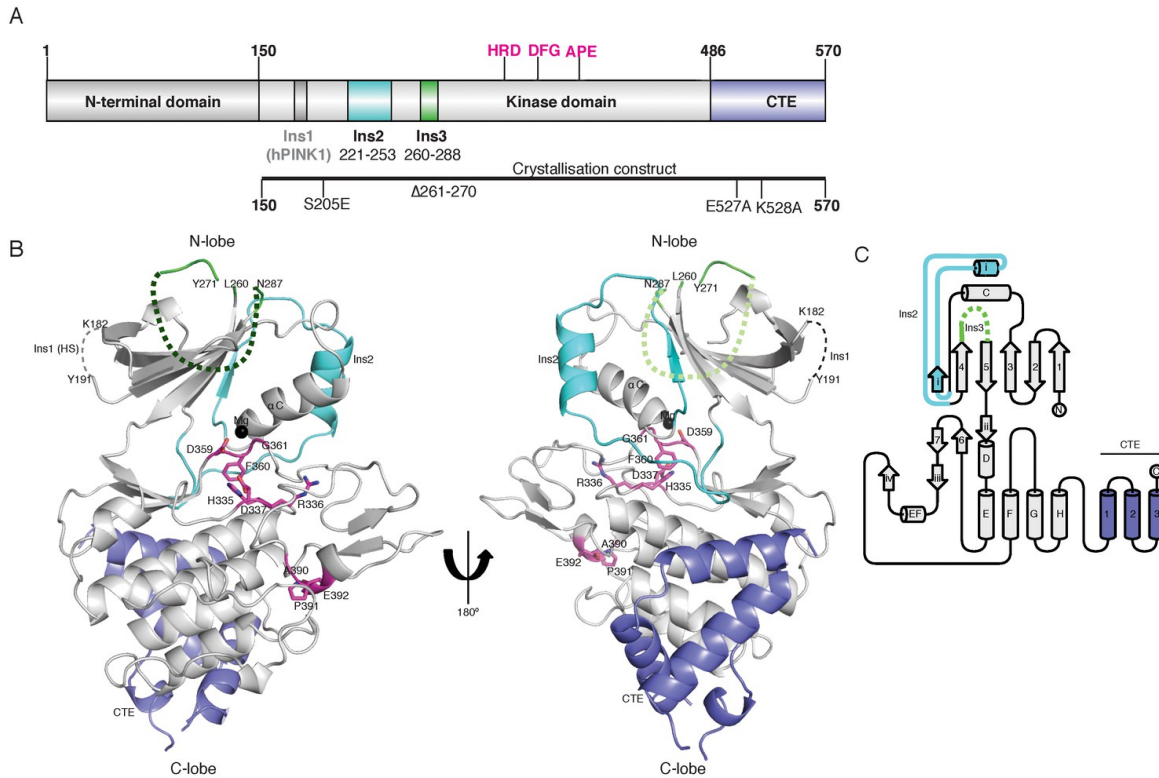


Figure 1.4. X-ray crystal structure of TcPINK1 150-570. (A) Domain depiction of TcPINK1. (B) Structure of TcPINK1. Grey = canonical N- and C-lobes; pink = catalytic and activation loops; dark grey = insert 1 (*HsPINK1*); cyan = insert 2; green = insert 3; dashed lines = disordered regions; black sphere = Mg^{2+} ; purple = C-terminal extension. (Adapted **with permission** from: Kumar, A., Tamjar, J., Waddell, A. D., Woodroof, H. I., Raimi, O. G., Shaw, A. M., Peggie, M., Muqit, M. M. K., van Aalten, D. M. F. (2017) *eLife*.)

deletion of residues 94 to 110 resulted in outer mitochondrial membrane localization⁸⁹. Okatsu *et al.* demonstrated that the first 90 amino acids, in particular hydrophobic residues from 70 to 94, are sufficient for PINK1 localization to the outer mitochondrial membrane, potentially operating as an alternative localization signal. Together, these results suggest the putative transmembrane domain of PINK1 is dispensable with regards to submitochondrial localization and that membrane retention of transmembrane deleted PINK1 must rely on other hydrophobic residues in PINK1 external to the putative transmembrane domain⁹⁶. Furthermore, these results lead to questions regarding the nature of PINK1 and if it indeed has a bonafide transmembrane domain. The idea that PINK1 transmembrane acts as a stop-transfer has been accepted in the field^{97,98} suggesting these residues comprising the transmembrane domain play a role in the membrane signaling or retention of PINK1^{89,96}.

The structure of PINK1 including the transmembrane segment has not been solved despite recent publication of PINK1 kinase structures solved by crystallography. *In silico* methods suggest PINK1[89-111] (AWGCAGPCRAVFLAFGLGLLI) forms a partial alpha helical structure (**Figure 1.5**). A report by Ulmschneider and Sansom suggests residues such as arginine, tryptophan, and cysteine do not have a high frequency in transmembrane segments of alpha helical proteins, whereas glycine and leucine are highly favourable transmembrane residues⁹⁹ and comprise a large portion of the putative PINK1 transmembrane domain. In contrast, Ulmschneider recently released a report supporting the claim of arginine being a thermodynamic-

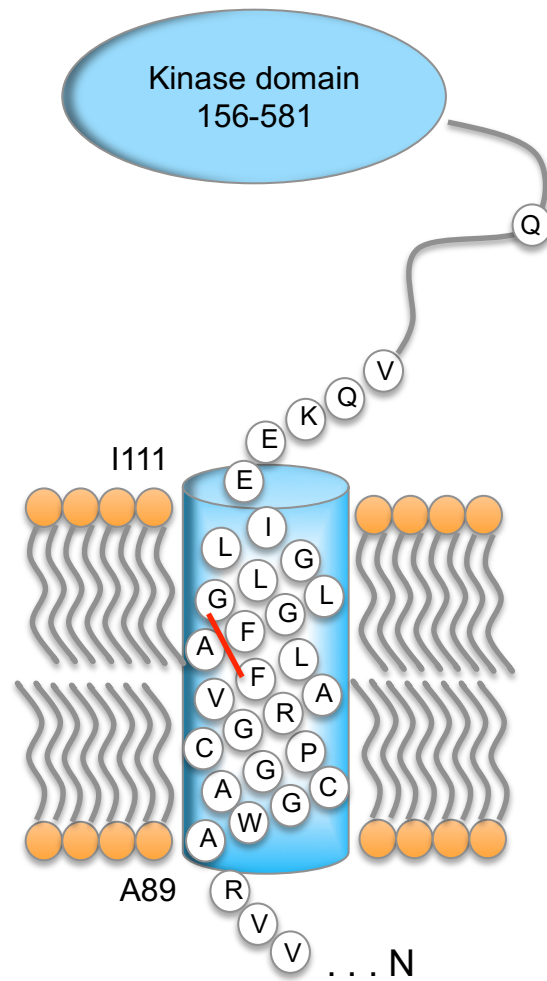


Figure 1.5. Helical representation of the putative transmembrane domain of PINK1. The transmembrane boundaries of PINK1 are predicted to be from residues 89 to 111. The red line denotes the PARL protease cleavage site. Orange circles represent lipid head components of the membrane bilayer.

ally stable member of transmembrane helices¹⁰⁰. Conflicting accounts of PINK1 amino acid energetics within a lipid bilayer demonstrate that there is still plenty to be understood about its transmembrane domain structure and dynamics.

1.4.2 PINK1 processing by PARL protease in the inner mitochondrial membrane

Presenilin-Associated Rhomboid-Like (PARL) protease is a human mitochondrial rhomboid protease (**Figure 1.6**). Localized to the inner mitochondrial membrane, its catalytic dyad, serine-277 and histidine-335, is responsible for the cleavage of *HsPINK1* between alanine-103 and phenylalanine-104, highly conserved residues in vertebrates⁸³. Rhomboid proteases typically cleave TM regions with helix destabilizing motifs, and the high glycine population in PINK1 may introduce kinks in the transmembrane domain to make it an excellent candidate for rhomboid protease cleavage¹⁰¹. Cleavage by PARL protease releases the N-terminal truncated form of PINK1 into the cytosol, where it is subsequently degraded by the proteasome. The constant cycle of inner mitochondrial import, PARL protease-mediated proteolysis, and cytosolic degradation results in a low measurable presence of PINK1 in healthy mitochondria¹⁰². Knockout of PARL protease in mouse embryonic fibroblasts (MEFs) resulted in accumulation of a 60kDa form of PINK1, corresponding to a suggested MTS-truncated form of PINK1⁹². In wild-type MEFs, accumulation of this “full-length”, mitochondrial targeting sequence (MTS)-

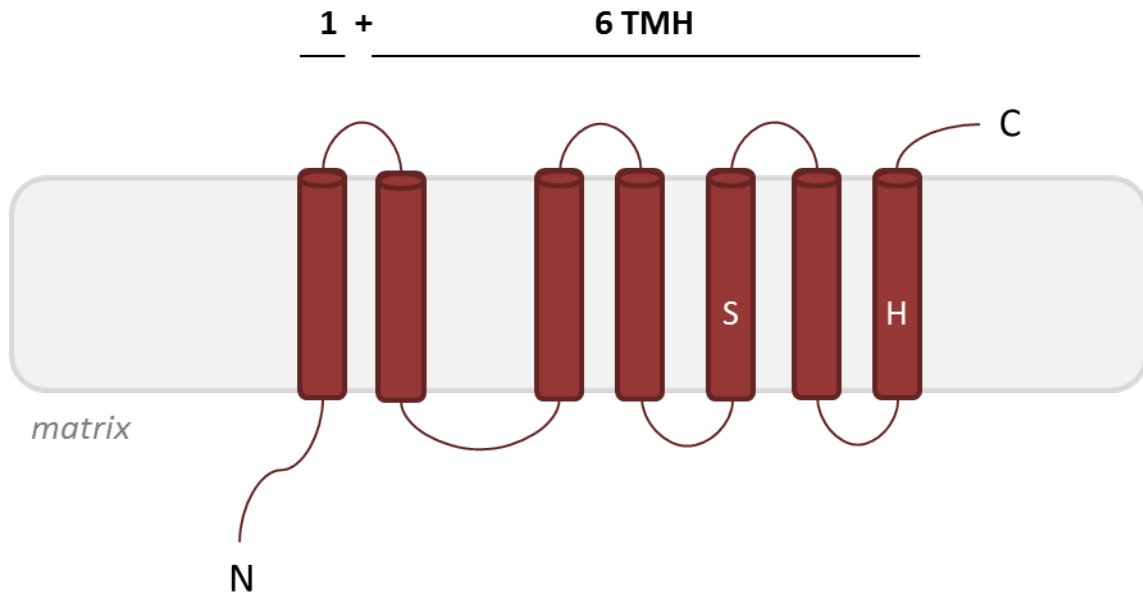


Figure 1.6. Topological diagram of the predicted structure of PARL protease in the inner mitochondrial membrane determined using TMpred and TMAP¹⁰³. The mitochondrial rhomboid protease is predicted to have 7 transmembrane helices, 6 core helices (similar to the structure of other members of the rhomboid family) with an additional helix appended at the N-terminus. S and H in white denote the positions of serine-277 and histidine-335, the two residues that form the catalytic dyad responsible for the hydrolytic activity of the protease. The grey rectangle is representative of the lipid bilayer forming the inner mitochondrial membrane.

truncated form of PINK1 is not observed; instead there is presence of a 52kDa PINK1 species⁹². Taken together, these results confirm the role of PARL protease in PINK1 processing, particularly the regulation of PINK1-mediated mitophagy.

1.4.2.1 The human mitochondrial rhomboid protease, PARL

PARL protease has a predicted 7 transmembrane domain topology (**Figure 1.6**). Rhomboid proteases generally share a conserved 6 transmembrane helix core. Though a structure of a PARL protease has not been solved, molecular modelling of the 6 transmembrane helix core demonstrates structural conservation with the bacterial rhomboid (**Figure 1.7**)¹⁰⁴. This additional N-terminal transmembrane helix in PARL is suggested to form a loop to the catalytic core¹⁰⁵. Intriguingly, the PARL protease experiences autoproteolysis as a mechanism of activity regulation in the N-terminal¹⁰⁴. α -, β - and γ -cleavage of PARL results in different truncations of PARL and their expression profiles are varied across different organs¹⁰⁴. The positioning of the γ -cleavage site is suggested to occur in the loop connecting the additional transmembrane helix to the 6 helix bundle. The occurrence of this cleavage event is controversial as it is difficult to imagine the accessibility the active site of PARL would have towards this particular site. Despite this, deletion of residues within this proposed cleavage site resulted in disruption of the distinct 1+6 transmembrane helix structure. Jeyaraju et al. suggest that this cleavage event is a mechanism of eliminating PARL activity in the mitochondrion. A mutation at serine-77, the site of β -cleavage, to an asparagine has been identified in two PD patients¹⁰⁶,

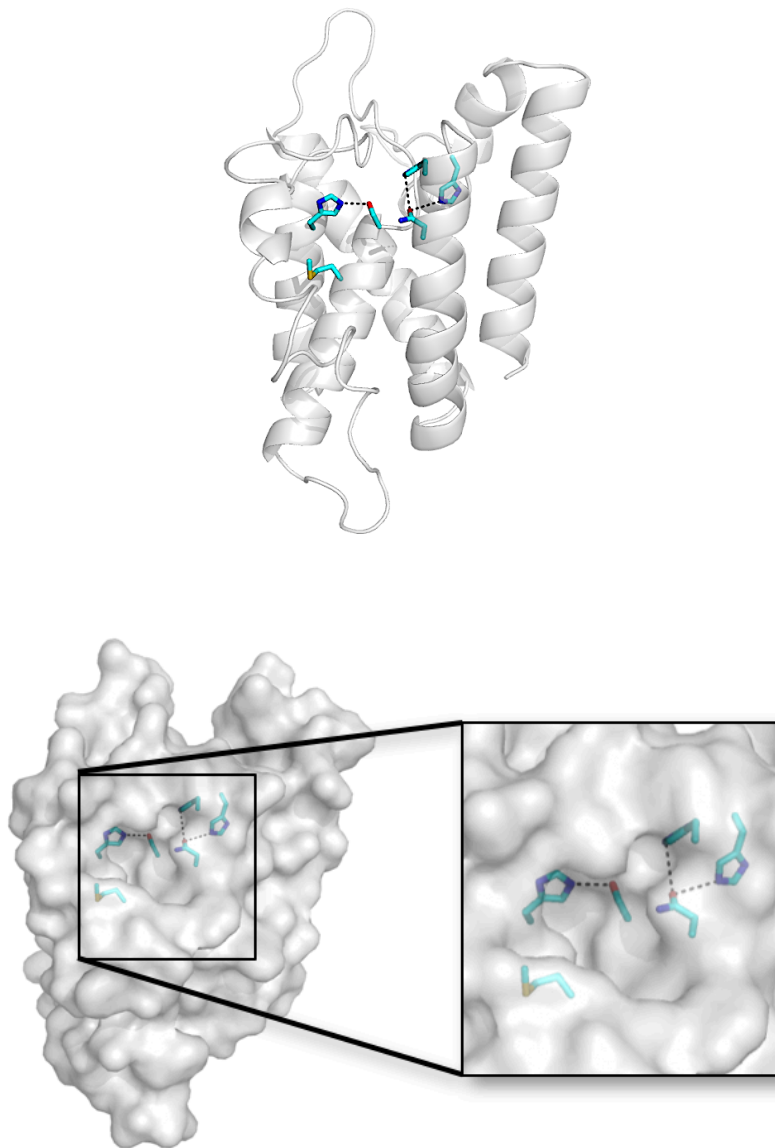


Figure 1.7. Homology model of PARL. The PARL protease homology model is based on the structure of the bacterial rhomboid, hiGlpG. Catalytic residues serine-277 and histidine-335 are coloured in cyan. Surface representation demonstrates a large binding pocket for substrates, demonstrating the active site of PARL could accommodate a large, hydrophobic residue such as the phenylalanine-104 found in the P1 position of PINK1.

suggesting an importance in this hydrolytic prone site. This particular mutation in the PARL protease is the only mutation that has been identified and linked to PD, suggesting mutations in PARL are an extremely uncommon genetic cause of PD^{107,108}

The PARL protease clearly plays an important role in mitochondrial quality control. Apart from its role in PINK1 turnover, the PARL protease is implicated in other cellular processes such as apoptosis and cellular homeostasis^{108,109}. The mitochondrial rhomboid is conserved between mammals, yeast, and *Drosophila*¹⁰⁸. Genetic knockout of the yeast mitochondrial rhomboid protease, rhomboid-1/processing of cytochrome c peroxidase protein 1 (Rbd1p/Pcp1p) resulted in the inability of Rbd1/Pcp1p-deficient yeast to grow on glycerol medium^{108,110}. In addition to this finding, rhomboid-deficient yeast demonstrated mitochondrial fragmentation, mitochondrial aggregation, and loss of mitochondrial DNA nucleoids^{108,110}. Similar to the finding in yeast, down regulation of the mitochondrial rhomboid resulted in mitochondrial fragmentation in *Drosophila*¹¹¹. Majority of *Drosophila* deficient in the mitochondrial rhomboid, rhomboid-7, died before pupation¹¹¹. Surviving rhomboid-7-deficient flies suffered from neurological defects, male sterility, and a lifespan of 3 days in adulthood¹⁰⁸. Interestingly, overexpression of rhomboid-7 resulted in an increase in *Drosophila* lethality¹¹², neurological defects¹¹², and mitochondrial aggregation similarly to what is seen in the overexpression of catalytically active PARL¹¹¹. Knockdown of PARL orthologues, Parla and Parlb, in zebrafish results in embryonic lethality, and notably altered expression of tyrosine hydroxylase mRNA and dopamine transporter¹¹³. PARL-

deficient mice developed normally until completion of embryogenesis when they would start to suffer from muscle atrophy and massive apoptosis in immune organs, and eventual death around three months of age¹¹⁴. The resulting debilitating and eventual detrimental phenotypes presented with downregulation or ablation of mitochondrial rhomboid proteases across these species demonstrate the importance of the protease.

Recently, the interaction of PARL with i-AAA protease YME1L and Stomatin-like protein 2 (SLP2) in the inner mitochondrial membrane has been uncovered. These proteases come together in complex forming a “proteolytic hub”¹¹⁵. Potential regulatory effects of this complex on PARL activity may have implications towards other processes of PARL beyond mitochondrial homeostasis. Additionally, association with these proteins may influence the activity of the PARL protease towards its mitochondrial substrates. Individual knockout of the substrates of PARL, PINK1 and Phosphoglycerate Mutase Family Member 5 (PGAM5) does not result in lethality, though they provide excellent Parkinsonian models^{116,117}. Taken together with the extensive work studying the effect of mitochondrial rhomboid downregulation or ablation, this suggests a larger role of the protease in mitochondrial function and likely cell vitality. Altogether, there is still much to be understood about the PARL protease and potential alternative roles it may have.

1.5 PINK1/Parkin-mediated mitophagy

PINK1/Parkin-dependent mitophagy is a well-characterized mode for removal of damaged mitochondria (**Figure 1.8**). This mechanism is important for mitochondrial quality control. In healthy mitochondria, PINK1 is targeted to the mitochondrion and is rapidly degraded. PINK1 localizes to the inner mitochondrial membrane by the translocase of the outer mitochondrial membrane (TOM) and the translocase of the inner mitochondrial membrane (TIM) complexes. When localized in the inner mitochondrial membrane, PINK1 is cleaved at alanine-103 by an inner mitochondrial membrane PARL protease⁸³. Upon cleavage, the kinase domain of PINK1 is released into the cytosol where it is subsequently degraded by the proteasome. In an old or damaged mitochondrion, or when membrane depolarization occurs disrupting the membrane potential and thereby preventing the complete translocation of PINK1, PINK1 accumulates on the outer mitochondrial membrane with the kinase domain facing the cytosol, results in its self-dimerization and formation of a supermolecular complex through association with the TOM complex¹¹⁸, leading to its autophosphorylation and recruitment of both Parkin – an E3 ubiquitin ligase, and ubiquitin⁸⁸. PINK1 phosphorylates these factors resulting in the recognition and engulfment of the mitochondrion by an autophagosome¹¹⁹.

Various mutations found in PINK1 and Parkin result in an autosomal recessive early-onset Parkinson's disease phenotype¹²⁰. PINK1 variants demonstrate aberrant functioning such as the inability to recruit Parkin as a result of impaired

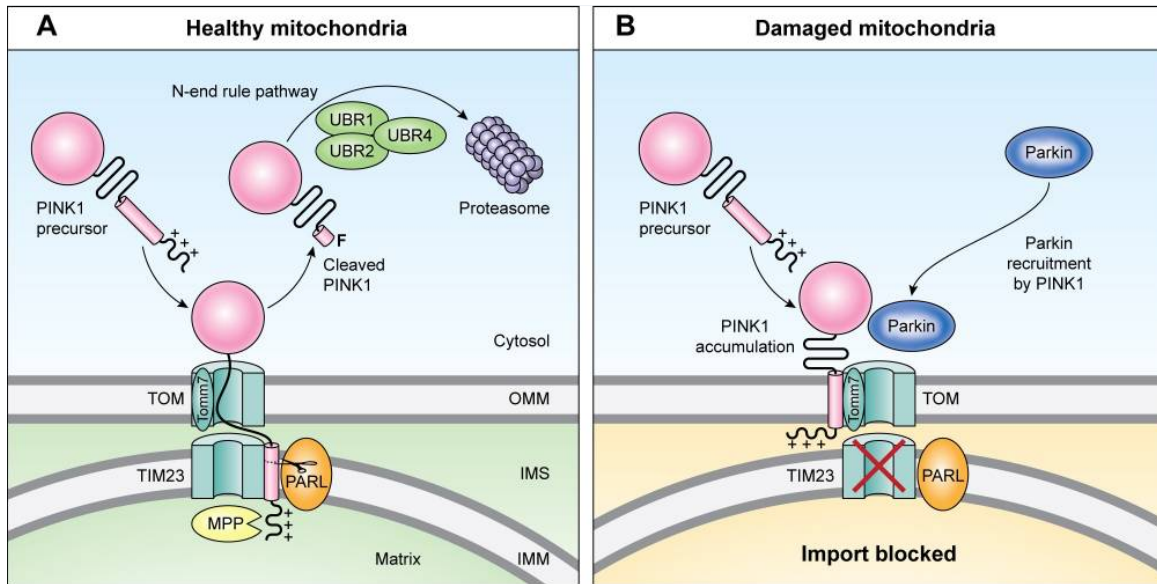


Figure 1.8. PINK1 proteolysis in the inner mitochondrial membrane. PINK1 is constitutively turned over in the inner mitochondrial membrane by the human rhomboid protease, PARL. In a healthy mitochondrion, PINK1 is imported into the inner mitochondrial membrane through the inner and outer mitochondrial translocases, TIM and TOM complexes, respectively. Once stabilized in the inner mitochondrial membrane, it presents to PARL protease as a transmembrane substrate where it is cleaved between alanine-103 and phenylalanine-104. The released kinase domain is then degraded by the proteasome, following the N-end rule pathway. When a mitochondrion is old or damaged, PINK1 accumulates on the outer mitochondrial membrane tagging the mitochondrion for removal by recruiting and then phosphorylating both Parkin and ubiquitin. (Adapted **with permission** from: Pickrell, A. M., Youle, R. J. (2015) The roles of PINK1, parkin and mitochondrial fidelity in Parkinson's disease. *Neuron* 85(2): 257-73.)

phosphorylation¹²¹⁻¹²³ or resistance to PARL-mediated cleavage¹²⁴, leading to a compromised mitochondrial quality control mechanism¹²¹. This imbalance in mitophagy is thought to be a major contributor to the premature cell death that is observed in various neuron types across different neurodegenerative pathologies, especially in PD (**Figure 1.9**).

1.6 Mutations found within the transmembrane domain of PINK1 have been linked to familial forms of PD

Mutations in *Pink1*, including nonsense, missense, splice site, and deletions have been identified in early-onset PD cases, both familial and sporadic forms¹²⁵⁻¹²⁷. Pathogenic mutations are found throughout the entire gene resulting in PINK1 protein variants (**Figure 1.3**). Variants of the kinase domain and C-terminal region have been thoroughly studied, often linking these kinase variants to loss of kinase function, affecting recruitment of Parkin and ubiquitin¹²⁸. Recently, more study has been directed at understanding PD-linked variants in the transmembrane region of PINK1. Preliminary studies using cellular extracts have demonstrated some single mutations made in the transmembrane domain of PINK1 result in alterations in protein integrity and function^{83,88,118,124,129-131}.

Variants of the transmembrane domain of PINK1 demonstrate altered processing, however it remains to be determined whether this is due to the PARL protease cleavage defects of trafficking to the IMM⁹², dictating effects on protein stability and

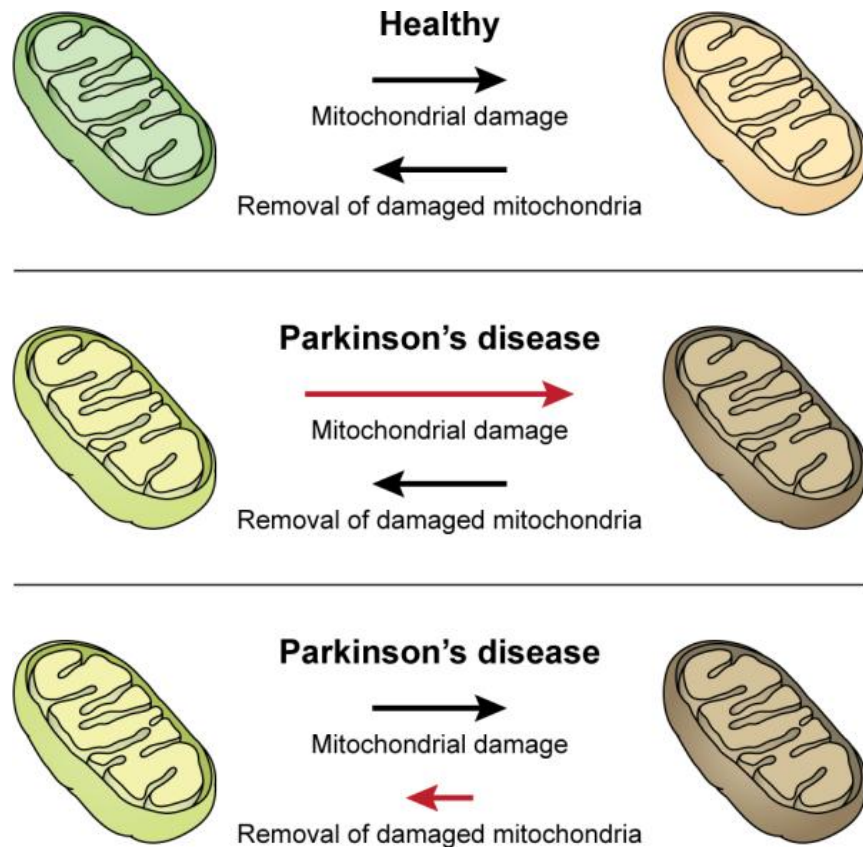


Figure 1.9. Imbalance in mitochondrial damage and damaged mitochondrion removal contributes to Parkinson's disease pathogenesis. In healthy cells, damaged organelles are removed and replaced. This is no exception for aged or damaged mitochondria, which undergo mitophagy as a means of removal. The mitochondrial damage and the subsequent removal of the damaged organelle constitute a very important homeostasis. In Parkinson's disease, two phenomena reported challenge this homeostasis: excess mitochondrial damage and insufficient damaged mitochondria removal. (Adapted **with permission** from: Pickrell, A. M., Youle, R. J. (2015) The roles of PINK1, parkin and mitochondrial fidelity in Parkinson's disease. *Neuron* 85(2): 257-73.)

downstream targets of the protein kinase (**Table 1.2, Figure 1.3**). Individual PD variants found in patients with mutations in the PINK1 TM will be highlighted below.

1.6.1 Compound heterozygous mutations in *Pink1* identified in PD patients results in substitution of cysteine-92 to phenylalanine and arginine-464 to histidine in PINK1 protein

Compound point mutations in the *Pink1* gene (c.275G>T, c.1391G>A) were found in a 37 year old PD patient^{127,128}. Cellular studies in SH-SY5Y cells revealed abnormal distribution and aggregation of mitochondria with expression of PINK1 C92F⁸³. The replacement of cysteine by phenylalanine introduces biochemical changes in the stability and functionality of the protein. Cysteine, a polar amino acid with a thiol side chain, has the ability to act as a nucleophile in enzymatic reactions in addition to its characteristic ability to form disulfide bonds. Okatsu *et al.* have reported the dimerization of PINK1 though the sites involved in the formation of the dimer-containing complex have not been identified. Membrane proteins typically dimerize using a GXXXG motif¹³². The sequence GLGLG, present in the transmembrane of PINK1 follows this motif though there is no evidence that supports its role in PINK1 dimerization. Individual mutations of the glycine to tryptophan did not appear to influence or interrupt the function of PINK1 under conditions of membrane depolarization with CCCP⁹². It has been suggested that dimerization of PINK1 is necessary for the auto-activation of PINK1 and subsequently its recruitment of

Table 1.2. Parkinson's disease-linked mutations found in (C92F, R98W, I111S) or near (Q126P) the transmembrane region of PINK1.

| Domain | Nucleotide change | Amino acid substitution | Mutation class | Mean onset ages | Inheritance |
|---------------|--------------------------|--------------------------------|-----------------------|------------------------|--------------------|
| TM | c.275G>T | C92F | Compound heterozygous | 37.0y | Nonfamilial |
| TM | c.282C>T | R98W | Single heterozygous | - | Familial |
| TM | c.332T>G | I111S | Single heterozygous | - | Familial |
| Extra-TM | c.377A>C | Q126P | Homozygous | 38.0y | Familial |

Parkin. If dimerization were affected, this would result in the disruption of PINK1 downstream kinase-involving events. It is possible that the cysteine-92 may play a pivotal role in the formation of the PINK1 dimer-containing complex. However, Okatsu *et al.* demonstrated that PINK1 C92F variant did not inhibit the formation of the dimeric PINK1-containing complex or the mitochondrial localization of Parkin. Regardless, there is evidence of disruption in PARL-mediated cleavage. Mutation of a polar residue to a non-polar, hydrophobic residue such as phenylalanine may result in protein aggregation – especially in a transmembrane region of a protein. In cellular studies, it is evident that processing of the PINK1 C92F variant is affected. This may be due to an induced disturbance in the helical structure of the transmembrane domain. Deas *et al.* demonstrate an accumulation of the full-length form of PINK1 in cells expressing the C92F variant, though there is still production of the mature, cleaved form of PINK1 consistent with that of the wild-type, indicating cleavage is not entirely inhibited though cleavage efficiency may be reduced. Intact structure is often imperative for the recognition, binding, and cleavage of a substrate by its respective enzyme.

1.6.2 Single heterozygous mutation in *Pink1* identified in PD patients results in substitution of arginine-98 to tryptophan in PINK1 protein

A mutation of arginine at residue 98 to an aromatic tryptophan in PINK1 has been found to be pathogenic in an Italian family^{133,134}. Sequence alignment shows high conservation of this residue among vertebrate species¹³⁴. Reports claim disease

manifestation began in lower limbs in addition to presentation of impaired gait, urinary urgency, and a slower disease progression¹³³. The significance of this residue may be attributed to its positive charge, where mutation from a charged residue to a bulky hydrophobic residue may cause misfolding or induce aggregation of the variant protein, thus affecting its ability to be localized to the mitochondrial membrane or its ability to be cleaved by PARL protease. A cell-based activity assay demonstrated a major reduction in the cleavage of the R98W variant compared to the wild-type¹³⁰. An accumulation of full-length PINK1 provides evidence to an alteration in the proteolysis of this variant¹³⁰. When PARL protease was knocked down there was no observable effect on the cleavage of PINK1 R98W in transfected HEK293 cells, signifying appreciable inhibited cleavage by PARL protease towards this variant *in vivo*¹³⁰. Notably in the absence of membrane depolarization, PINK1 R98W effectively influenced the translocation of Parkin to the mitochondrion¹²⁴. Additionally, the same group demonstrated cells expressing PINK1 R98W resulted in the formation of autophagosomes, a finding exclusive to this PD-linked variant in this study¹²⁴. Cellular studies done by Jin *et al.* show substitution of arginine-98 to a phenylalanine results in altered processing of the PINK1 variant, corroborating the findings of Meissner *et al.* In addition to the demonstration of disrupted PARL-mediated cleavage, there is an accumulation of the N-terminus fragment of PINK1 in a similar variant (R98F), suggesting interference in the ability of the proteasome to degrade this mature PINK1 fragment⁹². Together, these results suggest a PINK1 gain-of-function resulting in aberrant mitophagy in cells harboring this variant.

1.6.3 Single heterozygous mutation in *Pink1* identified in PD patients results in substitution of isoleucine-111 to serine in PINK1 protein

A mutation found downstream the PARL protease cleavage site, I111S, demonstrated a small alteration in PARL-mediated processing¹³⁰, though no aberrant Parkin recruitment or mitophagy initiation was observed¹²⁴. This mutation has also been found to be pathogenic in another Italian family¹³³ though understanding of the alteration in PINK1 I111S function or its claim to pathogenesis is underwhelming. The substitution of this isoleucine to a serine, a non-polar amino acid to a polar one, can significantly interrupt the integrity of the proteins secondary structure. This change may destabilize the alpha helical structure of the transmembrane domain, inducing misfolding and aggregation – influencing the variant's ability to effectively localize to the appropriate mitochondrial membrane for processing by PARL protease. *In vitro* functional studies of this variant will provide crucial insight into the role of PARL-mediated proteolysis and PD pathogenesis for this PD-linked mutation.

1.6.4 Homozygous mutation in *Pink1* identified in PD patients results in substitution of glutamine-126 to proline in PINK1 protein

In addition to the mutations found within the transmembrane domain, there is a series of mutations that have been identified clustered between the transmembrane domain and kinase domain: alanine-124, cysteine-125, and glutamine-126. These

residues are interesting because they suggest an importance in this extra-transmembrane region due to resulting pathogenicity when mutated. These PD-linked mutations, found in a highly conserved region, may imply their significance as potential residues recognized by an exosite in the PARL protease. An exosite is a secondary binding site on an enzyme, distinct from the active site. It is known that an exosite exists for rhomboid proteases and they influence rhomboid-substrate interactions¹³⁵⁻¹³⁷. These exosites are reported to exist within the rhomboid core. Though, PARL protease has not been reported to contain an exosite, mutations found at amino acid residues 124, 125, and 126 have been found in human patients, with two of the three being found in Parkinson's patients^{126,133,138}. A mutation from glutamine-126 to proline was identified in two PD-presenting sisters, with Parkinsonism developing at ages 36 and 40¹³⁸. This variant may provide insight towards the functionality of this extra-transmembrane, extra-kinase domain region. Interestingly, analysis of respiratory chain complexes I-IV and proteasomal activity, lactate, pyruvate, carnitine, and acylcarnitine levels in the two sisters provided no indication of mitochondrial dysfunction¹³⁸. Human PINK1 Q126P failed to recruit Parkin when co-expressed in HeLa cells indicating a kinase activity loss-of-function¹²⁸. Similarly to the other transmembrane variants of PINK1, there is much to uncover about the functional implications of PINK1 Q126P and how this variant contributes to PD pathogenesis.

1.7 Heterologous expression of membrane proteins

Studying membrane proteins outside of their natural environment often poses as a major challenge in the field of protein biochemistry. *In vitro* studies with recombinant protein, both structural and functional, often require sufficient yield and purity – both of which present as hurdles in the expression of these proteins. In biological membranes, the presence of an individual membrane protein species is typically low¹³⁹. There are certainly membrane proteins that can be isolated from their native sources. For example, SLC4A1 (solute carrier family 4 member 1) foundationally known as Band 3, is an anion transporter found in the membrane that can be isolated from red blood cells in sufficient quantity¹⁴⁰. Despite this, most membrane proteins are not able to be isolated in sufficient amounts from their native environments; therefore, attempts are made to recombinantly overexpress them.

The method of recombinant expression comes with its own set of challenges. Often the yield of the expressed protein is inadequate for *in vitro* studies. An expression screen of over one hundred membrane proteins from *Mycobacterium tuberculosis* in *Escherichia coli* demonstrated successful overexpression of only a quarter of the proteins screened^{141,142}. Low success in membrane protein overexpression is often due to protein instability, which in turn often leads to protein aggregation. In native environments, membrane proteins are stabilized by post-translational modifications. These post-translational modifications are often absent when protein

is expressed in other non-native hosts. This may contribute to the instability of a recombinant membrane protein, in addition to the lack of a natural membrane lipid bilayer and the general hydrophobicity of membrane proteins.

Protein structure knowledge is often a good indication on the stability and successful isolation or expression of said protein. Between the years of 1990 and 2017, the Protein Data Bank has grown from 507 known protein structures to over 136,000. Today, membrane proteins make up only 840 of those reported structures¹⁴³, likely as a result of the arduous tasks of generating sufficient yield. Developments in the biochemical techniques and protocols have led the field to a more productive approach for overexpression of proteins. Taken together, these findings highlight the importance for novel protocol development for the expression and purification of membrane proteins.

1.8 Expression systems for recombinant proteins

Advances in technology, molecular biology, and genetic engineering have allowed for increased feasibility of recombinant membrane protein expression. As a derivative of these advancements large-scale expression, or over-expression, of proteins has been optimized in addition to protocols for protease isolation. There is an abundance of protein expression systems that include and are not limited to bacteria, yeast, insects, plants, and mammalian cells. Innovation in the field of genetic engineering allowed for the expression of proteins in non-native systems,

such as the expression of Lipase B (PalB) a protein from *Pseudozyma antarctica* in *Escherichia coli* and *Pichia pastoris*¹⁴⁴. Advances in detergents have allowed for the gentle extraction of membrane proteins from bilayers while maintaining structural integrity¹⁴⁵. The recombinant or heterologous expression of proteins allows for an economical, and often simpler, alternative to expression from the native source.

Recombinant protein expression is a powerful biochemical tool for both structural and functional studies in protein biochemistry. Several factors influence the most suitable expression system to be used. Time, ease of use, protein yield, the desire of post-translational modifications and the protein destination protein post-expression all dictate the choice of expression system utilized.

1.8.1 The use of *Escherichia coli* as a recombinant expression system

Escherichia coli (*E. coli*) are a preferred host for recombinant expression of proteins as they offer several advantages as an expression system. The system and protocols for protein expression are well established. Advantages offered by *E. coli* include rapid expression, easy manipulation, simple scale up, and it is a less expensive method for protein expression. In addition to the aforementioned advantages, *E. coli* have well characterized genetics. The diverse range of bacterial strains allows for optimization between different bacterial protein phenotypes. This has been advantageous when, for example, expressing a protein such as *Providencia stuartii* TatA, a substrate of the rhomboid protease GlpG. By knocking out endogenously

expressed GlpG in the *E. coli* cells used to express TatA, premature cleavage is avoided and TatA is successfully expressed in its mature, full-length form for isolation and subsequent use^{146,147}. One disadvantage to recombinant expression of proteins in *E. coli*, especially when attempting to express eukaryotic membrane proteins, is the differences in translation machinery; including the absence of eukaryotic chaperones and other factors that may assist in protein folding and stability. Another shortcoming of this method is the absence of eukaryotic post-translational modifications. Post-translational modifications such as phosphorylation, acetylation, and ubiquitination may be necessary for the stability or functionality of a protein.

Additionally, the method calls for strenuous utilization of *E. coli* machinery responsible for protein expression. The high-energy exertion and speed of protein expression may compromise the folded protein product. A major distinguishing factor between eukaryotes and prokaryotes is in the basic processes of transcription and translation. In eukaryotes, RNA is transcribed in the nucleus and then translated in the cytoplasm. Conversely, in prokaryotes transcription and translation occur simultaneously. This major difference may play a role in eukaryotic protein folded fate when expressed in *E. coli*. Despite the source of expression, misfolding can lead to aggregation of the protein of interest. An additional challenge that may be encountered when working with *E. coli* is that as a bacterial species it is susceptible to bacteriophage infection. If infected, growth and subsequent protein expression

are severely compromised. Despite these potential disadvantages, *E. coli* remains a popular and reliable system for recombinant protein expression.

1.8.2 The use of *Pichia pastoris* as a recombinant expression system

Pichia pastoris (*P. pastoris*) is methylotrophic yeast that has been proven a well-established host for recombinant protein expression. Originally introduced and used for the production of single cell protein by Phillips Petroleum^{148,149}, it has transitioned its relevance towards biochemical uses. *P. pastoris* has been developed as a recombinant protein expression system by use of a tightly regulated promoter, P_{AOX1}. Alcohol oxidase 1 (AOX1), allows for the induction of gene expression by way of methanol. One advantage of this promoter is the uncoupling of growth and induction phases, allowing for the accumulation of biomass before protein overexpression¹⁵⁰. This relieves the cellular stress due to protein accumulation, allowing for expression during the growth phase and growth of otherwise *P. pastoris*-toxic proteins. When grown on glycerol, glucose, or ethanol, P_{AOX1} is repressed¹⁵¹. When yeast cells are depleted of these nutrients and supplemented with methanol the promoter is un-repressed and induced, respectively¹⁵⁰. One shortcoming of the use of this system for recombinant protein expression is the use of methanol, an extremely flammable substance. In industry, the use of such a hazardous substance is undesirable; however, in medial-scale lab expression, this is not a very significant drawback as these materials can be controlled more easily.

Use of *P. pastoris* as an expression hosts requires a fair amount of optimization. Unlike *E. coli*, expression of exogenously acquired DNA requires genomic integration. This determines protein expression levels via integration locus and the gene copy number. Importantly, the gene copy number refers to the number of copies of a particular gene in a genotype, discernibly influencing the amount of translated protein. This results in the need for screening of high expressing colonies by way of reporters such as GFP. Hydroxynitrile lyase, an enzyme derived from *Hevea brasiliensis*, was one of the first proteins recombinantly produced using the *P. pastoris* expression system¹⁵². Over 20 g of recombinant hydroxynitrile lyase per litre of culture was produced, proving as a very effective system¹⁵². Though, not all proteins are overexpressed to such an abundant yield, when optimized the amount of protein yielded can prove superior to other expression hosts. For example, eukaryotic membrane proteins, which are challenging to overexpress can be expressed in great quantity and stability by *P. pastoris*. *P. pastoris* possesses mammalian-like machinery that offers it advantages to its prokaryotic counterparts when expressing complex proteins¹⁵³. Overall, as a eukaryotic expression system, *P. pastoris* offers many advantages for the recombinant expression of proteins¹⁴¹.

1.9 Thesis objective

It is known and accepted that mutations found throughout the entire PINK1 protein influence its functionality in mitochondria. Despite the location of these mutations, resulting protein variants either demonstrate an imbalance in mitophagy due to

loss- or gain-of-function in signaling capabilities. With a primary focus on the transmembrane domain of PINK1, I aim to answer whether aberrant accumulation of PINK1 PD-linked variants are due to defects in cleavage by the PARL protease. Three mutations within the transmembrane region of PINK1 have been identified in PD patients: C92F, R98W, and I111S. An additional PD-linked mutation at glutamine-126 to a proline is found adjacent to the transmembrane domain. In this thesis, I establish a protocol to generate recombinant human PINK1 and I recombinantly produce human PARL protease. In addition, I will examine whether mutations in and surrounding the transmembrane domain influence the association with and cleavage by PARL protease. Adequate analysis of the cleavage parameters of PARL towards these PINK1 variants will provide insight into the effects these mutations have on PINK1 dynamics. A more comprehensive understanding of the effect of these variants on PINK1 processing may implicate a dysregulation of PINK1/Parkin-mediated mitophagy. Furthermore, these findings may uncover how effective identification of these mutations in PD patients may have the potential for targeted therapies.

CHAPTER 2: Expression and Purification of Human PINK1

2 Expression and Purification of His-FRET-HsPINK1[70-134]

2.1 Introduction

PINK1, introduced earlier as PTEN-induced putative kinase 1, is a mitochondrial protein kinase in which rare, inherited mutations have been associated with both familial and sporadic forms of PD. Study of these mutations have provided insight into the molecular mechanisms of the disease, particularly the importance of mitochondrial functioning. A key interaction in the mitochondrion that regulates the PINK1-dependent mitophagy pathway is between PINK1 and the PARL protease. Cleavage of PINK1 by PARL in the inner mitochondrial membrane of a healthy mitochondrion results in a rapid turnover of the substrate. Inhibition or disruption of this cleavage event may result in accumulation of PINK1, signaling mitophagy in an otherwise healthy mitochondrion. Mutations found in the transmembrane region of PINK1 may interfere with the ability of the PARL protease to appropriately process its substrate.

Given the importance of PINK1 in mitophagy, recombinant protein will be useful to determine its suitability as a substrate for PARL protease. While the kinase domains of PINK1 from *Pediculus humanus corporis* and *Tribolium castaneum* have been crystallized from recombinant protein^{81,82}, human PINK1 has not been recombinantly expressed and purified. With our interest in the transmembrane region significant effort for development and optimization of a protocol was

required for PINK1 overexpression given its high degree of hydrophobicity. The Lemieux lab has developed an *in vitro* FRET-based technique to study the kinetics of various bacterial intramembrane proteases¹⁴⁶ (**Figure 2.1**). This assay, adapted to for the mitochondrial rhomboid PARL, requires milligram amounts of purified recombinant protease and recombinant FRET-based substrate. This assay provides a powerful means to assess the catalytic capacity of the enzyme *in vitro*.

To measure the cleavage rate of the substrate PINK1 and its PD variants by PARL protease, recombinant FRET-based substrates of PINK1 are needed in sufficient milligram amounts and purity. A previous student in the Lemieux lab cloned the putative PINK1 transmembrane (residues 89-111) into a “FRET” vector, where the insert was flanked by two fluorescent proteins: cyan fluorescent protein for energy transfer (CyPet) and yellow fluorescent protein for energy transfer (YPet) resulting in the following DNA sequence: *XhoI-CyPet-BglIII-Pink1[89-111]-KpnI-YPet-stop-HindIII* (**Figure 2.2**). Kinetic studies using His-FRET-*HsPINK1*[89-111] expressed from this construct were unsuccessful; likely due to obstruction of the PINK1 cleavage site by the large fluorogenic proteins flanking PINK1, hindering protease accessibility. In the current study the boundaries of PINK1 cloned into the pBAD plasmid (Invitrogen) were extended to include residues phenylalanine-70 to glutamine-134,

FRQSVAGLAARLQRQFVVRAWGCAGPCGRAVFLAFGLGLGLIEEKQAESRRAVSACQEIQ
AIFTQ to mitigate potential steric effects. The corresponding DNA segment of PINK1

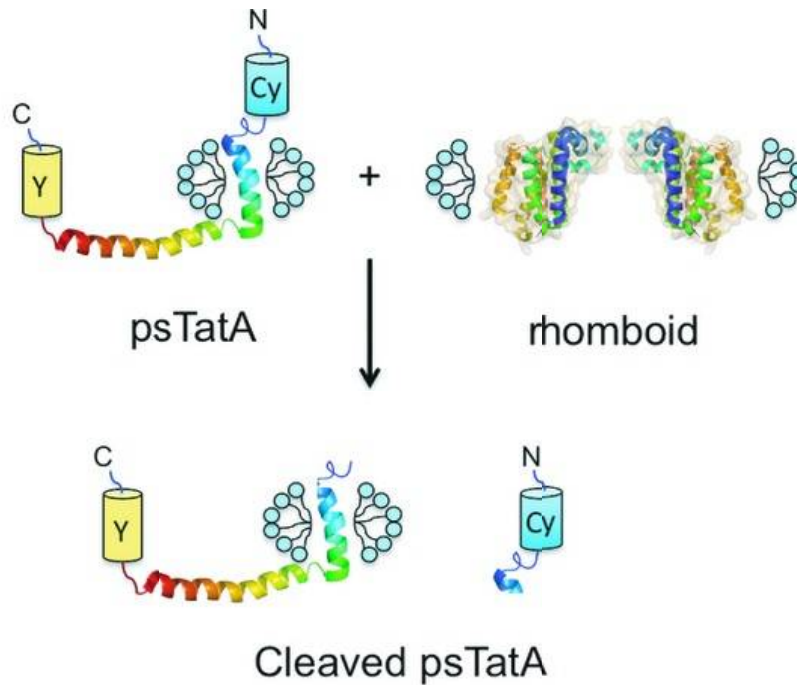


Figure 2.1. Fluorescence resonance energy transfer (FRET)-based kinetic assay concept. FRET-based activity assay used to assess catalytic parameters for the *Providencia stuartii* rhomboid protease, AarA-mediated cleavage of its physiologic substrate psTatA. psTatA is flanked by a CyPet fluorescent protein and a YPet fluorescent protein at the N- and C-termini, respectively. The structure of psTatA was determined by NMR¹⁵⁴. (Adapted **with permission** from: Arutyunova, E., Panwar, P., Skiba, P. M., Gale, N., Mak, M. W., Lemieux, M. J. (2014) Allosteric regulation of rhomboid intramembrane proteolysis. *EMBO J* 33(17): 1869-1881.)

was inserted into the pBAD:FRET vector resulting in the *XhoI-CyPet-BglII-Pink1[70-134]-KpnI-YPet-stop-HindIII* construct (Figure 2.2).

2.2 Generation of PINK1 transmembrane domain and mutations in the pBAD:His-FRET-HsPINK1[70-134] vector

To examine the effect of the various PD-linked transmembrane domain variants on PARL protease processing, it was necessary to have each variant, C92F, R98W, I111S, and Q126P, expressed in this FRET vector. Two methods were utilized to make the PINK1 PD-linked variants: classical cloning and site-directed mutagenesis. A challenge encountered with the cloning of PINK1 was the high GC content (>60%) in the DNA template. GC-rich DNA is often difficult to amplify due to the stronger hydrogen bonds formed between the guanines and cytosines, resulting in a higher melting temperature (T_m)¹⁵⁵. Primers designed for cloning are based on DNA template and therefore GC content of the primer is often reflective of that in the template region being amplified. High GC-containing primers often have unwanted secondary structures and interactions formed such as hairpins and self-annealing, respectively, inhibiting the success of primer-DNA annealing and thus DNA amplification^{156,157}. To overcome concerns linked to high GC content, the cloning protocol can be optimized. DNA denaturation temperature can be varied to ensure complete strand separation (NEB PCR protocol for Phusion High-Fidelity Polymerase (M0530)). The annealing temperature can be adjusted to enhance

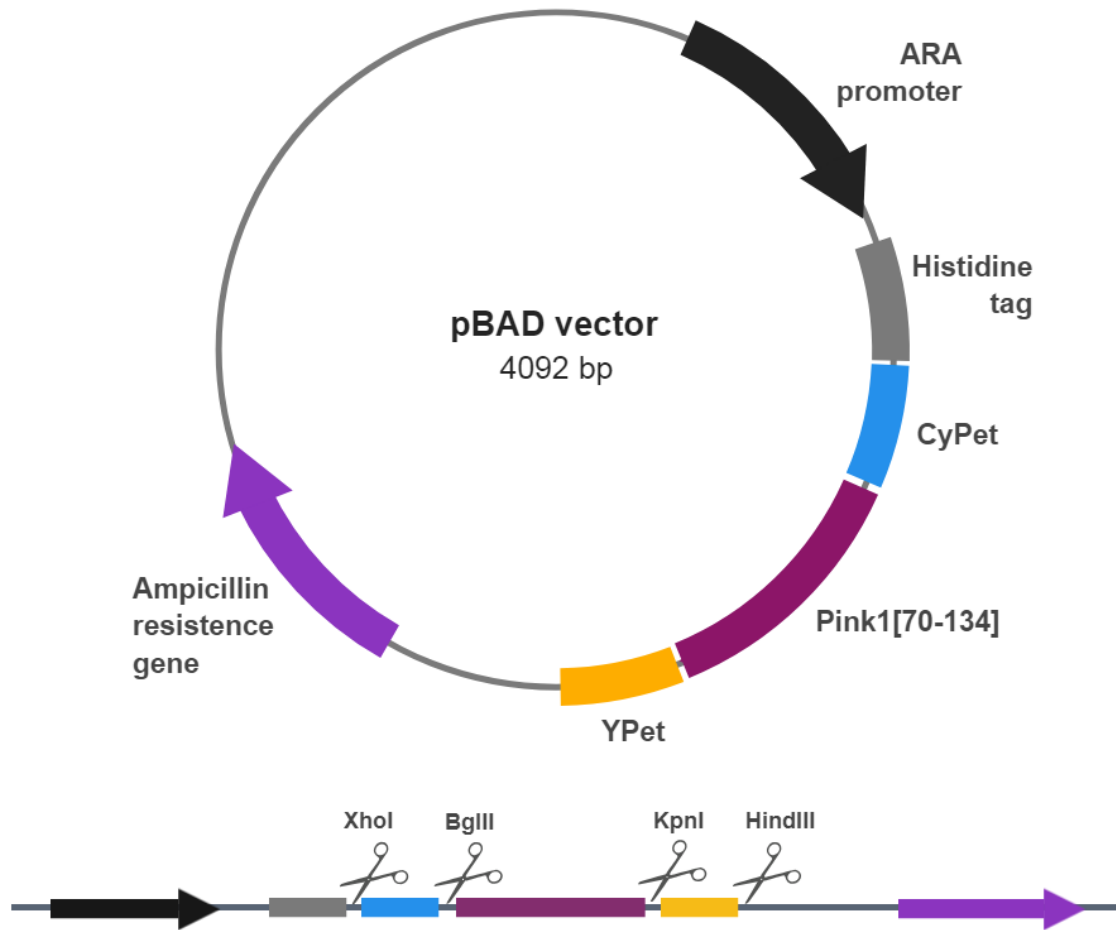


Figure 2.2. Condensed pBAD:FRET vector map. The black arrow represents the arabinose-inducible ARA promoter; the grey rectangle represents DNA encoding for the poly-His-tag; the blue rectangle represents DNA encoding for cyan fluorescent protein, CyPet; the pink rectangle represents DNA encoding for *HsPINK1*; and the yellow rectangle represents DNA encoding for yellow fluorescent protein, YPet. The adapted pBAD vector confers ampicillin resistance denoted by purple arrow, utilized for selection of positive *E. coli* clones.

primer-DNA annealing (NEB PCR protocol for Phusion High-Fidelity Polymerase (M0530)). Importantly, buffer additives such as DMSO and Mg^{2+} can be utilized to help DNA denaturation as well as polymerase activity efficiency, respectively¹⁵⁸ (NEB PCR protocol for Phusion High-Fidelity Polymerase (M0530)).

2.2.1 Cloning PINK1 variants into pBAD:His-FRET-HsPINK1[70-134] vector using restriction enzymes

All PINK1 variants of interest had already been successfully cloned in another construct for confocal imaging. Using the forward primer 5' – atc ata gat ctt tcc gcc agt cgg tgg ccg ggc t – 3' and the reverse primer 5' – cac tgg tac cct ggg taa aaa ttg cct gga tct cct gac a – 3', DNA encoding PINK1 residues 70-134 was amplified using Polymerase Chain Reaction (PCR). Reactions were set up to include 100 ng dsDNA template, 10 μ M forward primer, 10 μ M reverse primer, 10 μ L 5X Phusion GC buffer, 1.5 μ L DMSO, 1 μ L 10 mM dNTPs, and ddH₂O to a final reaction volume of 50 μ L. The protocol followed for the PCR amplification is outlined in **Table 2.1**. Typically, PCR follows three steps: first, denaturation of the dsDNA template into single strands, secondly, annealing of primers to each strand of the now single-strand template DNA (ssDNA), and finally, extension of the primers complementary to the ssDNA it is bound to¹⁵⁹. The initial DNA denaturation step occurs at 98 °C. The DNA-primer annealing temperature can range between 45-72 °C depending on the T_m of the primers. Input of the primer sequences into the online New England Bio T_m

Table 2.1. Polymerase Chain Reaction settings for amplification of *HsPINK1*[70-134] variants.

| Segment | Number of cycles | Temperature (°C) | Time |
|-------------------------|-------------------------|-------------------------|---------------|
| Denaturation | 1 | 98 | 5 minutes |
| Annealing and extension | 40 | 98 | 30 seconds |
| | | 72 | 1 minute |
| Final extension | 1 | 72 | 10 minutes |
| | 1 | 4 | Infinite hold |

calculator resulted in a suggested annealing temperature of 72 °C. The extension is typically carried out at 72 °C. Because the primers required an annealing temperature of 72 °C, a 2-step thermocycler protocol was required where both the annealing and extension steps were combined into one.

Using a 2% agarose gel, the PCR amplification product was purified, appearing at the expected 216 bp mark (**Figure 2.3**). Purification was followed by a gel extraction using the Qiagen QIAquick Gel Extraction Kit and protocol. The amplified DNA was then subject to a double digestion using the Thermofisher Fast Digest system. Restriction enzymes *BglII* and *KpnI* were used to digest both the pBAD vector and the PINK1⁷⁰⁻¹³⁴ inserts, creating sticky ends for their subsequent ligation (**Table 2.2**). The first digestion was done by incubating either 200 ng of the insert or 1 µg of the vector with 1 U *BglII* for 2 hours at 37 °C. *BglII* was then heat inactivated at 67 °C for 20 minutes. The second digestion was done using 1 U *KpnI* with the same incubation conditions. Digestions were run on either 2% agarose gels or 0.5% agarose gels for the inserts and the vector, respectively. Following this purification, digested fragments were extracted using the Qiagen QIAquick Gel Extraction Kit and protocol.

Following successful digestion of both the PINK1 inserts and the pBAD vector, ligation reactions were assembled. Input of the insert DNA length, the vector DNA length, and the mass of the vector DNA into the New England Bio online ligation calculator resulted in calculated amount of mass of insert required for ligation at different ratios of insert-to-vector. Ligation reactions were made at a 3:1 insert-to-

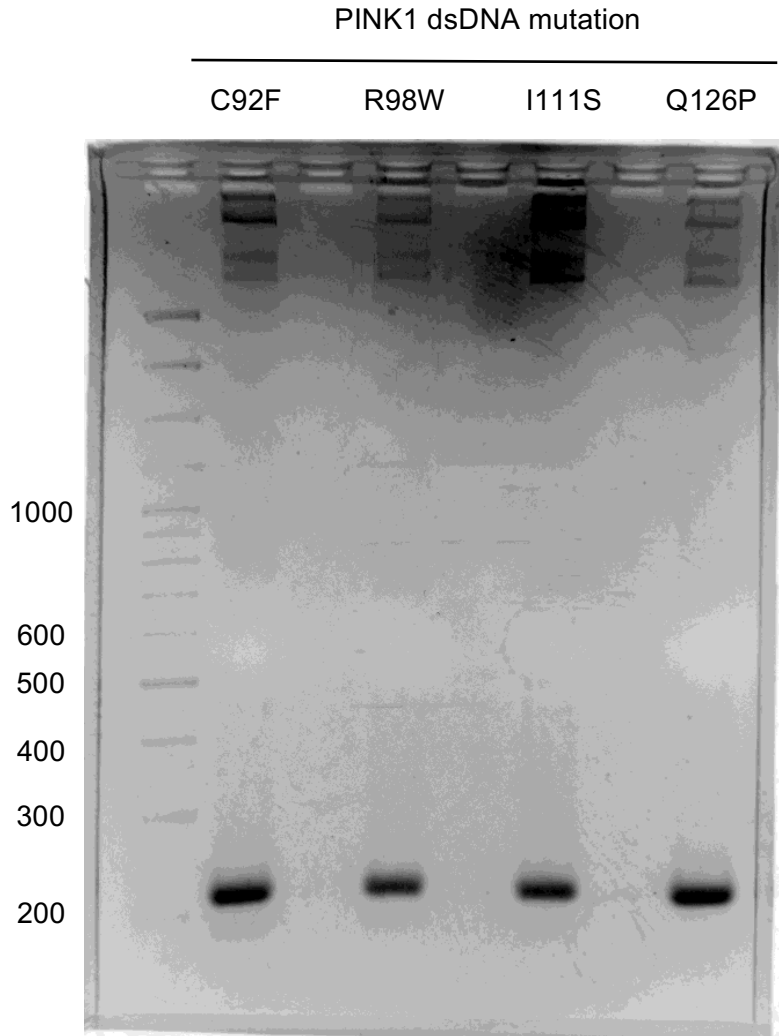


Figure 2.3. PCR amplification of PINK1 70-134 C92F, R98W, I111S, and Q126P dsDNA. PCR products run on a 2% agarose gel. Product bands appear at expected size of 216 bp. Imaged using the ImageQuant LAS 4000.

Table 2.2. Restriction enzymes *BglII* and *KpnI* DNA recognition sequences. ^ = sites of cleavage.

| Restriction enzyme | Recognition site |
|---------------------------|--|
| <i>BglII</i> | 5' – A ^ G A T C T – 3' 3' – T C T A G ^ A – 5' |
| <i>KpnI</i> | 5' – G G T A C ^ C – 3' 3' – C ^ C A T G G – 5' |

vector ratio with 4 μL 5X reaction buffer, 11.35 ng insert, 75.5 ng vector, 1 μL T4 ligase, and ddH₂O to a volume of 20 μL . The ligation reaction was incubated overnight at 25 °C. 5-10 μL of the ligation products were used to transform *E. coli* Top10 cells for identification of successful transformants.

2.2.2 Cloning PINK1 transmembrane domain mutations into pBAD:His-FRET-HsPINK1[70-134] vector using site-directed mutagenesis

Site-directed mutagenesis (SDM) is a technique used to introduce site-specific changes to DNA sequence¹⁶⁰. This method requires purified DNA template, short primers that are complementary to the template that contain the desired mutation, and certain buffers dependent on the kit used. Primers designed and ordered for the four variants of PINK1 are found in **Table 2.3**.

Reactions were set up to include 5 μL 10X reaction buffer, 5-50 ng dsDNA template, 125 ng forward primer, 125 ng reverse primer, 1 μL 10 mM dNTPs, 1 μL DMSO, ddH₂O to a final reaction volume of 50 μL . Immediately before beginning the reaction, 1 μL Phusion DNA polymerase was added to each reaction. PCR protocol followed the general procedure outlined by the SDM manual and **Table 2.4**. DMSO was added to the reaction mixture to moderate the problems encountered by the high GC content of the template.

Table 2.3. Forward and reverse primers designed for Site-Directed Mutagenesis of His-FRET-*HsPINK1*[70-134] PD variants.

| PD-linked variant | Primers (5' -> 3') |
|--------------------------|--|
| C92F | Forward: 5' – cag ttc gtg gtg cgg gcc tgg ggc ttc – 3' Reverse: 5' – gaa gcc cca ggc ccg cac cac gaa ctg – 3' |
| R98W | Forward: 5' – ttg cgg ctg ggc agt ctt tct ggc ctt cg – 3' Reverse: 5' – ctt ccg gtg aaa gac tgc cca gcc gca a – 3' |
| I111S | Forward: 5' – ggg cta ggg ctg ggc ctc agc gag gaa – 3' Reverse: 5' – tgt ttt tcc tcg ctg agg ccc agc cct a – 3' |
| Q126P | Forward: 5' – gtc tcg gcc tgt ccg gag atc cag gca at – 3' Reverse: 5' – att gcc tgg atc tcc gga cag gcc gag ac – 3' |

Table 2.4. Polymerase Chain Reaction settings for Site-Directed Mutagenesis of His-FRET-*HsPINK1*[70-134] variants.

| Segment | Number of cycles | Temperature | Time |
|-------------------------|-------------------------|--------------------|---------------|
| Denaturation | 1 | 95 | 30 seconds |
| Annealing and extension | 16 | 95 | 30 seconds |
| | | 55 | 1 minute |
| | | 68 | 3 minutes |
| | 1 | 4 | Infinite hold |

After PCR, each reaction was subjected to a 30 minute *DpnI* incubation, and then 10 μ L was used to transform Top10 *E. coli* cells for selection of positive clones. *DpnI* is a restriction enzyme that recognizes and cleaves methylated DNA. This step is incorporated post-SDM PCR to digest any template DNA present in the site-directed PCR product mixture¹⁶¹, minimizing the likelihood of false-positive transformants. Site-directed mutagenesis was not successful for all variants of PINK1 so traditional cloning was utilized for remaining PD-linked variants.

2.3 Transformation of *E. coli* Top 10 with pBAD:His-FRET-*HsPINK1*[70-134]

Chemo-competent Top10 cells, stored in 50 μ L aliquots at -80 $^{\circ}$ C, were thawed on ice. 3 μ L of vector was added to the competent cells and incubated on ice for 20 minutes. Cells were heat shocked at 42 $^{\circ}$ C for 1 minute, then returned to ice for 2 minutes. After this cooling incubation step, 1 mL of LB was added to the competent cells and incubated at 37 $^{\circ}$ C for 1 hour with agitation. Following this incubation, cells were sterilely plated onto LB agar and ampicillin plates for selection of successful transformants. Plates were incubated overnight at 37 $^{\circ}$ C.

2.4 Growth of *E. coli* Top10 pBAD:His-FRET-*HsPINK1*[70-134] and expression of His-*HsPINK1*[70-134] WT and variants

Standard protein purification protocol relies on induced expression of a protein of interest through introduction of an inducing agent; forcing transcription and

translation of the inserted vector containing the gene of interest¹⁶². The translated protein usually includes an affinity tag that allows for isolation of the protein of interest from other expressed proteins¹⁶³. This affinity step may result in sufficient protein purity, or there may still be some contaminating proteins that one would try to remove using further purification efforts. These could include techniques such as an additional affinity chromatographic step, or other modes of chromatography. Alternative protein purification methods include anion exchange chromatography – a chromatographic technique used for the separation of proteins based on the charge they carry using a resin that contains positively charged groups, or size exclusion chromatography – a method used to separate proteins based on size.

2.4.1 Initial expression and purification of His-FRET-*HsPINK1*[70-134]

A standard protocol for the expression and purification of a FRET-tagged protein in the lab was followed. Human PINK1 had been cloned into the pBAD:FRET vector, a derivative of the pBAD vector (Invitrogen)¹⁴⁶. pBAD:His-FRET-*HsPINK1*[70-134] WT (His-FRET-*HsPINK1*[70-134] WT) was transformed into the Top10 *E. coli* cell line, which has a genotype to prevent arabinose catabolism. A single colony from a fresh transformation was used to inoculate 125 mL of LB + 100 µg/mL ampicillin for an overnight growth at 37 °C. The following day, 20 mL of the overnight culture was used to subinoculate 1 L of LB + 100 µg/mL ampicillin (x6), for a total culture volume of 6 L. These grew at 37 °C with shaking (180 RPM) until the optical density at 600 nm (OD₆₀₀) reached an optical density of 0.7. At this OD₆₀₀ the shaker

temperature was changed to 18 °C, and they were induced with 0.02% L-arabinose for an overnight induction period. At the end of the induction period the cells were harvested at 8000 $\times g$ for 20 minutes using the Avanti JLA8.1 rotor. Cell pellets were either stored at -20 °C or used immediately. Pellets were resuspended using a buffer containing 50 mM Tris-HCl pH 8.0, 150 mM NaCl, and 5% glycerol. The cellular suspension was then passed through the Emulsiflex C3 homogenizer three times for cell lysis in the presence of serine protease inhibitor, PMSF. Following lysis, the cell lysate was subjected to a slow centrifugation spin at 20 000 $\times g$ to pellet unbroken cells and cellular debris. Due to the two soluble fluorescent proteins flanked to both ends and the expansion of PINK1 boundaries beyond its transmembrane domain, His-FRET-*HsPINK1*[70-134] was soluble and present in the soluble supernatant fraction post-centrifugation. The supernatant was then incubated with Nickel-nitrilotriacetic acid (Ni-NTA) resin for 2 hours so that His-FRET-*HsPINK1*[70-134] would bind to the matrix. This protein-resin slurry was then passed through a gravity flow column where the resin packed at the bottom, allowing for the wash and subsequent elution of His-FRET-*HsPINK1*[70-134].

Presence of the YPet fluorescent protein on the C-terminal allows for a fluorescence visual of His-FRET-*HsPINK1*[70-134] under blue light. This is extremely convenient as it mimics the outcome of a Western blot, which utilizes antibodies, and fluorogenic visualization probes; indicative of exactly where His-FRET-*HsPINK1*[70-134] and any *HsPINK1*-YPet tagged derivatives are on a gel. This protocol resulted

in His-FRET-*HsPINK1*[70-134] expression, though the yield, evidence of proteolysis, and purity were evident obstacles to overcome.

2.4.2 Expression tests to optimize growth and induction conditions

Standard tests often utilized when expressing a new recombinant protein in *E. coli* are small-scale expression tests^{164,165}. This requires testing different parameters within the protein expression protocol. There are standard variables that are typically tested, including: cell line used, amount of induction agent used to induce protein expression, induction time, and induction temperature^{164,166}.

2.4.2.1 Cell lines tested for expression of His-FRET-*HsPINK1*[70-134]

A multitude of different cell lines were tested for the most optimal expression of His-FRET-*HsPINK1*[70-134]. Different cell lines tested varied slightly in their genotypes (**Table 2.5**). Variability in the genes present and expressed offers different advantages when navigating through the different *E. coli* strains for protein expression. **Table 2.5** outlines the different cell lines trialed throughout optimization of the expression procedure for His-FRET-*HsPINK1*[70-134] and their respective genotypes.

Small cultures of 5-6 mL were grown at 37 °C until the OD₆₀₀ was 0.7 and induced with 0.02% L-arabinose. The temperature was decreased to 24 °C for an 8 hour

Table 2.5. *Escherichia coli* cell lines used for optimization of His-FRET-*HsPINK1*[70-134] expression. Chromosomal genotype outlines the genetic differences between the cell lines.

| Cell line | Chromosomal Genotype | Source |
|----------------------|--|--|
| Top10 | <i>mcrA</i> , $\Delta(mrr-HsdRMS-mcrBC)$, <i>Phi80lacZ(del)M15</i> , $\Delta lacX74$, <i>deoR</i> , <i>recA1</i> , <i>araD139</i> , $\Delta(ara-leu)7697$, <i>galU</i> , <i>galK</i> , <i>rpsL(SmR)</i> , <i>endA1</i> , <i>nupG</i> | Invitrogen |
| C43(DE3) | F ⁻ <i>ompT gal dcm HsdS_B(r_B⁻ m_B⁻)</i> (DE3) | Openwetware |
| Rosetta(DE3) | F ⁻ <i>ompT HsdS_B(r_B⁻ m_B⁻) gal dcm</i> (DE3) pRARE (Cam ^R) | Millipore |
| Rosetta2 | F ⁻ <i>ompT HsdS_B(r_B⁻ m_B⁻) gal dcm</i> pRARE2 (Cam ^R) | Millipore |
| Rosetta2(DE3) | F ⁻ <i>ompT HsdS_B(r_B⁻ m_B⁻) gal dcm</i> (DE3) pRARE2 (Cam ^R) | Millipore |
| DH5 α | F ⁻ <i>endA1 glnV44 thi-1 recA1 relA1 gyrA96 deoR nupG purB20</i> $\phi 80dlacZ\Delta M15$ $\Delta(lacZYA-argF)U169$, <i>HsdR17(r_K⁻ m_K⁺)</i> , λ^- | Openwetware |
| BL21 | F ⁻ <i>ompT gal dcm lon HsdS_B(r_B⁻ m_B⁻)</i> [<i>malB</i> ⁺] _{K-12} (λ^S) | Openwetware |
| BL21(DE3) pLysS | F ⁻ <i>ompT gal dcm lon HsdS_B(r_B⁻ m_B⁻)</i> λ (DE3 [<i>lacI lacUV5-T7p07 ind1 sam7nin5</i>]) [<i>malB</i> ⁺] _{K-12} (λ^S) pLysS[T7p20 <i>ori_{p15A}</i>](Cm ^R) | Openwetware |
| BL21 pLemo | <i>fhuA2 [lon] ompT gal</i> (λ DE3) [<i>dcm</i>] Δ <i>HsdS</i> / pLemo(Cam ^R) λ DE3 = λ <i>sBamHlo</i> Δ <i>EcoRI-B int::(lacI::PlacUV5::T7 gene1) i21</i> Δ <i>nin5</i> pLemo = pACYC184- <i>PrhaBAD-lysY</i> | NEB |
| BL21(DE3) | F ⁻ <i>ompT gal dcm lon HsdS_B(r_B⁻ m_B⁻)</i> λ (DE3 [<i>lacI lacUV5-T7p07 ind1 sam7nin5</i>]) [<i>malB</i> ⁺] _{K-12} (λ^S) | Openwetware |
| K12 BW25113 glpG::Kn | <i>rnnB3</i> Δ <i>lacZ4787 HsdR514</i> Δ (<i>araBAD</i>)567 Δ (<i>rhaBAD</i>)568 <i>rph-1</i> | Baba <i>et al.</i> , 2006; Arutyunova <i>et al.</i> , 2014 |

induction. After 8 hours, cells were harvested and stored at -20 °C. The cells were thawed and lysed using a cell lysis buffer (50 mM Tris-HCl pH 8.0, 150 mM NaCl, 1% Triton X-100, 1 mM PMSF, 1 mM EDTA, 10 µg/mL DNase). The high concentration of Triton X-100 permeabilizes the *E. coli* cell membranes, thus lysing the cells. After lysis, cells were centrifuged at 15 000 x *g* for 30 min to remove unbroken cells, cellular debris, and inclusion bodies. Supernatant from centrifugation step was then subjected to SDS-PAGE electrophoresis and imaged under blue light to visualize His-FRET-*HsPINK1*[70-134]. Based on the signal observed for each lysate, cell lines expressing relatively high levels of His-FRET-*HsPINK1*[70-134] were identified (**Figure 2.4**).

2.4.2.2 Induction time and temperature study for His-FRET-*HsPINK1*[70-134] expression

Time and temperature are important variables to consider when optimizing the expression of a recombinant protein¹⁶⁶. A lower temperature results in slower protein production, this often means improved protein folding and stability. Lower temperatures result in decreased protein aggregation, which is typically favored at higher temperatures due to an established temperature dependence on hydrophobic interactions¹⁶⁷. In addition to this, temperature is known to have a substantial impact on cellular processes, proteins expressed, and activity of various proteins such as proteases and chaperones. Certain chaperones act exactly as such in low temperature conditions, but in high temperature they may behave as

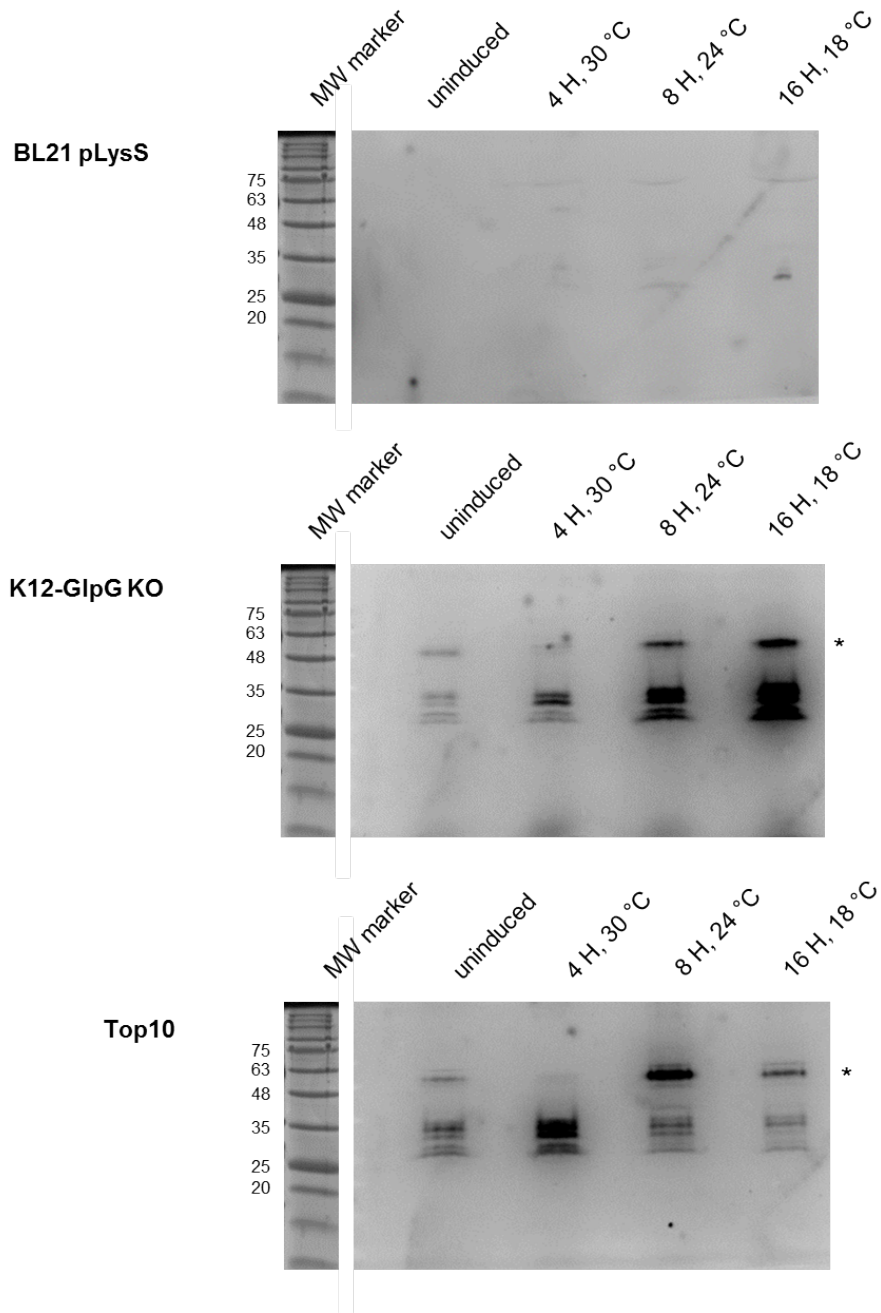


Figure 2.4. Relative expression of His-FRET-*HsPINK1*[70-134] WT in different *E. coli* cell lines. Fluorescence images of untreated cell lysates (soluble fraction) subjected to SDS-PAGE. Different induction conditions resulted in variable amount of proteolysis as demonstrated by the fluorescence images. Full-length His-FRET-*HsPINK1*[70-134] is 61.5 kDa and marked by the asterisks (*). H=hours.

proteases¹⁶⁸. Therefore, the balance between getting sufficient yield and mitigating effects that may be offset by the temperature is important during expression optimization. Time of induction is usually dependent on the temperature at which induction takes place. A higher induction temperature usually results in a lower expression time, and vice versa. **Figure 2.4** demonstrates optimal His-FRET-*HsPINK1*[70-134] expression in *E. coli* Top10 cells when induction is carried out for 8 hours at 24 °C.

2.4.2.3 Testing different concentrations of L-arabinose for induction of His-FRET-*HsPINK1*[70-134] expression

The pBAD vector contains the tightly regulated, arabinose-inducible araBAD promoter¹⁶⁹. Introduction of L-arabinose into a pBAD-transformed *E. coli* cell line induces protein expression, which can be modulated by a range of L-arabinose concentrations. In addition to the variation of temperature and time, the amount of inducing agent used to induce protein expression is often a simple variable to test. Lowering the concentration of the inducing agent may result in better-folded protein due to the reduced amount of translated protein. This effect is not always observed and is highly protein dependent. The amount of L-arabinose required to induce protein expression in the pBAD:FRET vector was previously optimized for the expression of His-FRET-*PsTatA*, and this convention was adapted for the expression of His-FRET-*HsPINK1*[70-134]¹⁴⁶. When optimizing parameters for the low expression of His-FRET-*HsPINK1*[70-134] R98W, a titration of L-arabinose

concentrations was tested. No variation from the 0.02% concentration of L-arabinose was noted to have a positive effect on protein production.

2.5 Lysing *E. coli* Top10 cells expressing His-FRET-HsPINK1[70-134]

Cell pellets were resuspended in 4:1 volume-to-pellet weight in resuspension buffer. Buffer composition is important because it will carry throughout the protein purification process and influences protein stability. Throughout various trials, the resuspension buffer composition changed. Varying amounts of NaCl and glycerol were used to determine the optimal concentration to minimize nonspecific interactions with contaminating proteins. The final resuspension buffer composition was 50 mM Tris-HCl pH 8.0, 500 mM NaCl, 20% glycerol, 1 mM PMSF supplemented with protease inhibitor tablets without EDTA. Upon complete resuspension of cells, cell suspension was passed through an Avestin Emulsiflex C3 homogenizer three times for cell lysis. After cell lysis, the lysate was subject to a detergent incubation prior to IMAC. Different detergents were tested: n-Dodecyl- β -D-maltoside (DDM), Triton X-100, and n-Octyl- β -D-glucopyranoside (OG). No discernable differences were noted between use of these three detergents between protein purifications, though a difference in purity was observed in the absence of a detergent incubation. Following detergent incubation, the “solubilized” cell lysate was subject to a centrifugation step at 20 000 x *g* before incubation with IMAC resin. This protocol later changed incorporation of the detergent incubation step to follow the

centrifugation to further mitigate interactions with contaminating proteins during purification.

2.6 Optimizing immobilized metal affinity chromatography (IMAC) parameters to increase His-FRET-*HsPINK1*[70-134] purity

Initially, the FRET-based substrate purification protocol called for a 2 hour incubation of the supernatant with Ni-NTA resin at 4 °C on a nutator. Batch resin was poured through gravity flow column, where the flowthrough was collected. The Ni-NTA resin was washed with 20 column-volumes (CV) buffer containing 20 mM imidazole, the column-eluting component of the buffer. His-FRET-*HsPINK1*[70-134] was eluted with a titration of imidazole in buffer ranging from 100 mM to 1 M in 1 CV aliquots. This resulted in a number of problems with the final protein product. In initial studies over 50% of the His-FRET-*HsPINK1*[70-134] expressed was found in the flow through, indicating the His-tagged PINK1 fusion protein was not binding to the resin, despite this relatively long incubation time. Additionally, His-FRET-*HsPINK1*[70-134] accounted for only about 10% of the total protein eluted from the Cobalt resin resulting in a low His-FRET-*HsPINK1*[70-134]-to-contaminant protein ratio. A final concern was a substantial amount of proteolysis observed; contributing to the low yield of purified His-FRET-*HsPINK1*[70-134]. Several steps were taken to mitigate these concerns. Cobalt resin has a lower binding capacity and higher specificity than Nickel resin¹⁷⁰, so a transition was made from Ni-NTA resin to HisPur Cobalt resin. In conjunction with this change, the site-directed mutagenesis

protocol, mentioned in Section 2.2.2, was used to elongate the histidine tag of His-FRET-*HsPINK1*[70-134] from a tag encoding for 6 histidines (6x) to 10 histidines (10x) to increase the affinity of the Co resin towards His-FRET-*HsPINK1*[70-134]. A forward primer (5' – gtt ctc atc atc atc atc atc atc atc atc atc atg gta tgg cta gca tga c – 3') and a reverse primer (5' – gtc atg cta gcc ata cca tga gaa c – 3') were designed using Agilent Technologies SDM primer design online tool. Successful elongation of the N-terminal located histidine tag and incubation with HisPur Co resin made an observable difference in the purity of His-FRET-*HsPINK1*[70-134], though there was still a notable degree of proteolysis. This observation resulted in the transition from batch purification in the original protocol to flow-through purification, where the resin was packed and equilibrated with buffer before introduction of the His-FRET-*HsPINK1*[70-134]-containing supernatant. This change led to a decrease in observable proteolysis. In addition to decreased proteolysis, the presence of co-purifying contaminants decreased by modifying the column wash protocol. Instead of adding a designated column volume wash of buffer, the optical density at 280 nm (OD_{280}) of the wash buffer flowing off the column was measured as an indication of contaminating protein elution. Once the OD_{280} was less than 0.1, the bound His-FRET-*HsPINK1*[70-134] can be eluted off the column (**Figure 2.5**). Elutions containing the greatest amount of His-FRET-*HsPINK1*[70-134] were pooled and then subjected to further purification.

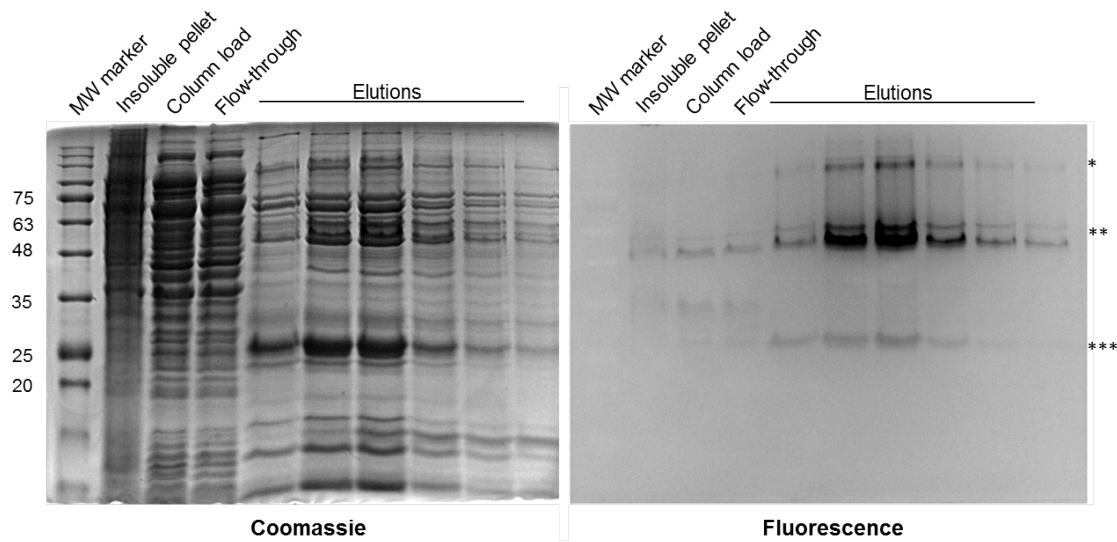


Figure 2.5. 14% SDS-PAGE gel for immobilized metal affinity chromatography purification of His-FRET-*HsPINK1*[70-134] WT using Cobalt resin. Full-length His-FRET-*HsPINK1*[70-134] is 61.5 kDa but appears as a doublet when subject to SDS-PAGE without heat treatment (Required to maintain YPet fluorophore structural integrity). * = Speculated His-FRET-*HsPINK1*[70-134] dimer; ** = Full-length His-FRET-*HsPINK1*[70-134]; *** = Free YPet.

2.7 Size exclusion chromatography of His-FRET-*HsPINK1*[70-134] as a final purification step

Following IMAC purification, an additional chromatography step was included to the His-FRET-*HsPINK1*[70-134] purification protocol. Eluted protein was immediately concentrated to 2-3 mL. This protein was then loaded onto a Superdex 200 10/300 GL column and run at 0.2 mL/min. The buffer used for this column was composed of 50 mM Tris-HCl pH 8.0, 300 mM NaCl, 5% glycerol, 0.05% DDM, 1mM TCEP. The gel filtration chromatogram for each PD-linked variant of His-FRET-*HsPINK1*[70-134] followed the same trend. His-FRET-*HsPINK1*[70-134] began to elute around 8.5 mL, as demonstrated in **Figure 2.6**. The elution of His-FRET-*HsPINK1*[70-134] at 8.5 mL has been confirmed by SDS-PAGE fluorescent gel analysis (**Figure 2.7**). Following gel filtration, fractions containing His-FRET-*HsPINK1*[70-134] were pooled together and concentrated no more than 12 times to stay below the critical micelle concentration (CMC) of DDM to prevent protein aggregation. After concentration to approximately 1 mg/mL, His-FRET-*HsPINK1*[70-134] was distributed in small aliquots and flash frozen to be stored at -80 °C.

2.8 Expression and purification of His-FRET-*HsPINK1*[70-134] PD-linked variants

The protocol established for the expression and purification of His-FRET-*HsPINK1*[70-134] WT was followed for all PD-linked variants of focus in this thesis.

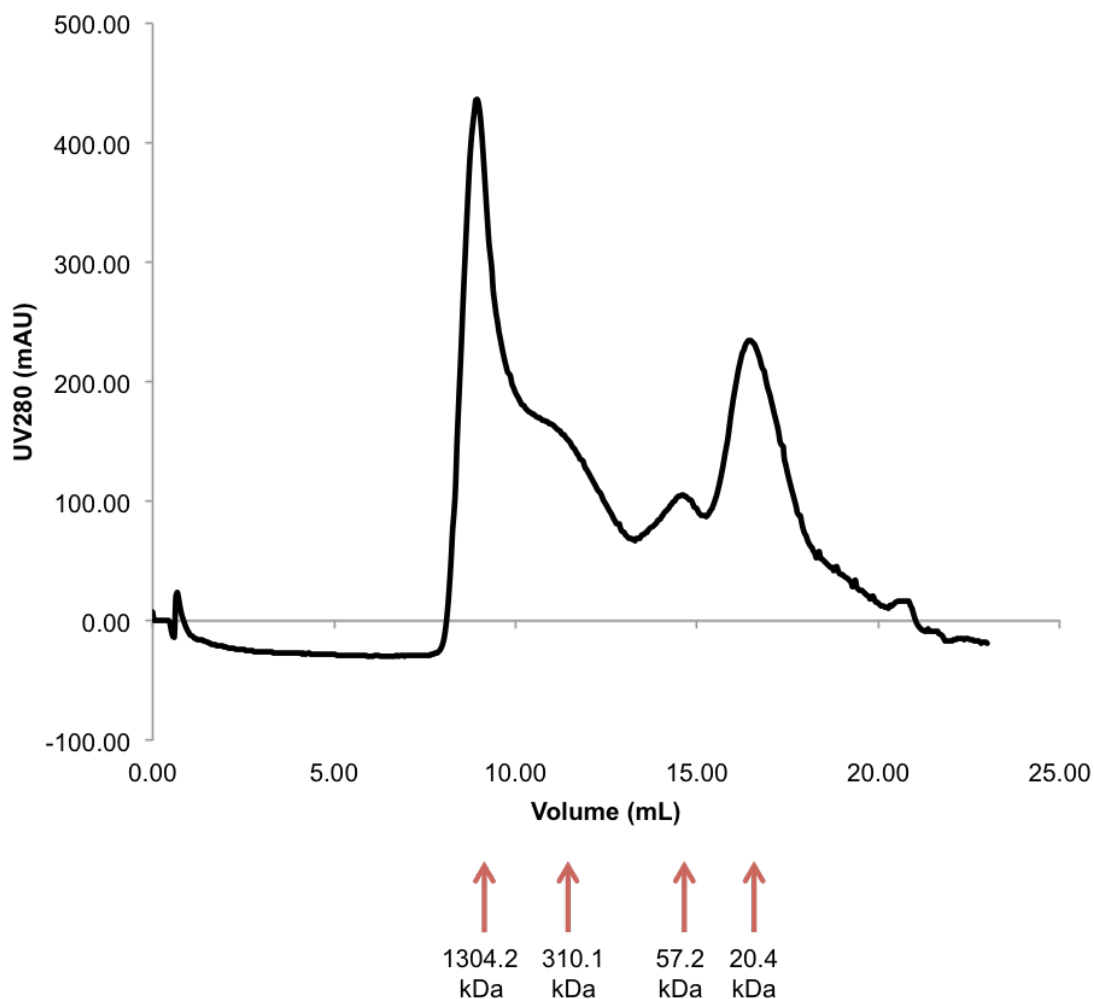


Figure 2.6. Size exclusion chromatogram of His-FRET-*HsPINK1*[70-134] WT. The final size exclusion column serves as both an additional purification step as well as a quality control step. His-FRET-*HsPINK1*[70-134] begins to elute around 7.5 mL in what appears to become a skewed bimodal distribution. First elution peak resides in the void volume, so likely this first population containing His-FRET-*HsPINK1*[70-134] is the result of protein aggregates. The second, broader distribution elutes stable His-FRET-*HsPINK1*[70-134].

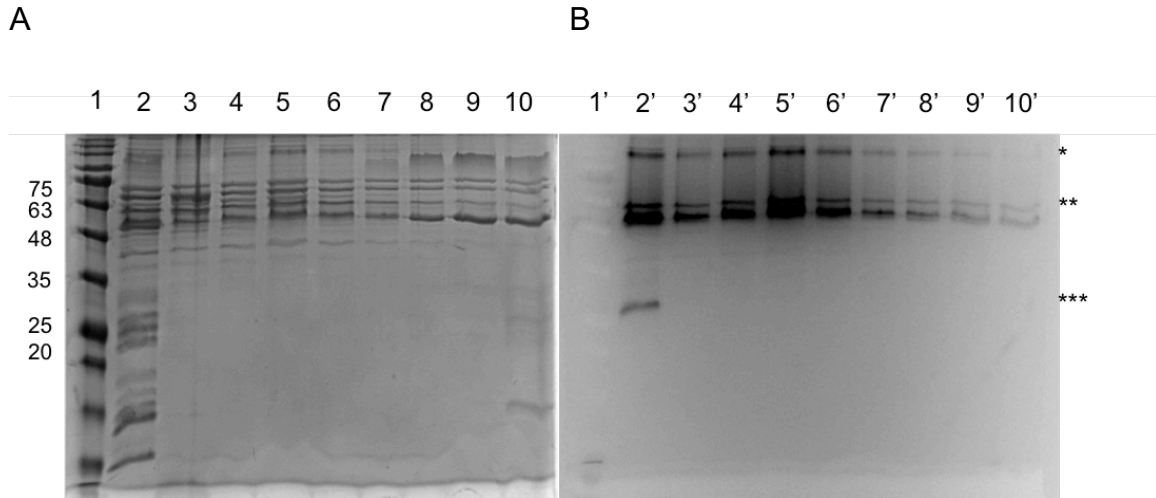


Figure 2.7. SDS-PAGE gel for SEC column elution fractions. Full-length His-FRET-*HsPINK1*[70-134] is 61.5 kDa but appears as a doublet when subject to SDS-PAGE without heat treatment. (A) Coomassie-stained gel. 1 = molecular weight marker (kDa); 2 = column load; 3-10, fractions A4, A6, A8, A10, A12, B11, B9, and B7, that correspond to 0.5 mL elutions from 10 to 12.5 mL on the column respectively. (B) Fluorescence gel. 1'-10' of the Fluorescence-imaged gel correspond respectively to 1-10 on the Coomassie-stained gel. * = Speculated His-FRET-*HsPINK1*[70-134] dimer; ** = Full-length His-FRET-*HsPINK1*[70-134]; *** = Free YPet.

Expression and purification of His-FRET-*HsPINK1*[70-134] R98W was unsuccessful, despite efforts to optimize expressed levels of protein, His-FRET-*HsPINK1*[70-134] R98W consistently demonstrated toxicity to all cell lines tested. In addition to observed toxicity to *E. coli*, the poorly expressed His-FRET-*HsPINK1*[70-134] R98W was extremely susceptible to proteolysis. Together, this suggests that this variant in particular is unstable when expressed in the pBAD:FRET vector. With exception of R98W, all variants of human PINK1 were successfully expressed and isolated to sufficient yield and purity for use in our FRET-based *in vitro* kinetic assay.

On gel, His-FRET-*HsPINK1*[70-134] appears as a doublet. To ensure that there was not two species of His-FRET-*HsPINK1*[70-134] being purified, the samples were subject to a brief incubation at 60 and 100 °C. A brief 60 °C incubation resulted in the doublet merging into a single band (**Figure 2.8**).

2.8.1 Expression and purification of His-FRET-*HsPINK1*[70-134] C92F

His-FRET-*HsPINK1*[70-134] C92F was expressed in a 12 L *E. coli* Top10 cell culture. After growth at 37 °C, at OD₆₀₀ of 0.7 cells were induced with 0.02% L-arabinose. The induction temperature was 24 °C and after 8 hours the cells were harvested and stored at -80 °C until subsequent use for purification. Purification of His-FRET-*HsPINK1*[70-134] C92F followed the standard protocol established for the wild-type. Protein expressed and purified was comparable in yield and purity to His-FRET-*HsPINK1*[70-134] WT (**Figure 2.9**).

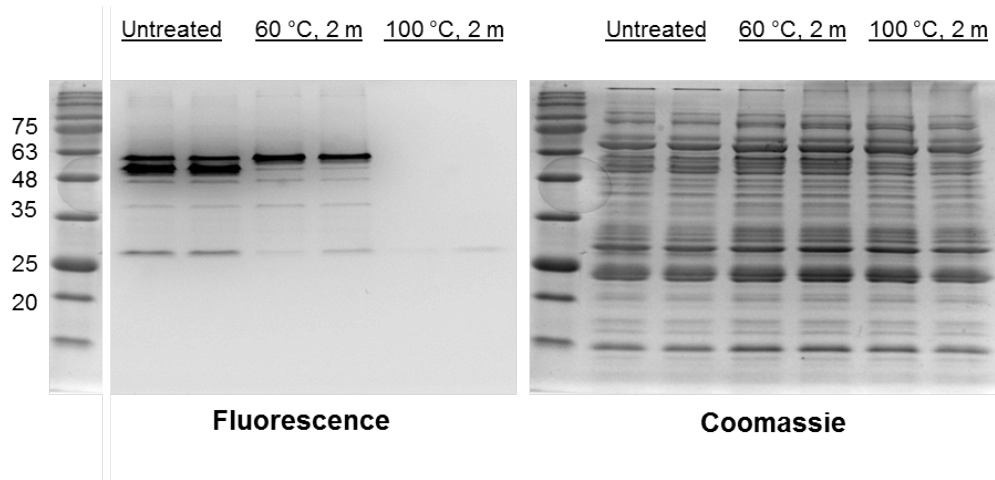


Figure 2.8. Incubation of His-FRET-*HsPINK1*[70-134] at 60 °C demonstrates recombinant PINK1 exists as a single species.

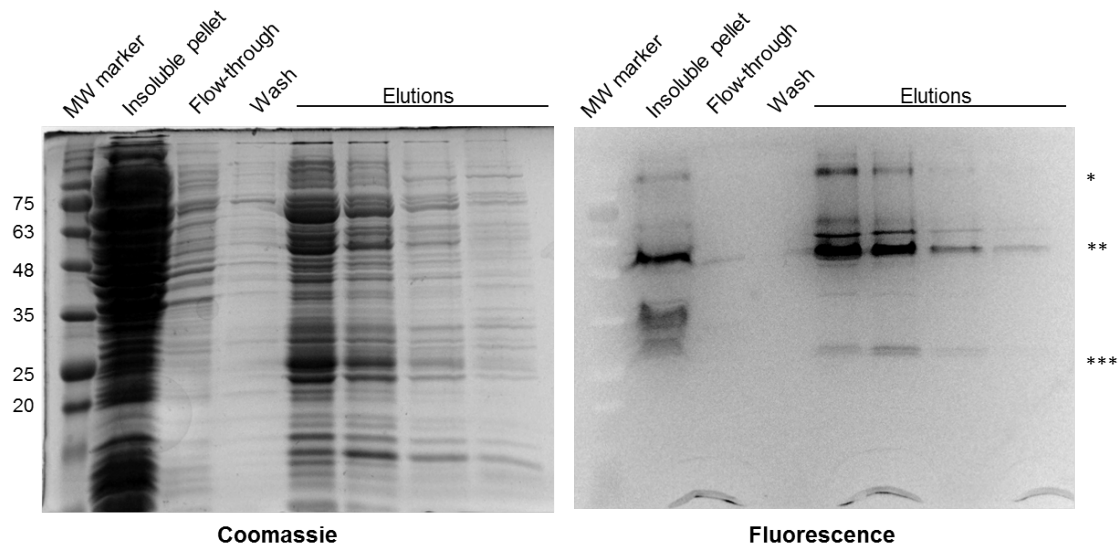


Figure 2.9. 14% SDS-PAGE gel for purification of His-FRET-*HsPINK1*[70-134] C92F. Full-length His-FRET-*HsPINK1*[70-134] is 61.5 kDa but appears as a doublet when subject to SDS-PAGE without heat treatment. * = Speculated His-FRET-*HsPINK1*[70-134] dimer; ** = Full-length His-FRET-*HsPINK1*[70-134]; *** = Free YPet.

2.8.3 Expression and purification of His-FRET-*HsPINK1*[70-134] R98W

Several conditions of growth were tested to determine optimal expression conditions for this particular variant. Following the same protocol established for the expression and purification of His-FRET-*HsPINK1*[70-134] WT, R98W did not have comparable expression. As seen in **Figure 2.10** there was an extremely low detection of protein purified from a 12 L Top10 *E. coli* culture. Upon concentration and size exclusion chromatography of this variant, the protein is extremely diluted in the column buffer resulting in a low detection of protein when subject to SDS-PAGE. The primary cause of the low His-FRET-*HsPINK1*[70-134] R98W yield was the low expression in the *E. coli* culture. As mentioned previously, several parameters play a role in protein expression. Varying amounts of L-arabinose, different cell lines, and several induction conditions were tested on a small-scale to determine optimal growth and induction conditions for this particular variant. As seen in **Figure 2.11** His-FRET-*HsPINK1*[70-134] R98W expressed best when cells were induced with 0.02% L-arabinose. Moving forward, subsequent His-FRET-*HsPINK1*[70-134] R98W expression tests were done using this concentration of arabinose. Next, induction conditions were tested in *E. coli* Top10 cells. This test determined that His-FRET-*HsPINK1*[70-134] R98W expressed best at 24 °C for 8 hours (**Figure 2.12**). Several cell lines were utilized to identify a strain of *E. coli* that expressed an adequate or WT-comparable amount of the R98W variant (**Table 2.5**). An initial screen resulted in three potential high His-FRET-*HsPINK1*[70-134] R98W expressing cell lines: DH5 α , C43, and C43(DE3) (**Figure 2.13**). Upon further

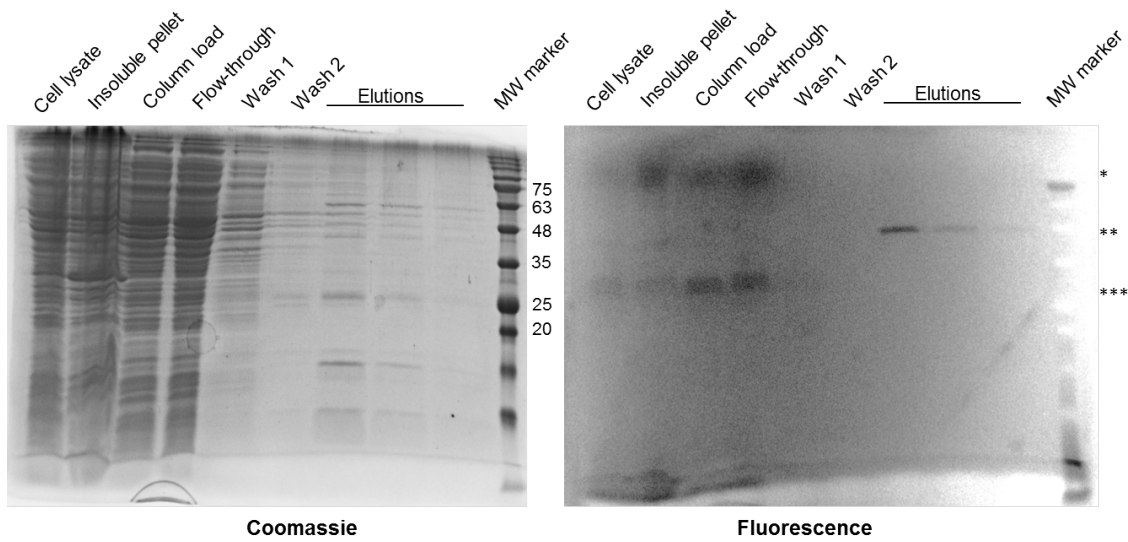


Figure 2.10. 14% SDS-PAGE gel for purification of His-FRET-*HsPINK1*[70-134] R98W. Full-length His-FRET-*HsPINK1*[70-134] is 61.5 kDa but appears as a doublet when subject to SDS-PAGE without heat treatment. * = Full-length His-FRET-*HsPINK1*[70-134]; ** = Full-length His-FRET-*HsPINK1*[70-134]; *** = Free YPet.

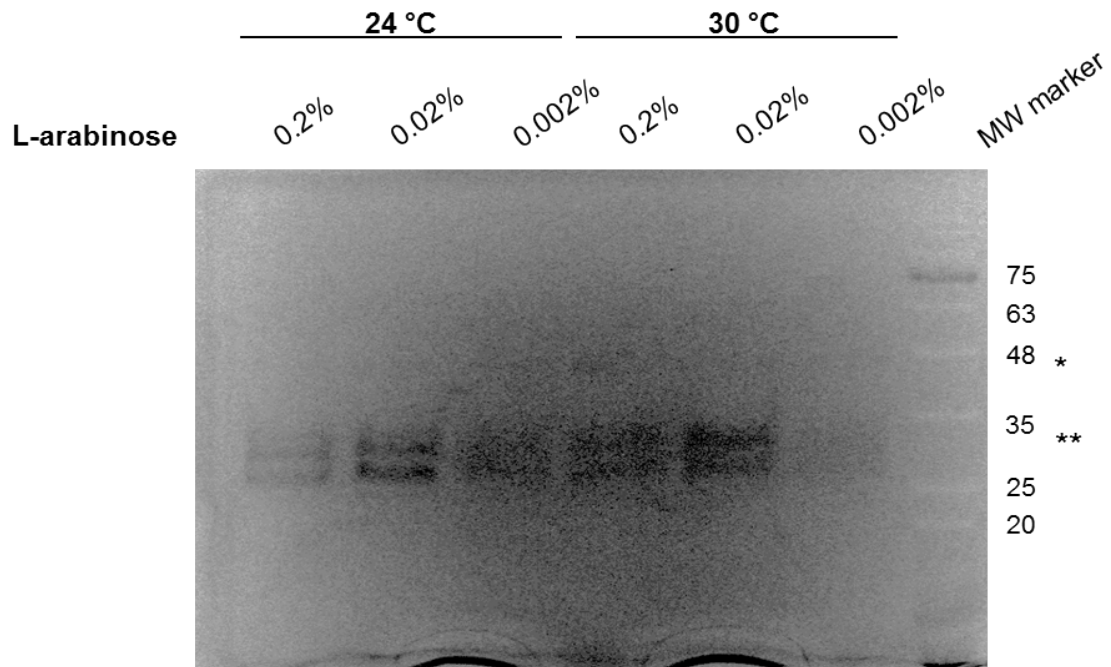


Figure 2.11. Induction screen for expression of His-FRET-*HsPINK1*[70-134] R98W in small-scale *E. coli* culture. Varying amounts of L-arabinose were assessed for optimal protein expression in liquid LB culture at two temperatures (24 and 30 °C) for 8 hours. * = Full-length His-FRET-*HsPINK1*[70-134], ** = partially proteolysed His-FRET-*HsPINK1*[70-134]

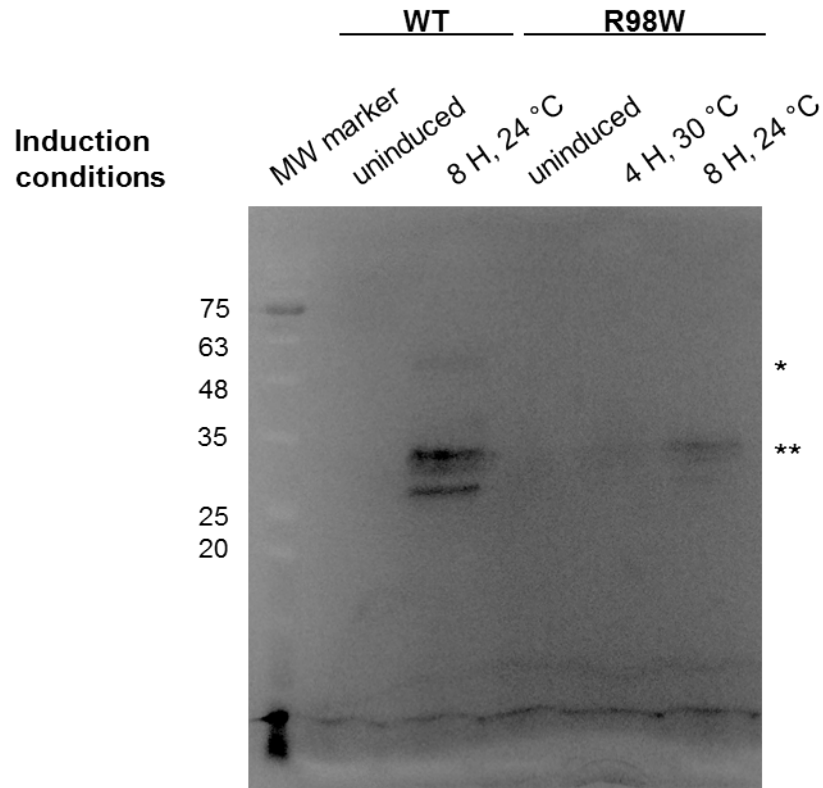


Figure 2.12. Induction screen for expression of His-FRET-*HsPINK1*[70-134] R98W in small-scale *E. coli* culture. Varying amounts of L-arabinose were assessed for optimal protein expression in liquid LB culture at two temperatures (24 and 30 °C) with a wild-type control. * = Full-length His-FRET-*HsPINK1*[70-134], ** = partially proteolysed His-FRET-*HsPINK1*[70-134]

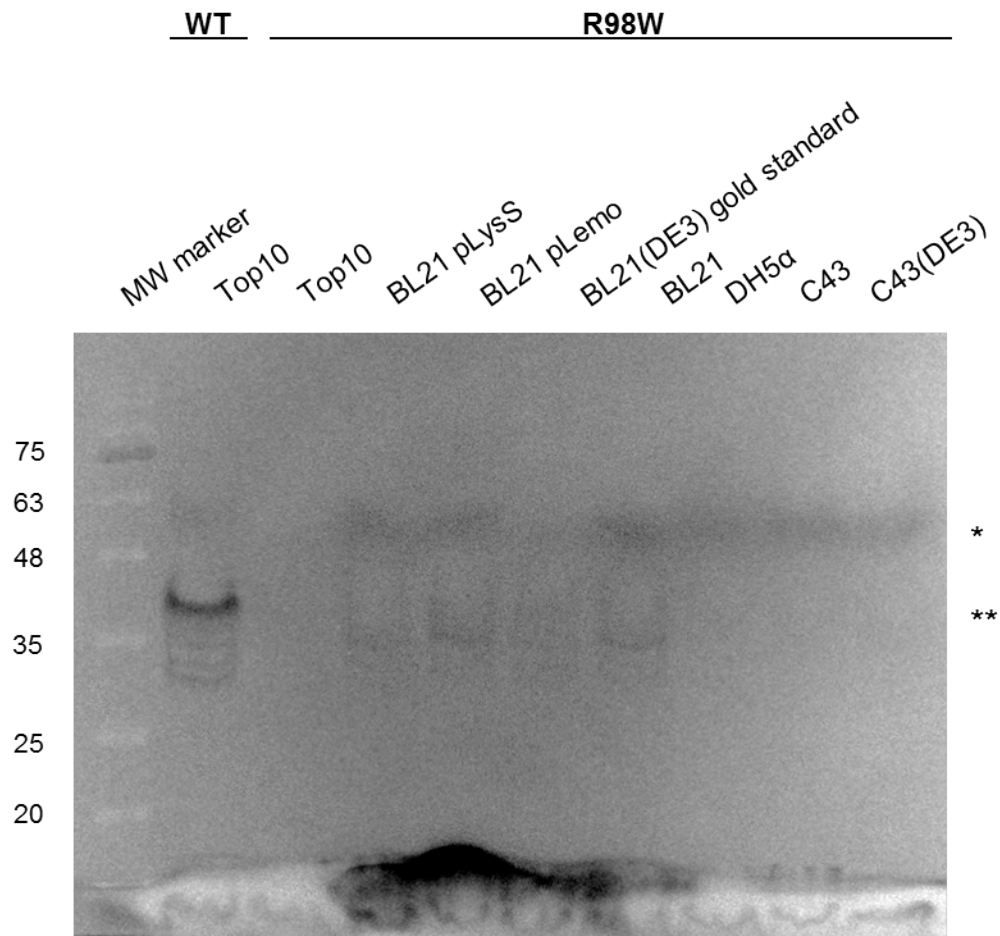


Figure 2.13. Induction screen for expression of His-FRET-*HsPINK1*[70-134] R98W in small-scale *E. coli* culture. Different cell lines were assessed for optimal protein expression in liquid LB culture at 24 °C for a total induction period of 6 hours. His-FRET-*HsPINK1*[70-134] WT was expressed in Top10 cells as a positive control. * = Full-length His-FRET-*HsPINK1*[70-134], ** = partially proteolysed His-FRET-*HsPINK1*[70-134]

investigation, these initial results appeared to be false positives (**Figure 2.14**). From these tests and subsequent large-scale expression of His-FRET-*HsPINK1*[70-134] R98W was underwhelming in comparison to WT and other variants. Additionally, the extensive protocol for purification which results in low protein yield retention contributed to the inability to successfully produce and purify this variant.

2.8.4 Expression and purification of His-FRET-*HsPINK1*[70-134] I111S

For the expression of His-FRET-*HsPINK1*[70-134] I111S a 12 L culture of *E. coli* Top10 cells was induced with 0.02% L-arabinose at an OD₆₀₀ of 0.7. Cells were induced for 8 hours at 24 °C. At the end of this period, cells were harvested and stored at -80 °C. Similarly, the expression parameters, protein purification followed the same protocol established for that of the wild-type. His-FRET-*HsPINK1*[70-134] was successfully expressed and purified, resulting in comparable product to His-FRET-*HsPINK1*[70-134] WT for use in the *in vitro* kinetic assay (**Figure 2.15**).

2.8.5 Expression and purification of His-FRET-*HsPINK1*[70-134] Q126P

The His-FRET-*HsPINK1*[70-134] Q126P variant was successfully expressed in *E. coli* Top10 cells following the protocol established for the wild-type counterpart: 12 L culture growth until OD₆₀₀ reached 0.7 for a subsequent 8 hour induction of protein expression at 24 °C. Q126P demonstrated comparable expression to His-FRET-

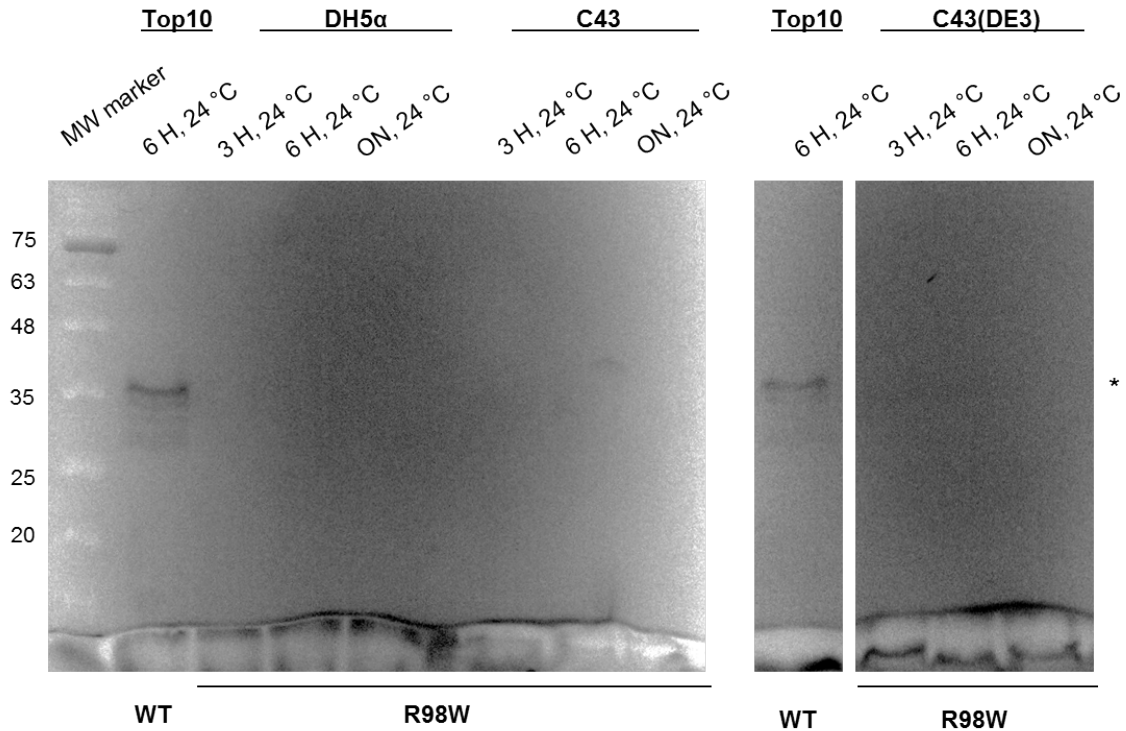


Figure 2.14. Induction screen for expression of His-FRET-*HsPINK1*[70-134] R98W in small-scale *E. coli* culture. Previously identified potentially high expressing His-FRET-*HsPINK1*[70-134] R98W cell lines (DH5 α , C43, and C43(DE3)) were assessed for optimal protein expression in liquid LB culture at 24 °C. His-FRET-*HsPINK1*[70-134] WT was expressed in Top10 cells as a positive control. * = partially proteolysed His-FRET-*HsPINK1*[70-134]

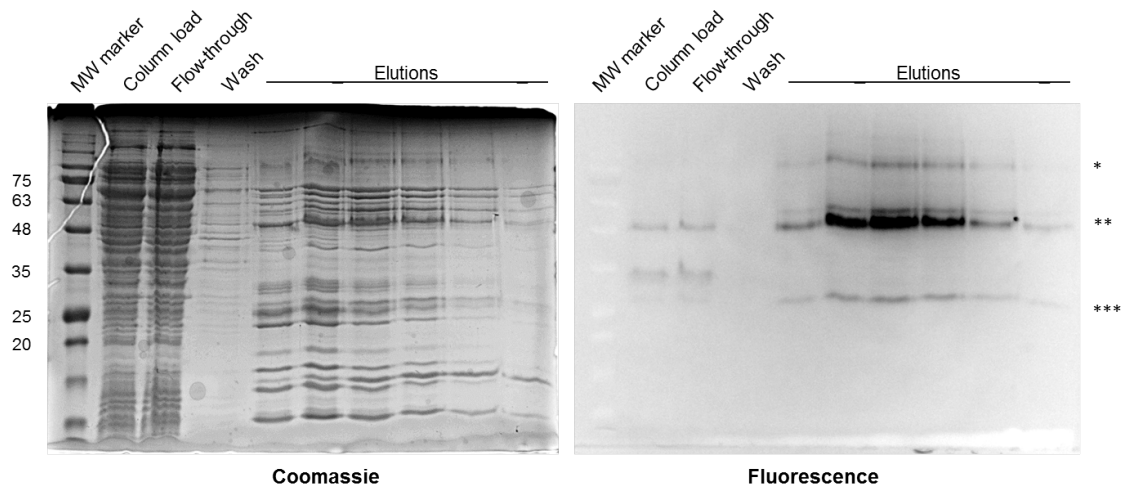


Figure 2.15. 14% SDS-PAGE gel for purification of His-FRET-*HsPINK1*[70-134] I111S. Full-length His-FRET-*HsPINK1*[70-134] is 61.5 kDa but appears as a doublet when subject to SDS-PAGE without heat treatment. * = Speculated His-FRET-*HsPINK1*[70-134] dimer; ** = Full-length His-FRET-*HsPINK1*[70-134]; *** = Free YPet.

HsPINK1[70-134] WT and subsequent purification steps resulted in comparable purity of the product (**Figure 2.16**).

2.9 Discussion

Human PINK1 variants C92F, R98W, I111S, and Q126P were all successfully cloned into the pBAD:FRET vector using traditional cloning methods and site-directed mutagenesis. Additionally, a protocol for the expression and purification of His-FRET-*HsPINK1*[70-134] was successfully developed. A high purity of His-FRET-*HsPINK1*[70-134] was obtained through immobilized metal affinity chromatography using HisPur Cobalt resin immediately followed by a gel filtration step using the Superdex200 30/100 GL column (**Figure 2.17**).

As mentioned throughout the chapter, there were multiple areas that required attention for optimization. After multiple expression trials, an 8 hour induction with 0.02% L-arabinose at 24 °C demonstrated the highest yield of His-FRET-*HsPINK1*[70-134]. It is not atypical to start the induction of low expressing proteins at higher OD₆₀₀, around 1.0. Though for His-FRET-*HsPINK1*[70-134], when induced at an OD₆₀₀ greater than 1.0, there was an observed decrease in the protein produced by the Top10 *E. coli* cells, so cells were consistently induced at an OD₆₀₀ of 0.7.

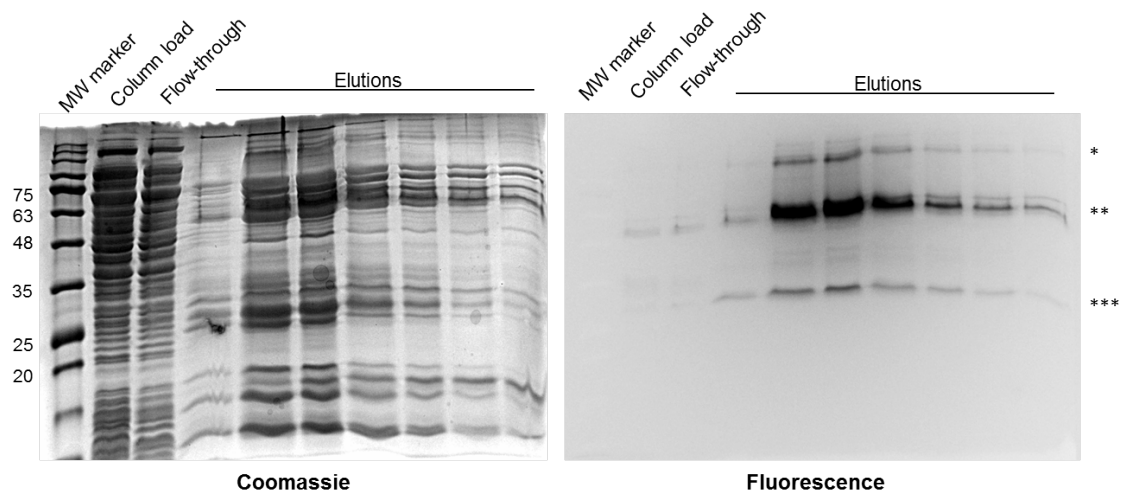


Figure 2.16. 14% SDS-PAGE gel for purification of His-FRET-*HsPINK1*[70-134] Q126P. Full-length His-FRET-*HsPINK1*[70-134] is 61.5 kDa but appears as a doublet when subject to SDS-PAGE without heat treatment. * = Speculated His-FRET-*HsPINK1*[70-134] dimer; ** = Full-length His-FRET-*HsPINK1*[70-134]; *** = Free YPet.

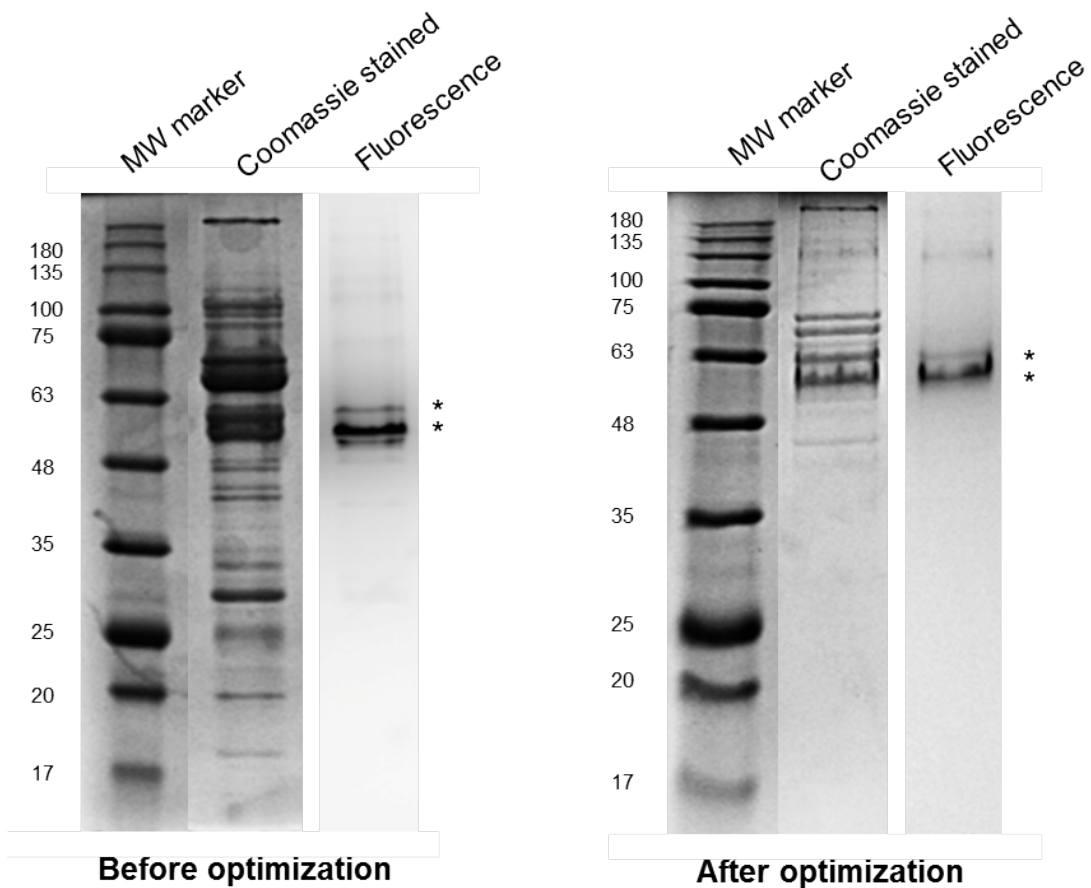


Figure 2.17. SDS-PAGE gels of His-FRET-*HsPINK1*[70-134] before and after optimization. Comparison of His-FRET-*HsPINK1*[70-134] purity post-size exclusion chromatography highlights the progression made with regards to protein purity. 1 = molecular weight marker (kDa); 2 = Coomassie-stained gel of purified His-FRET-*HsPINK1*[70-134]; 3 = Fluorescence gel of purified His-FRET-*HsPINK1*[70-134]; * = His-FRET-*HsPINK1*[70-134] appears as a doublet when subject to SDS-PAGE electrophoresis.

A multitude of different cell lines were tested for the optimization of His-FRET-*HsPINK1*[70-134] expression. As outlined in **Table 2.5**, some cell lines varied greater from the rest encoding for certain factors including phage resistance and protease deficiencies. Top10 is a standard *E. coli* strain typically used for plasmid purification, though it is sometimes utilized in protein expression, especially when using the pBAD vector. It is not deficient in any proteases, nor does it confer any phage resistance. The *E. coli* BL21 cell line is deficient in two proteases: Lon protease, a cytosolic protease, and OmpT, an outer membrane protease. This deficiency was thought to have made a difference in the proteolysis observed during protein expression and purification, though no comparable difference was seen when compared to the Top10 control. BL21(DE3), BL21(DE3) pLemo, BL21(DE3) pLysS, and Rosetta(DE3) cell lines were also tested. A main factor in each of these cell lines is the presence of the λ DE3 lysogen, which carries a gene for T7 RNA polymerase. This is not beneficial or useful for expression of proteins under control of the Ara promoter, as such in the pBAD vector. Not surprisingly, there was no enhancement in protein expression with use of these cell lines. Derived from the BL21 strain, the *E. coli* Rosetta cell line includes a pRARE plasmid. This vector supplies tRNAs for “rare” eukaryotic codons: AGG AGA AUA CUA CCC GGA; encoding for arginine, isoleucine, and leucine. Despite this seemingly advantageous cell line for expression of our human PINK1 construct, it appeared the yield of protein expressed was lower than our Top10 standard/control. Similar to Top10 cells, DH5 α cells are optimized for use to purify plasmids. These have been used in the lab to express MBP-tagged *HsPINK1*, so the rationale was that it might be able to

express the His-FRET-*HsPINK1*[70-134] construct. MBP-*HsPINK1*[70-134] was expressed via the pMAL vector, which contains a T7 inducible promoter. This may account for the difference in success between the two PINK1 constructs expressing the same 70-134 boundaries of PINK1. Despite these differences amongst the *E. coli* cell lines there wasn't a significant difference or expression enhancement amongst the different cell types in the yield of His-FRET-*HsPINK1*[70-134], though there was less proteolysis observed and less contaminating proteins expressed by Top10 *E. coli* cells in cellular lysates.

With a low amount of about 1 mg His-FRET-*HsPINK1*[70-134] produced by a 6 L *E. coli* Top10 culture, subsequent steps had to be scrutinized to protect and maintain the integrity of the protein expressed. The protein purification buffers used in the original protocol adapted in the lab composed of only 150 mM NaCl and 5% glycerol. The main reason for this was to keep buffer component concentrations, particularly the salt concentration; similar to what would be found physiologically. To increase stability and simultaneously decrease non-specific interactions with other proteins, both the salt and glycerol concentrations were increased. The established protocol now uses a buffer that contains 500 mM NaCl and 20% glycerol to disrupt any electrostatic interactions and non-specific hydrophobic reactions, respectively, between His-FRET-*HsPINK1*[70-134] and other proteins. As anticipated, the increase of both these entities appeared to improve the purity of the resulting protein product.

Detergent has an important role in protein biochemistry, especially in protein purification. As previously mentioned, three detergents were trialed for efficacy in isolation and purification of His-FRET-*HsPINK1*[70-134]: DDM, TX, and OG. These are all classified as non-ionic detergents but differ slightly. OG belongs to the glucoside family of detergents, whereas DDM is a maltoside derivative. Triton X-100 varies in the number of repeating ethoxy (oxy-1,2-ethanediyl) groups, with an average number of 9.5, classifying it as a polyoxyethylene. The structures of these detergents are found in **Figure 2.18**. DDM is a mild detergent often used for membrane protein purification. Despite differences in these non-ionic detergents, there was no observable difference in purified protein yield between these three. Though incorporation of a detergent solubilization step, regardless of the detergent, resulted in a purer His-FRET-*HsPINK1*[70-134] product.

When subject to SDS-PAGE electrophoresis, His-FRET-*HsPINK1*[70-134] appears as a doublet. SDS-PAGE is a method that allows sample separation based on charge attributed to SDS-association. Addition of SDS, an anionic detergent and main component of SDS-PAGE sample buffer, results in the denaturation of the protein. Protein denaturation disrupts the secondary and tertiary structures of proteins, reducing them to an unfolded, linear form. Typically, a boiling step is included before loading the samples onto a gel to ensure complete protein denaturation. Disruption of secondary structure of the fluorescent proteins results in the inability to observe His-FRET-*HsPINK1*[70-134] under blue light. For this reason, samples were not boiled prior to electrophoresis. As a result, some molecules of His-FRET-

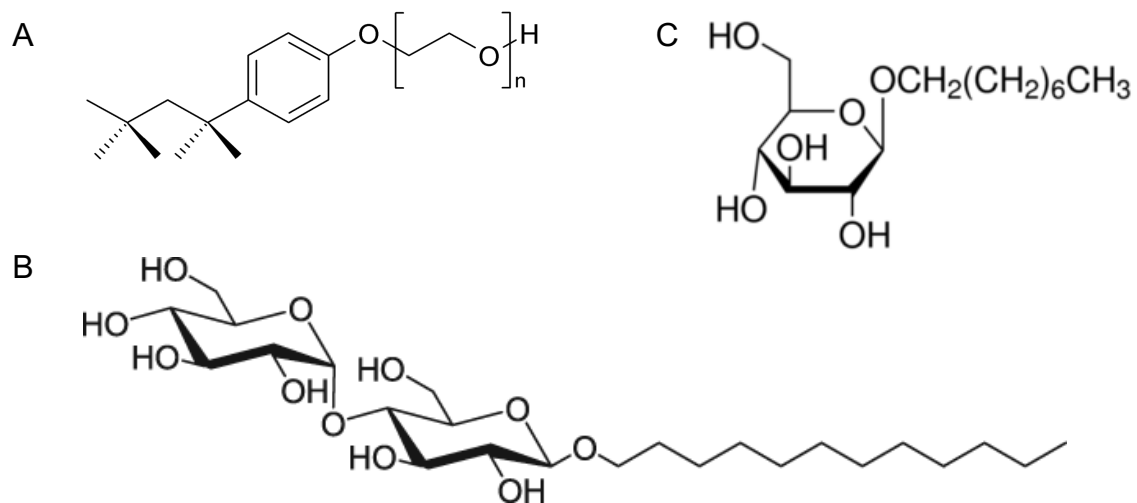


Figure 2.18. Popular detergents used in membrane protein purification. Molecular structures of (A) Triton X-100, (B) DDM, and (C) OG.

HsPINK1[70-134] are not completely denatured; resulting in the appearance of two species of partially unfolded and completely unfolded His-FRET-*HsPINK1*[70-134]. To confirm this, a brief incubation of the protein sample at either 60 °C or 100 °C was done before electrophoresis. The fluorescence-imaged gel shows the His-FRET-*HsPINK1*[70-134] doublet merges into a single band with the 60 °C incubation. A quick incubation at 100 °C results in a similar phenomenon, though this is not observed in the fluorescence gel due to denaturation of the YPet fluorescent protein.

All variants of human PINK1, with the exception of R98W, were successfully expressed and isolated to sufficient yield and purity for use in out FRET-based *in vitro* kinetic assay using this adapted protocol (**Figure 2.19**). **Figure 2.20** demonstrates comparable protein purification quality following the final size exclusion step. Arguably the most interesting mutation in the transmembrane domain, Chapter 4 will outline a strategy to assess the effect of the R98W variant on PARL-mediated cleavage, overcoming the inability to produce sufficient His-FRET-*HsPINK1*[70-134] R98W.

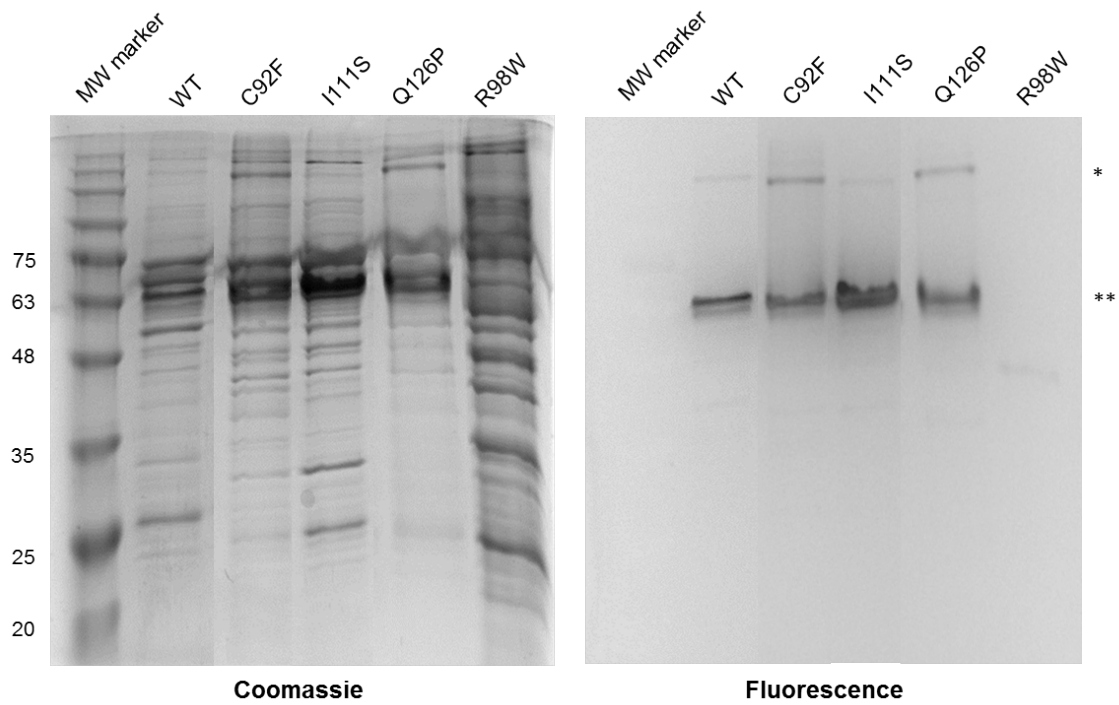


Figure 2.19. 14% SDS-PAGE gel of final purified His-FRET-*HsPINK1*[70-134] variants. Full-length His-FRET-*HsPINK1*[70-134] is 61.5 kDa. * = Speculated His-FRET-*HsPINK1*[70-134] dimer; ** = Full-length His-FRET-*HsPINK1*[70-134]

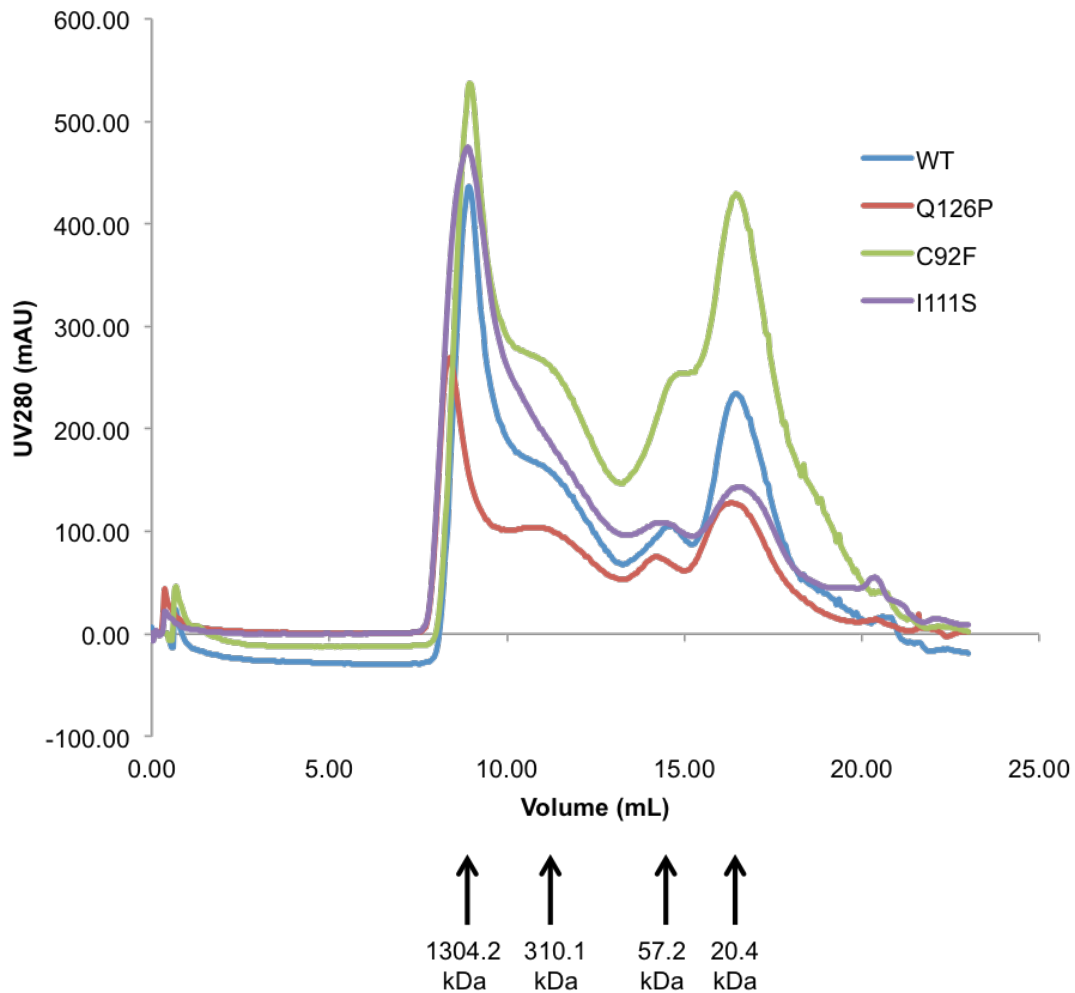


Figure 2.20. Superimposed size exclusion chromatograms of His-FRET-*HsPINK1*[70-134] WT, C92F, I111S, and Q126P. In addition to its main purpose as a purification step, size exclusion chromatography serves as a quality control step to ensure consistency between protein preparations across all variants. First elution peak resides in the void volume. Second, broader peak elutes stable His-FRET-*HsPINK1*[70-134]. Fractions A4, A6, A8, A10, A12, B11, B9, and B7 containing elutions between 10 and 12.5 mL from a wild-type purification are imaged on an SDS-PAGE gel in Figure 2.7.

CHAPTER 3: Expression and purification of human PARL protease

3 Expression and purification of GFP-*Hs*PARL protease

3.1 Introduction

The PARL protease, as introduced above is an intramembrane rhomboid protease found in the inner mitochondrial membrane. PARL is known as the mitochondrial rhomboid, though its name is kept from its historical roots, stemming from its original identification in a screen aiming to identify interacting partners of Presenilin 1 and Presenilin 2^{108,171}. Rhomboid proteases are a highly conserved family of serine proteases that hydrolyze peptide bonds of both soluble and transmembrane substrates^{172,173}. A catalytic serine found on transmembrane helix 4 (TMH4), highly conserved amongst rhomboids, is hydrogen bonded to the catalytic histidine found on transmembrane helix 6 (TMH6) of PARL. Together, these residues form the catalytic dyad responsible for the peptide bond hydrolysis mediated by the mitochondrial rhomboid protease.

Similarly to PINK1, human PARL protease has never been recombinantly expressed and purified. As an intramembrane protein, the expression and purification of PARL protease needs to be optimized before a protocol can be established. In contrast to the expression of His-FRET-*Hs*PINK1[70-134] in *E. coli*, PARL protease is expressed in *Pichia pastoris* cells. As previously mentioned, to assess the effect of PD-linked mutations on PARL protease-mediated processing, a FRET-based assay has been adapted. In addition to purified substrate, recombinant protease is required in

milligram amounts. To do so, a His-GFP-PARL protease fusion is expressed in *P. pastoris*. Following expression, His-GFP-PARL protease is purified based on an established protocol in the Lemieux lab. Following this initial purification, the His-GFP-PARL protease fusion is incubated with TEV protease for cleavage at a TEV cleavage site located between GFP and PARL allowing for the isolation of pure, untagged PARL protease.

3.2 Screen for high GFP-PARL expressing *P. pastoris* GS115 colonies

In order to obtain a sufficient yield of recombinant protein in *P. pastoris*, the Lemieux lab has developed a screen to identify high expressers of the protein of interest¹⁴¹. This has been adapted below for the human rhomboid protease, PARL.

3.2.1 Transformation of *P. pastoris* GS115

3.2.1.1 Linearizing pPICZ α plasmid DNA for *P. pastoris* transformation

Double-stranded DNA was purified using a Mini Prep kit from Geneaid. 5 μ g of purified dsDNA was then digested using *MssI*. A sample of the digested dsDNA was subject to a 0.5% agarose gel to confirm successful linearization. Linearized dsDNA was purified by adding 1/10th volume of 3 M NaOAc and thoroughly mixed. Three times the volume of 95% ethanol was added and mixed, causing the DNA to precipitate. Precipitated dsDNA was harvested by centrifugation at 21 000 $\times g$ for 5

minutes at room temperature. Supernatant was decanted, and dsDNA was washed with 200 μ L 70% ethanol. dsDNA was then subject to another round of centrifugation at 21 000 $\times g$ for 3 minutes at room temperature. Again, supernatant was decanted and the Eppendorf tube was left open on its side and incubated at room temperature for 5 minutes to allow residual ethanol to evaporate. dsDNA, clear and gelatinous in appearance, was resuspended in sterile ddH₂O, resulting in successfully double-digested and purified linear dsDNA. DNA concentration was determined using a ThermoFisher NanoDrop.

3.2.1.2 Preparation of electrocompetent *P. pastoris* GS115 cells

A glycerol stock of *P. pastoris* GS115 WT was streaked out onto a YPD + 100 μ g/mL ampicillin plate and incubated at 28 °C for 48 hours until adequately sized colonies were grown. A single *P. pastoris* GS115 colony from this streaked plate was then used to inoculate 5 mL YPD + 100 μ g/mL ampicillin in a tilted 50 mL conical tube, and incubated overnight at 28 °C, 220 RPM. The following day, this overnight culture was used to subinoculate 50 mL of YPD + 100 μ g/mL ampicillin to a starting culture OD₆₀₀ of 0.02. This day culture was incubated at 28 °C, 220 RPM for *P. pastoris* growth. At OD₆₀₀ of 1.2, cells were harvested at 500 $\times g$ for 15 minutes at 4 °C. Supernatant was removed and cells were resuspended in 50 mL cold sterile ddH₂O. Cells were then again harvested at 2000 $\times g$ for 5 minutes at 4 °C. Supernatant decanted, and wash step was repeated with 25 mL cold sterile ddH₂O, followed by cell harvesting at 2000 $\times g$ for 5 minutes. Again, supernatant was

removed and the wash step was repeated with 10 mL cold sterile 1 M sorbitol. A final centrifugation step was done at $2000 \times g$ for 5 minutes, and the supernatant was discarded. The *P. pastoris* GS115 WT cell pellet remaining was resuspended in 1 mL of cold sterile 1 M sorbitol and the cell suspension was kept on ice.

3.2.1.3 Transformation of *P. pastoris* GS115 with pPICZ α :His-GFP-PARL

The transformation began with transfer of 95 μ L of the *P. pastoris* GS115 WT cell suspension into a 2mm Bio-Rad cuvette, pre-incubated on ice. 5 μ g of linearized dsDNA was added to the cells in the cuvette, mixed, and incubated on ice for 3 minutes. Cells were electroporated at 2.5 kV and 1 mL of cold sterile 1 M sorbitol was immediately added post-electroporation. Transformation reaction was then kept in the cuvette and incubated at 28 °C for 4 hours to ensure yeast recovery and successful expression of the zeocin resistance gene encoded by the linearized plasmid. 5 μ L, 15 μ L, 50 μ L, and 200 μ L of the transformation was plated onto YPDS + zeocin plates and incubated at 28 °C for 3 days, allowing for individual colony growth of successful transformants.

3.2.2 Transfer of successful *P. pastoris* GS115 transformants to YPDS master plates

Following growth and identification of successful transformants, individual colonies were transferred onto YPDS + 100 μ g/mL ampicillin plates in a grid orientation.

These plates represented our master plates that would be used to streak out and make glycerol stocks of high GFP-PARL expressing colonies. After transferring colonies, these master plates were inverted and incubated at 28 °C for an additional 2 days.

3.2.3 Transfer of successful *P. pastoris* GS115 transformants from YPDS master plates to BMMY induction plates

Colonies from the master plates were transferred to BMMY + 100 µg/mL ampicillin plates, corresponding to their positions on the YPDS master plates. Plates were inverted and incubated at 28 °C. After 24 hours of induction, plates were imaged under blue light using ImageQuant LAS 4000. Due to the presence of GFP in the GFP-PARL fusion, the relative expression of GFP-PARL can be assessed. High expressing colonies of GFP-PARL or the positive control pEMT-GFP appeared black, whereas the negative control, wild-type *P. pastoris* GS115, and low expressing colonies of GFP-PARL appeared grey (**Figure 3.1**).

3.2.4 Screening for high GFP-PARL expressing *P. pastoris* GS115 colonies

High expressing colonies were used to inoculate 5 mL of YPD + 100 µg/mL ampicillin media and grown overnight at 28 °C. These overnight cultures were then used to make glycerol stocks to be used for subsequent large-scale expression cultures.

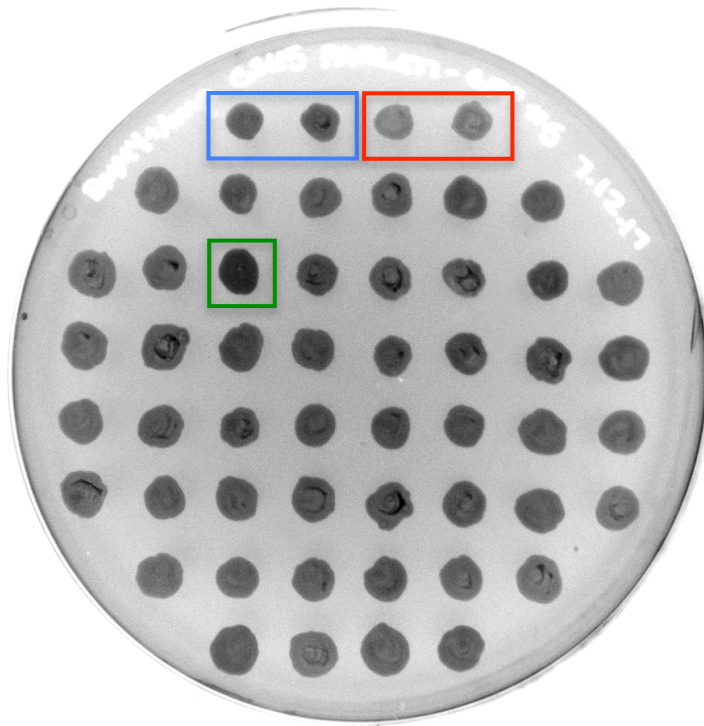


Figure 3.1. Induction plate expression screen for GFP-PARL protease. Colonies of *P. pastoris* GS115 yeast transformed with the pPICZ α :His-GFP-PARL plasmid were spotted onto BMMY agar plates and incubated at 28 °C for 48 hours. Enclosed in blue are positive control colonies from pEMT-transformed *P. pastoris* GS115. Enclosed in red are negative control colonies from untransformed wild-type *P. pastoris* GS115. In green is a positively identified high expressing colony of GFP-PARL. Plate imaged under blue light using an ImageQuant LAS 4000.

3.3 Growth of *P. pastoris* GS115 and expression of GFP-PARL

A glycerol stock made from a high GFP-PARL expressing colony identified by the expression screen was used to inoculate 100 mL YPD + 100 µg/mL ampicillin. This culture was incubated overnight at 28 °C, with shaking. The following day, the starter culture was used to subinoculate 1 L BMGY media + 100 µg/mL ampicillin (x6), for a total culture volume of 6 L. These grew at 28 °C with shaking (200 RPM) until the OD₆₀₀ reached 8, typically taking 20 hours. At this OD₆₀₀, the cells were harvested using the Avanti JLA8.1 rotor for 30 minutes at 800 *x g*. Cell pellets were resuspended in 1 L BMMY media + 100 µg/mL ampicillin and returned to the shaker for a 48 hour induction period at 24 °C. At the end of the induction period the cells were harvested at 800 *x g* for 30 minutes using the Avanti JLA8.1 rotor. Cell pellets were then transferred to 50 mL falcon tubes and frozen at -20 °C for storage until subsequent use.

3.4 Purification of GFP-PARL

Frozen cell pellets were thawed on ice and resuspended in 5:1 buffer-to-pellet weight in TBS buffer. Cells were then lysed using the Constant Systems Cell Disruptor with two passes at 40 kPSI. Immediately, after cell lysis, 1 mM PMSF and protease inhibitor tablets without EDTA were added to the cell lysate. Cell lysate was then centrifuged at 20 000 *x g* for 2 – 20 minute spins to pellet unbroken cells and cellular debris using the Beckman TI45 rotor. Following these centrifugation

steps, supernatant was subjected to a 2 hour ultracentrifugation step at 35 000 $\times g$ to harvest the GFP-PARL-containing cell membranes, again using the TI45 rotor. The supernatant from this ultracentrifugation step was discarded, and cell membranes were stored at -20 °C.

Isolated membranes were manually homogenized in a solubilization buffer (50 mM Tris-HCl pH 8.0, 200 mM NaCl, 20% glycerol, 20 mM imidazole, 1mM PMSF) using a Dounce homogenizer. Triton X-100 was added to the homogenized membranes to a final concentration of 1% for a 2 hour incubation on ice at 4 °C. Following this detergent solubilization step, the solubilized sample was subjected to another 35 000 $\times g$ ultracentrifugation spin for 30 minutes to pellet any insoluble material.

3.4.1 Immobilized metal affinity chromatography

2 mL of HisPur Co resin was packed into a column and equilibrated with 10 CV of equilibration buffer (50 mM Tris-HCl pH 8.0, 300 mM NaCl, 10% glycerol, 0.1% DDM). The supernatant from the final ultracentrifugation step was then passed through the Co column 2 times. The column was with 20 CV of wash buffer (50 mM Tris-HCl pH 8.0, 300 mM NaCl, 10% glycerol, 0.1% DDM, 10 mM imidazole). Protein was eluted off the column using 6 mL of 500 mM imidazole in buffer. Elutions were collected in 1 mL aliquots, and those with the highest concentration of GFP-PARL were pooled together (**Figure 3.2**). GFP-PARL was incubated with TEV protease and 1 mM DTT overnight at 4 °C to separate PARL protease and the GFP-His tag.

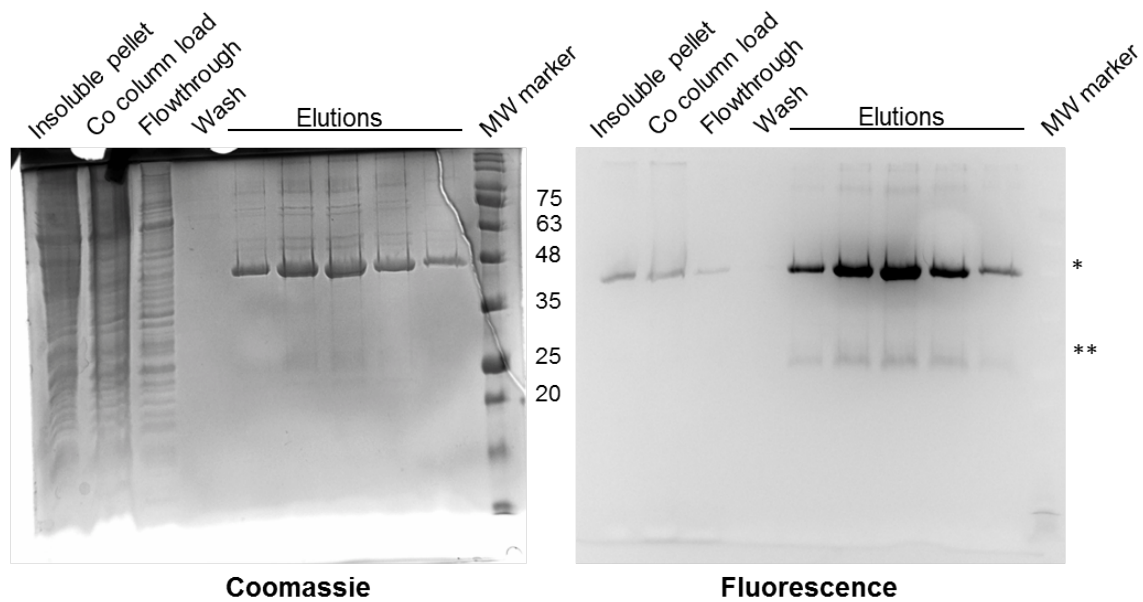


Figure 3.2. SDS-PAGE gel for purification of GFP-PARL. Full-length GFP-PARL is 55.5 kDa, though on gel appears just below 48 kDa. PARL is eluted from the Co column using buffer containing 500 mM imidazole. * = GFP-PARL; ** = Free GFP.

3.4.2 Negative immobilized metal affinity chromatography

After the overnight TEV protease-mediated digestion of PARL-GFP, this reaction was subject to a 2-hour dialysis to remove DTT and imidazole from the sample. The dialysis buffer was made of 50 mM Tris-HCl pH 8.0, 300 mM NaCl, 10% glycerol. The dialysis bag had a molecular weight cut-off of 12-14 kDa, mitigating concerns of loss of detergent as DDM micelles are 72 kDa.

To isolate PARL protease from the free GFP, a negative IMAC column was utilized. This method is based on the premise that the protein of interest is untagged; therefore as the sample is poured through the column the untagged protein flows through as the unwanted, tagged protein is bound to the resin. The dialyzed sample was passed through 2 mL of settled and equilibrated Ni-NTA resin. Flow-through, containing purified PARL protease, was collected (**Figure 3.3**). Resulting flow-through had a slight tinge of green, indicating GFP contamination. To remove this free GFP, a second negative IMAC column was prepared and the sample was passed through 2 mL of Ni-NTA resin again, collecting the colourless flow-through. This PARL protease-containing fraction was then concentrated using a 30 kDa Amicon concentrator. Concentration was determined to be 1.0 mg/mL using a BCA assay. Protein distributed into small 30 μ L aliquots and flash frozen using liquid nitrogen, to be stored at -80 °C for subsequent use.

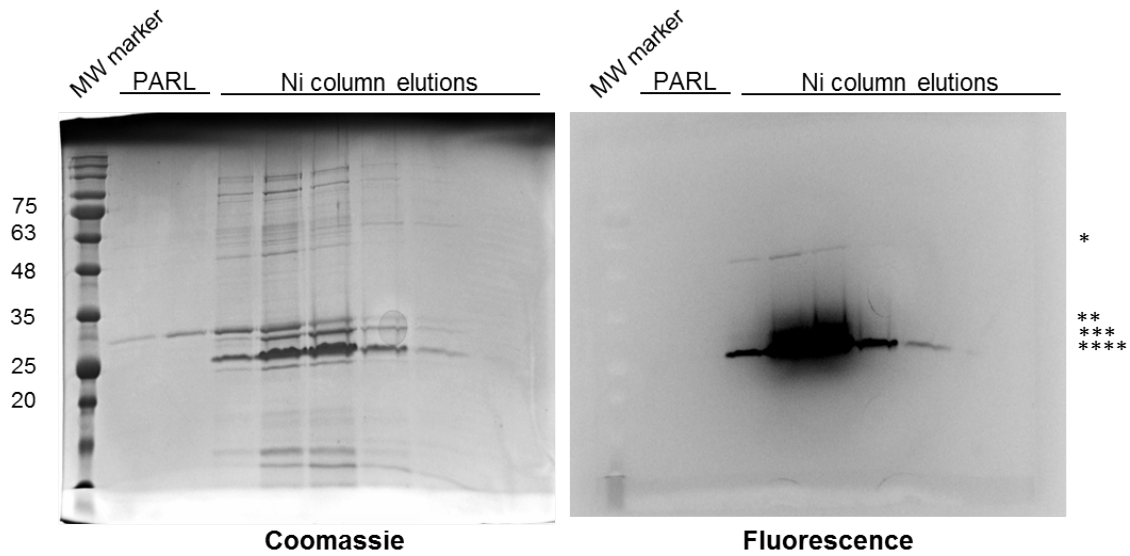


Figure 3.3. SDS-PAGE gel for negative-Ni column post-TEV protease cleavage. Removal of His tag with incubation of TEV protease allows PARL to be isolated in the column flow-through, whereas the Ni resin captures the His-tagged GFP and TEV protease. Elution of the resin with buffer containing imidazole shows both GFP and TEV bind to the column, in addition to some PARL protease (thought to associate with GFP through strong hydrophobic reactions). * = uncleaved GFP-PARL; ** = Full-length PARL protease; *** = TEV protease; **** = Free GFP.

3.5 Discussion

The GFP-PARL expression screen proved to be useful for identification of high GFP-PARL expressing *P. pastoris* colonies. The purification of GFP-PARL required slight optimization. Though the protocol had already been established in the lab, there were some issues that arose throughout the progression of the project. The main issue was declining yield of PARL protease. Though identification of high GFP-PARL expressing colonies was successful, oftentimes these findings didn't translate when transitioning to large-scale cultures for expression. Expression screens for *P. pastoris* expressing PARL are required approximately twice a year. Around the 6-month mark, post-screen, glycerol stocks lose their high expressing capacity. Additionally, following the 24-hour mark post-induction, additional methanol is added to the cultures. The standard amount of methanol added 24 hours post-induction was 10 mL, but after measuring fluorescence a gradient was observed between flasks depending on position in the shaker. To compensate for this, an additional 5-10 mL of 100% methanol are added to the cultures demonstrating hindered expression. By the time the 48-hour induction period has come to an end, the variability in fluorescence between flasks is greatly decreased. The surveillance of culture fluorescence during induction has certainly aided in ensuring optimal GFP-PARL expression. Purification of GFP-PARL follows a standard protocol that works well for the protein of interest. One change that was made was the transition from batch-resin purification to a pass-through method, similar to the change made in the His-*HsPINK1*[70-134] purification protocol. This resulted in the observation

that there is less proteolytic degradation of PARL with expulsion of the batch-resin incubation step. Shifting from large IMAC elution volumes to smaller ones equivalent to the column volume resulted in higher concentrated GFP-PARL, also contributed to increased protein integrity by decreasing the amount PARL needed to be concentrated.

Genomic integration of the expression cassette was never verified so this may be a contributing factor among others to the variable expression of GFP-PARL^{141,174}. Integration into the *P. pastoris* genome allows for the possibility of multi-copy integration. This multi-copy integration has been proposed to influence the yield of protein expressed in *P. pastoris* due to an increase in gene dosage¹⁷⁵. Another factor that could contribute to the low yield of the pastors or very low yield of protein expressed is differences in the unfolded protein response (UPR). The UPR is a cellular response to experienced stress by the endoplasmic reticulum, the primary site for protein folding in eukaryotes. Activation of the UPR could result when the demand for protein folding exceeds that of the folding capacity¹⁷⁶. Consequences of its activation include death of living cells and activation of various signaling pathways¹⁷⁷, which could result in protein of interest degradation.

Further work on the expression of PARL protease could focus on the confirmation of genomic integration via colony PCR amplification. If there is confirmation of a high copy number and protein expression is still low that will be an indication that there are other factors playing a role in the relatively low or medial expression of GFP-

PARL. For our purposes expression and purification of PARL protease was successful and sufficient for use in downstream applications and assays.

CHAPTER 4: Analysis of PD-linked PINK1 variants in FRET-based kinetic assay

4 Analysis of PD-linked PINK1 variants in FRET-based kinetic assay

The procedure for this assay was developed and optimized by Dr. Elena Arutyunova from the Lemieux lab. As an already established protocol, this assay proves as a powerful tool to determine kinetics of various proteases¹⁴⁶.

4.1 FRET-based assay adapted to measure kinetic parameters of PARL protease

Varying amounts of CyPet-PINK1-YPet, final concentrations ranging from 0.1 to 10 μM , were incubated at 30 °C in buffer (50 mM Tris-HCl pH 7.0, 150 mM NaCl, 20% glycerol, 0.1% DDM) for 30 minutes in an OptiPlate-384 F HB, Black 384-well Microplate. Following this pre-incubation step, PARL protease was added to each well to a final concentration of 0.8 μM . There was a blank prepared at each substrate concentration without any PARL protease. A shift in the emission spectra was measured as it directly corresponded to the cleavage events ongoing in the reaction wells (**Figure 4.1**).

In the FRET-based assay, the emission intensities of CyPet and YPet were measured, 475 nm and 530 nm respectively, with the excitation wavelength of 414 nm in a fluorescence multi-well plate reader from BioTek. The fluorescence emission of YPet was measured every 5 minutes for 2 hours. Using **Equation 1**, developed by Liu *et*

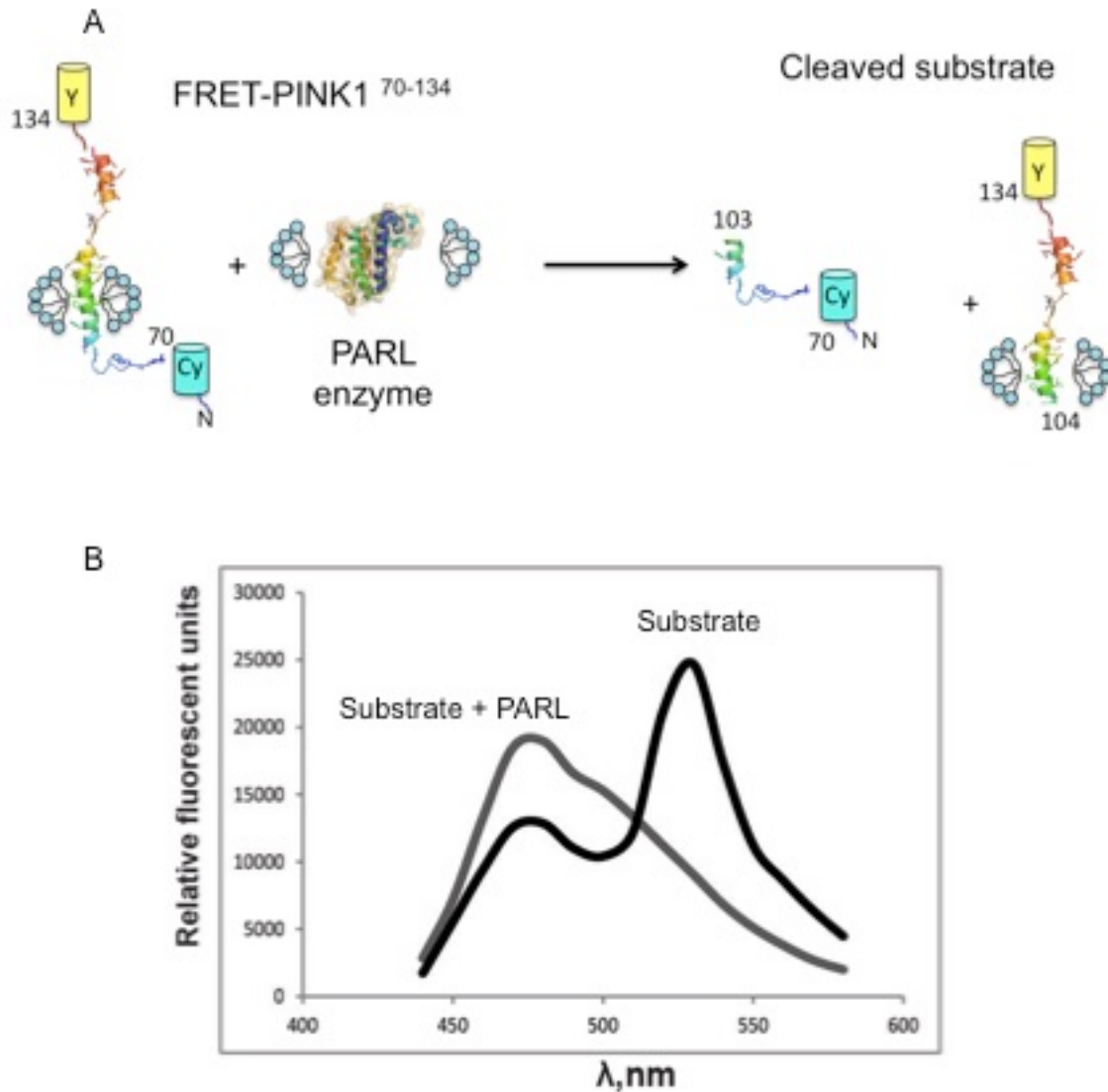


Figure 4.1. FRET-based kinetic assay using FRET-based PINK1 substrate. (A) Schematic representation of FRET-based kinetic assay using detergent solubilized PARL protease and detergent purified His-FRET-*HsPINK1*[70-134] substrate. (B) Emission spectrum of His-*HsPINK1* before (black) and after (grey) cleavage of FRET substrate by the PARL protease. Relative change of fluorescence at 480 nm is measured, directly corresponding to the rate of cleavage by PARL protease.

al., the concentration of the cleaved substrate was determined^{146,178}.

$$FL'_{\frac{530}{414}} = \frac{M - x}{M} \left(FL_{\frac{530}{414}} - \alpha FL_{CyPet(\frac{475}{414})} - \beta FL_{YPet(\frac{530}{475})} \right) + \alpha \left[k(M - x) + \frac{30}{68} jx \right] + \beta FL_{YPet(\frac{530}{475})}$$

$FL_{530/414}$ and $FL'_{530/414}$ correspond to the fluorescence emission of YPet at an excitation wavelength of 414 nm before and after cleavage of the substrate, respectively¹⁴⁶. M is the total amount of CyPet-PINK1-YPet, whereas x is the amount of digested CyPet-PINK1-YPet¹⁴⁶. α represents a ratio of fluorescence emission by CyPet at 530-475 nm under excitation at 414 nm. Similarly, β represents the ratio of fluorescence emission by YPet at 530-475 nm under 475 nm excitation. As such $\alpha FL_{CyPet(475/414)}$ is a direct measure of CyPet emission when excited at 414 nm, and $\beta FL_{YPet(530/475)}$ is the YPet direct emission at 530 nm when excited at 475 nm. Constants j and k are calculated based on standard plots of fluorescence emission versus known amount of protein. Initial velocities were plotted against substrate concentrations. Data was fit to Michaelis-Menten kinetics.

4.1.1 Recombinant His-FRET-HsPINK1[70-134] as a substrate of PARL protease

As mentioned before, all parameters of the FRET-based assay were optimized prior to use for the analysis of the kinetics of the PARL protease towards the FRET-based

PINK1 substrate. Cleavage of all successfully purified FRET substrates was successfully demonstrated (**Figures 4.2A-D**). Kinetic results of PARL protease towards the His-FRET-*HsPINK1*[70-134] PD-linked variants are found in **Figure 4.3**. Our kinetic analysis reveals that the K_M parameter is comparable between wild-type and all PINK1 PD-linked variants tested. However, for the substrate turnover rate, k_{cat} , a significant decrease is observed with the PD-variants of PINK1, C92F, I111S, and Q126P, compared to the wild-type, suggestive of a turnover defect (**Figure 4.3**). The catalytic efficiency, k_{cat}/K_M , however, is not statistically different. We do observe with this FRET-based assay a great deal of variability with the cleavage of PINK1-wild type (**Figure 4.2A**). This may be attributed to an outlier in the kinetic analysis or a larger data pool is needed. More analysis of the wild-type cleavage is needed to demonstrate statistical confidence. Furthermore, other assays may be incorporated to provide stronger evidence, such as peptide cleavage assays.

4.1.2 Internally quenched (IQ)-*HsPINK1* peptide as a substrate of PARL protease

To mitigate the inability to produce a sufficient yield of His-FRET-*HsPINK1*[70-134] R98W for the kinetic assay a short internally quenched (IQ), fluorescent peptide was ordered harboring this mutation, IQ-*HsPINK1*[97-107] R98W. A corresponding control wild-type peptide, IQ-*HsPINK1*[97-107] WT, was ordered. **Table 4.1** outlines the sequence of each internally quenched peptide designed and ordered for synthesis (Biomatik).

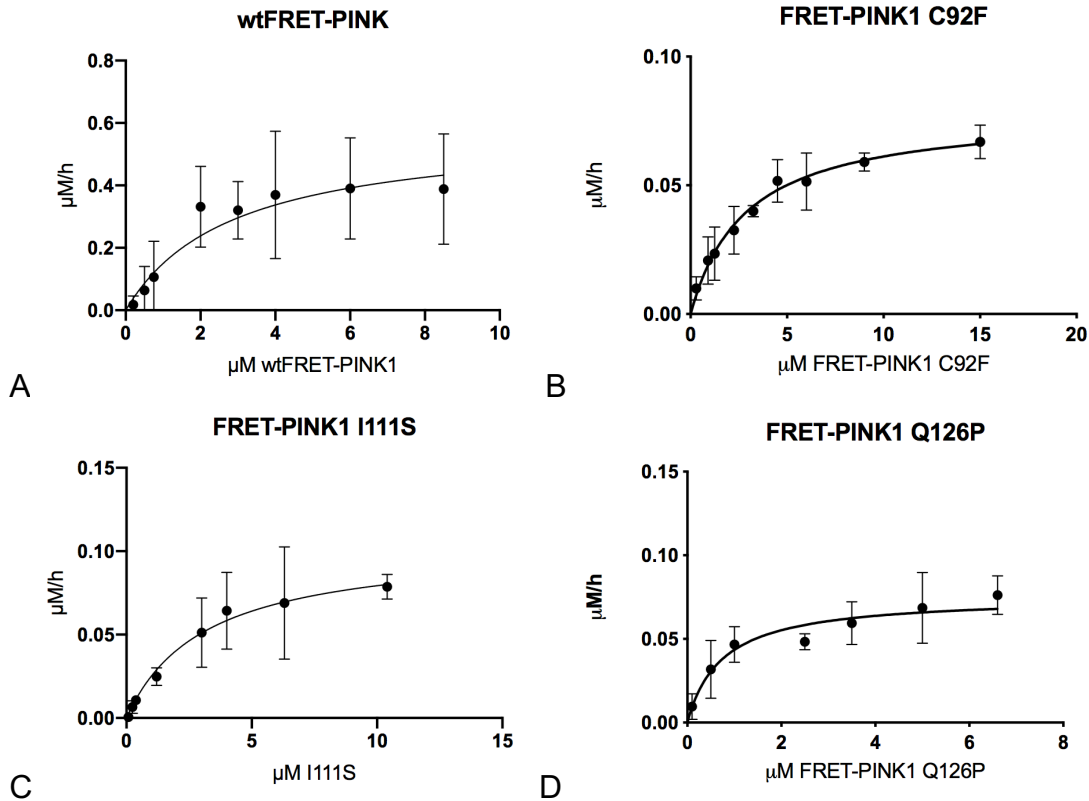


Figure 4.2. (A) Michaelis-Menten curve of PARL-mediated cleavage of His-FRET-*HsPINK1*[70-134] WT. Range of substrate concentration was 0 to 9 μM . FRET substrate was incubated with 0.8 μM PARL protease at 30 $^{\circ}\text{C}$ for 2 hours (n=4). **(B)** Michaelis-Menten curve of PARL-mediated cleavage of His-FRET-*HsPINK1*[70-134] C92F. Range of substrate concentration was 0 to 15 μM . FRET substrate was incubated with 0.8 μM PARL protease at 30 $^{\circ}\text{C}$ for 2 hours (n=3). **(C)** Michaelis-Menten curve of PARL-mediated cleavage of His-FRET-*HsPINK1*[70-134] I111S. Range of substrate concentration was 0 to 10 μM . FRET substrate was incubated with 0.8 μM PARL protease at 30 $^{\circ}\text{C}$ for 2 hours (n=3). **(D)** Michaelis-Menten curve of PARL-mediated cleavage of His-FRET-*HsPINK1*[70-134] Q126P. Range of

substrate concentration was 0 to 9 μM . FRET substrate was incubated with 0.8 μM PARL protease at 30 $^{\circ}\text{C}$ for 2 hours (n=3).

A

| | K_M (μM) | k_{cat} (h^{-1}) | k_{cat}/K_M ($\mu\text{M}^{-1} \text{h}^{-1}$) |
|----------------------|-------------------------|--------------------------------------|---|
| WT (n = 4) | 3 \pm 1 | 0.46 \pm 0.09 | 0.16 \pm 0.09 |
| C92F (n = 3) | 3 \pm 1 | 0.06 \pm 0.01 | 0.02 \pm 0.01 |
| I111S (n = 3) | 3 \pm 1 | 0.08 \pm 0.02 | 0.03 \pm 0.02 |
| R98W | --- | --- | --- |
| Q126P (n = 3) | 0.7 \pm 0.5 | 0.06 \pm 0.01 | 0.08 \pm 0.07 |

B

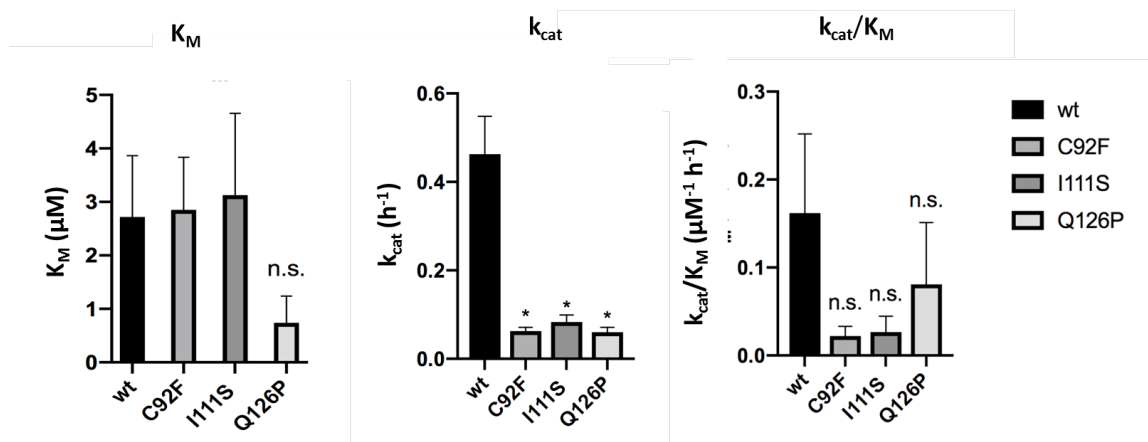


Figure 4.3. PARL-mediated cleavage of His-FRET-*HsPINK1*[70-134]. **(A)** Kinetic parameters of PARL protease-mediated cleavage of His-FRET-*HsPINK1*[70-134] WT and PD-linked variants. **(B)** Graphical representation of kinetic parameters comparing PARL-mediated cleavage of PINK1 PD-linked variants to that of the wild-type. Paired t-tests were performed; K_M demonstrated no statistical significance between wild-type and variants. There is a statistical significance observed for the k_{cat} between wild-type and each of the variants (* p <0.05). k_{cat}/K_M demonstrates no statistical significance.

Table 4.1. Peptide design of small IQ-*HsPINK1* peptides used in FRET-based kinetic assay.

| Peptide name | Peptide construct |
|----------------------------------|---|
| IQ- <i>HsPINK1</i> [97-107] WT | Arg-(DABCYL)-GRAVFLAFGLG-Glu(EDANS)-Arg |
| IQ- <i>HsPINK1</i> [97-107] R98W | Arg-(DABCYL)-GWAVFLAFGLG-Glu(EDANS)-Arg |

The design of these internally quenched peptides falls in line with the traditional FRET concept. EDANS, 5-((2-Aminoethyl)amino)naphthalene-1-sulfonic acid, is a fluorescent donor often paired with the DABCYL quencher, or 4-((4-(dimethylamino)phenyl)azo)benzoic acid (**Figure 4.4, Figure 4.5**). EDANS is excited at 336 nm and emits at 490 nm, the same absorbance wavelength of DABCYL. This overlap in the excitation and absorbance spectra of EDANS and DABCYL, respectively, is responsible for the quenching activity of DABCYL (**Figure 4.4C**). Similarly to the FRET-based assay utilizing CyPet-PINK1-YPet, incubation of IQ-*HsPINK1* peptides with PARL protease results in a measurable change in fluorescence over time (ex = 336 nm, em = 490 nm). With substrate concentration matched blanks, increasing amount of IQ-*HsPINK1* versus shift in normalized fluorescence were used to form initial velocity plots. Values from these plots were then used to fit Michaelis-Menten kinetic plots. The values obtained for the K_M and k_{cat}/K_M of IQ-*HsPINK1* peptide, encompassing residues 97-107, were comparable with the His-FRET-*HsPINK1* WT protein, encompassing residues 70-134 (**Figure 4.6**). No statistically significant change was observed with these two parameters between the two wild-type PINK1 substrates. This finding enabled us to move forward to assess the PARL-mediated cleavage of PINK1 R98W.

IQ-*HsPINK1*[97-107] WT and R98W were both successfully cleaved by PARL protease in our *in vitro* assay (**Figure 4.7**). Cleavage of IQ-*HsPINK1*[97-107] R98W by PARL protease indicated a higher K_M value, suggesting a lower affinity of PARL to the substrate. The turnover rate however was faster for the R98W mutant,

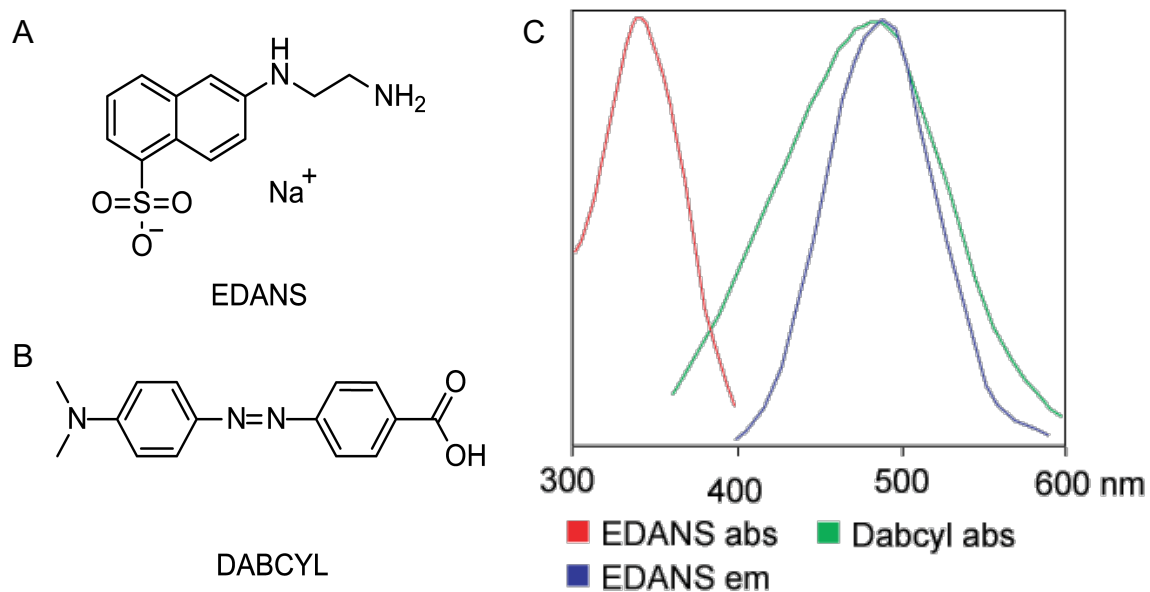


Figure 4.4. Fluorophore-quencher pair concept. **(A)** Chemical structure of EDANS fluorophore, **(B)** Chemical structure of DABCYL fluorescent quencher. **(C)** Graph demonstrating absorbance and emission spectra of EDANS and DABCYL. When in close proximity of one another, the absorbance of DABCYL at 490 nm overlaps with the emission of EDANS at 490 nm, thereby interfering with the fluorescence emission of EDANS.

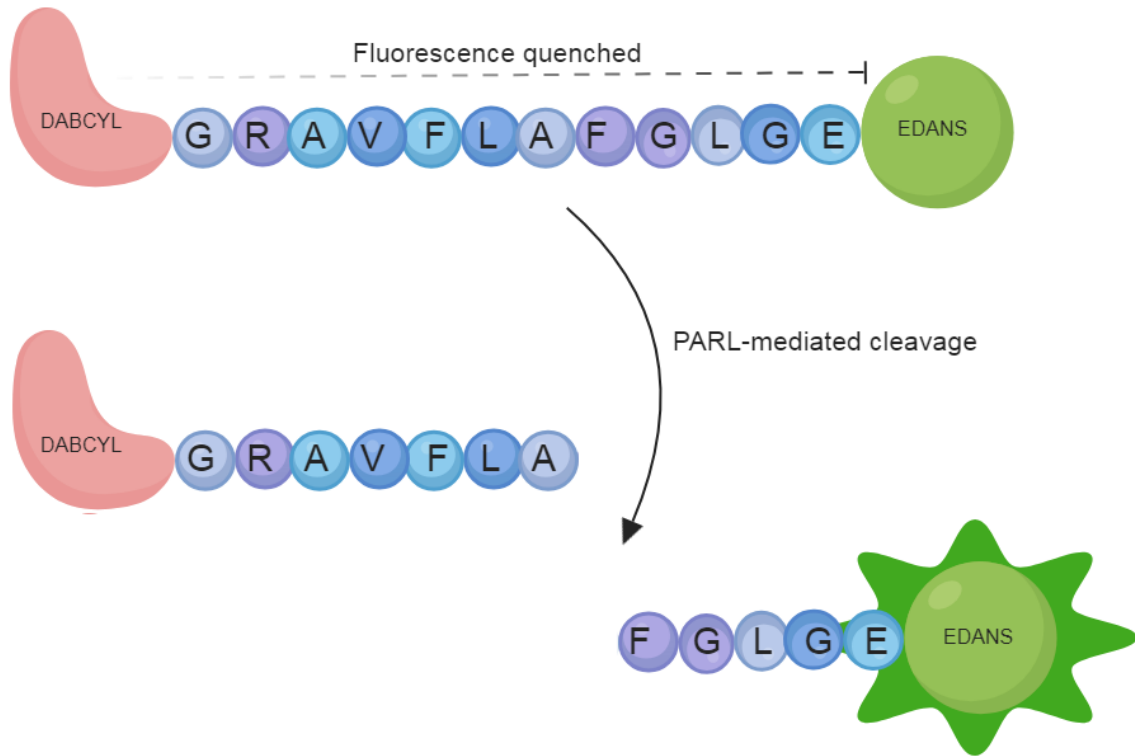


Figure 4.5. FRET-based kinetic assay using IQ-peptide substrate. Schematic representation of kinetic assay using detergent solubilized PARL protease and synthetic IQ-*HsPINK1*⁹⁹⁻¹⁰⁸ WT peptide substrate. Upon incubation with PARL protease, the quenched EDANS fluorophore of the peptide results in the measurement of an increase in fluorescence due to separation of the fluorophore and the quencher.

A

| | His-FRET- <i>HsPINK1</i> [70-134] WT (n=4) | IQ- <i>HsPINK1</i> [97-107] WT (n=10(x2)) |
|--|---|--|
| PARL protease | $\Delta 77$ | $\Delta 77$ |
| K_M (μM) | 3 ± 1 | 2.1 ± 0.4 |
| k_{cat} (h^{-1}) | 0.46 ± 0.09 | 0.26 ± 0.02 |
| k_{cat}/K_M ($\mu\text{M}^{-1} \text{h}^{-1}$) | 0.16 ± 0.09 | 0.13 ± 0.03 |

B

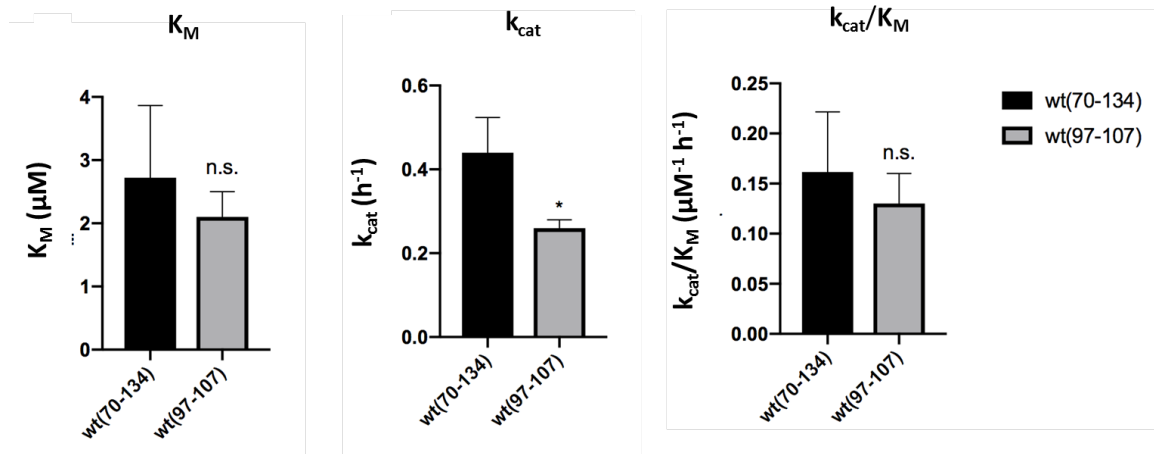


Figure 4.6. PARL-mediated cleavage of different wild-type PINK1 transmembrane constructs. **(A)** Kinetic parameters of PARL protease-mediated cleavage of His-FRET-*HsPINK1*[70-134] WT and IQ-*HsPINK1*[97-107] WT. **(B)** Graphical representation of kinetic parameters comparing PARL-mediated cleavage of PINK1: IQ-*HsPINK1*[97-107] and His-FRET-*HsPINK1*[70-134]. Paired t-tests were performed; K_M demonstrated no statistically significant change in affinity for the different PINK1 lengths. A statistically significant change was observed in turnover rate between IQ-*HsPINK1*[99-108] (* $p < 0.05$) and IQ-*HsPINK1*[97-107] (** $p < 0.005$)

compared to His-FRET-*HsPINK1*[70-134]. k_{cat}/K_M demonstrates no statistical significance.

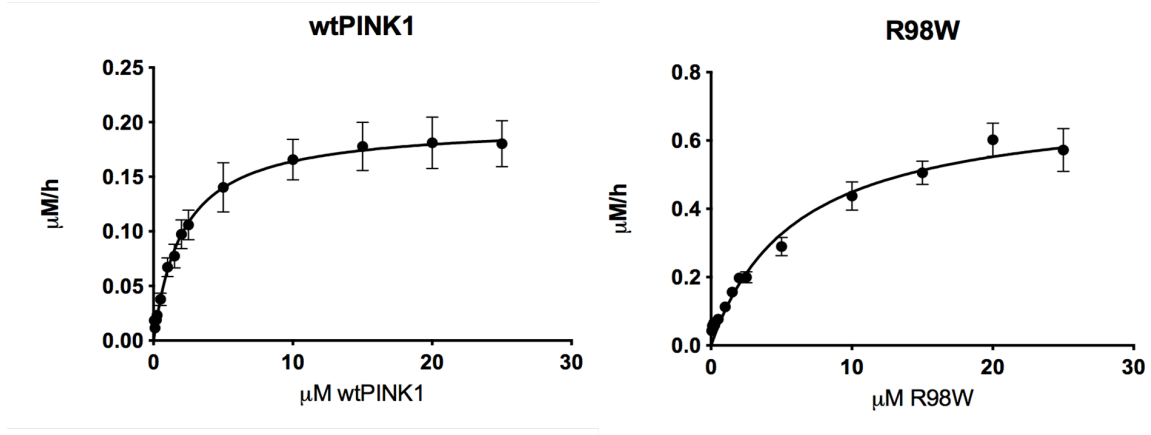


Figure 4.7. Michaelis-Menten curves of PARL-mediated cleavage IQ-*HsPINK1*[97-107] WT and R98W. Range of substrate concentration was 0 to 25 μM . FRET substrate was incubated with 0.8 μM PARL protease at 30 $^{\circ}\text{C}$ for 2 hours (WT n=10; R98W n=8).

suggesting enhanced substrate turnover. However the R98W mutant did not show a statistical significant change in catalytic efficiency for cleavage compared to the control wild-type peptide (**Figure 4.8**). These results suggest the PD-linked variant R98W does experience an alteration in PARL-mediated cleavage as otherwise suggested in previous studies¹³⁰.

4.2 Discussion

An *in vitro* assay was developed and assessed for the study of PARL mediated cleavage. Kinetics of the intramembrane protease, PARL, has been well characterized in the lab with our recombinant human His-FRET-*HsPINK1* substrate as well as with small synthetic PINK1 transmembrane peptide. A well-established protease-substrate pair is AarA and its physiological substrate psTatA. With a Michaelis constant (K_M) of $7.6 \pm 1.1 \mu\text{M}$, a substrate turnover rate (k_{cat}) of 1.06 ± 0.05 molecules per minute, and a catalytic efficiency (k_{cat}/K_M) of $13.9 \times 10^{-2} \pm 2.4 \times 10^{-2} \mu\text{M}^{-1} \text{min}^{-1}$, AarA proves to be a very efficient intramembrane protease when cleaving its physiological substrate¹⁴⁶, and is faster than the PARL mediated cleavage of PINK1, that has a k_{cat} of 0.46 per hour. Assessment of other prokaryotic rhomboids, ecGlpG and hiGlpG, using the TatA substrate demonstrated specificity or preference for cleavage of transmembrane substrates. With higher K_M values and lower k_{cat} values, this FRET-based assay revealed the broad but preferential proteolytic activity of prokaryotic rhomboid proteases¹⁴⁶.

A

| | IQ-HsPINK1[97-107] WT (n=10(x2)) | IQ-HsPINK1[97-107] R98W (n=8(x2)) |
|---|--|---|
| K_M (μM) | 2.1 \pm 0.4 | 6.0 \pm 0.9 |
| k_{cat} (h^{-1}) | 0.26 \pm 0.02 | 0.96 \pm 0.05 |
| k_{cat}/K_M ($\mu\text{M}^{-1} \text{h}^{-1}$) | 0.13 \pm 0.03 | 0.16 \pm 0.03 |

B

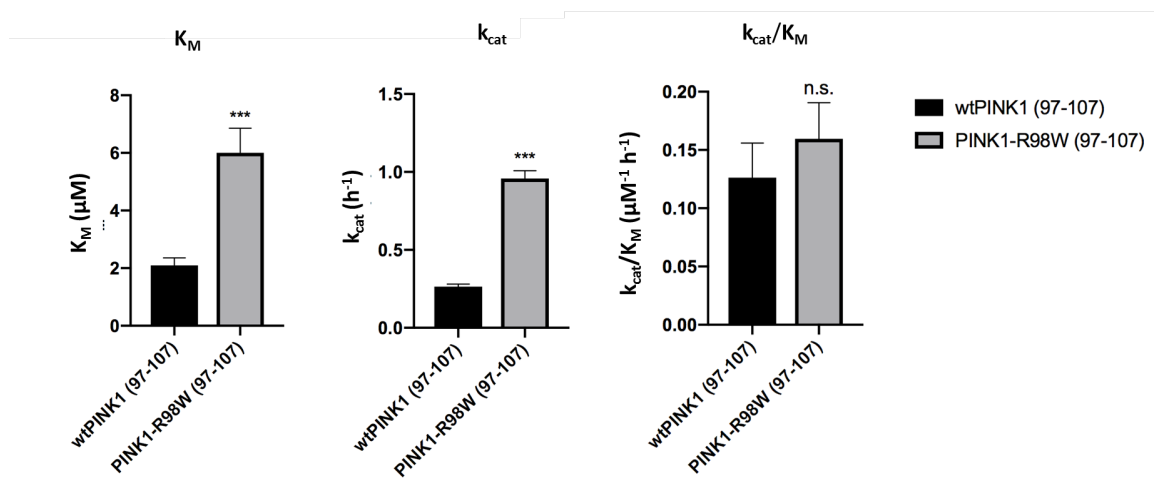


Figure 4.8. PARL-mediated cleavage of IQ-HsPINK1[97-107] WT and R98W. **(A)** Kinetic parameters of PARL protease-mediated cleavage of IQ-HsPINK1[97-107] WT and PD-linked variant R98W. **(B)** Graphical representation of catalytic parameters of PARL-mediated cleavage. Paired t-tests were performed; statistically significant difference in both the K_M and the k_{cat} between the wild-type peptide and the R98W variant (***) $p < 0.0005$) was observed. k_{cat}/K_M demonstrated no statistical change in catalytic efficiency between wild-type and the R98W variant.

Two constructs of PINK1 were used as substrates of PARL protease: recombinantly expressed proteins His-FRET-*HsPINK1*[70-134], and synthetic peptides IQ-*HsPINK1*[97-107]. Catalytic parameters, such as the K_M and catalytic efficiency revealed comparable cleavage between the two lengths of PINK1 (**Figure 4.6**). This suggests that the peptide boundaries surrounding the cleavage site at alanine-103 are sufficient enough to measure PARL-mediated cleavage. Proteases are quickly emerging as principal regulators of cellular signaling and thus a wide range of cellular processes^{109,179}, and PARL protease is no exception. PINK1, Phosphoglycerate Mutase Family Member 5 (PGAM5), Second Mitochondria-derived Activator of Caspases/Direct IAP-Binding protein with Low PI (Smac/Diablo), StAR Related Lipid Transfer Domain Containing 7 (STARD7), Caseinolytic Peptidase B protein homolog (CLPB), and Tetratricopeptide Repeat Domain 19 (TTC19) were all identified in a proteomic study as potential or already known substrates of PARL protease¹⁰⁹. Mutations found in TTC19 have been associated with respiratory chain complex III impairment and resulting neurological abnormalities¹⁸⁰. Variants of CLPB have been associated with mitochondrial disorder¹⁸¹. Identification of these new substrates demonstrates the importance PARL plays in mitochondrial function and homeostasis, and how impairment in its regulatory function may result in disorder.

After establishing adequate and measurable cleavage of PINK1 by PARL protease using the His-FRET-*HsPINK1* protein, the different PD-linked PINK1 variants were assessed. Though there was no statistical difference between the wild-type and the

variants for the K_M and the k_{cat}/K_M there was a significant difference in the turnover rate, k_{cat} , between the wild-type and the PD-linked variants. These results suggest that though the wild-type substrate is cleaved significantly quicker, the catalytic efficiencies between WT and the variants are comparable. There is some discrepancy within these results that are primarily attributed to the relatively high error of the wild-type control. As demonstrated by the Michaelis-Menten plot in **Figure 4.2A**, there is wide variability in the cleavage of His-FRET-*HsPINK1*[70-134] WT. This variability suggests questionable reproducibility of the control. In addition to the need for a larger data pool, there is concern that the two fluorescent proteins on each terminus of the PINK1 protein and the contaminating proteins co-purified with His-FRET-*HsPINK1* (**Figure 2.19**), may be occluding consistent access for the protease to cleave the substrate uniformly between assays. Therefore conclusions made from this assay need to be repeated to increase confidence in the data gathered, or supplemented with kinetics done using synthetic peptides as done for the R98W PD-linked variant. An additional consideration is the two cysteines that reside within the residues 70 to 134. A PINK1 dimer-containing complex has been reported in the literature though the residues or interactions responsible for this phenomenon are not known¹¹⁸. It is possible that there are some self-interacting elements of PINK1 within the region recombinantly expressed that are altering the PARL-mediated cleavage being measured. In particular, though there is no evidence, PINK1 molecules may be forming disulfide bonds. The incorporation of reducing agents such as DTT or TCEP may negate this effect if PINK1 is indeed forming thiol bonds. This may result in more consistent cleavage by PARL in the *in vitro* assay.

Deas *et al.* report an abnormal distribution and aggregation of mitochondria in cells expressing PINK1 C92F⁸³. Studies demonstrated an increased ratio between the full-length PINK1 and the mature PARL-cleaved form when SH-SY5Y cells were transfected with PINK1 C92F in comparison to the results reported for that of the wild-type⁸³. Conclusions made by Deas *et al.* neither emphasized nor supported a specific defect in PARL-mediated cleavage. The K_M was comparable between His-FRET-*Hs*PINK1[70-134] WT and C92F. The k_{cat}/K_M was also comparable. However, there was a statistically significant decrease in turnover for the PD-linked variant than that of the wild-type, suggesting a cleavage defect. Our results demonstrate that the increased presence of full-length PINK1 in the mitochondrion may be due to a defect in the cleavage by PARL protease but does not discount the possibility of defective localization to the inner mitochondrial membrane, where the protease resides.

In vivo studies emphasized a severe defect in PARL-mediated proteolysis of the PINK1 transmembrane variant R98W^{124,130}. *In vitro* kinetic results gathered suggest PINK1 R98W is successfully cleaved by the PARL protease, in fact with a higher turnover than the wild-type. The accumulation demonstrated may be a result of inner mitochondrial membrane import defects. Ulmschneider *et al.* conducted studies that demonstrate transmembrane helices containing arginine are thermodynamically stable in POPC bilayers¹⁰⁰, contrasting previous reports about the instability of a charged residue, such as arginine, in a primarily hydrophobic

environment. Intermolecular interaction analyses revealed “burial” of centrally located arginine via multiple mechanisms: “local bilayer distortion, guanidium snorkeling, and peptide shifting along the bilayer normal”. Interruption of these interactions with introduction of a hydrophobic residue such as tryptophan may result in helix distortion in relation to the lipid bilayer. PINK1 protein interaction with the lipid components of the bilayer, as consequent of the R98W mutation, may have negative downstream effects in its ability to be correctly trafficked to the inner mitochondrial membrane. In addition to a localization defect, one finding that has not been demonstrated in previous literature is the apparent and significant increase in the PINK1 R98W turnover. Consequences of increased accumulation or decreased cleavage have been implied but the same has not been done for an increase in PINK1 turnover and how this may be implicated in disease. If PINK1 is being turned over at a rate more rapid than what would occur for the wild-type, then there is likely an imbalance of mitophagy occurring. Mitochondria that should have PINK1 accumulating to tag them for degradation are not being flagged. This may result in an increased presence of damaged and old mitochondria in the mitochondrial network, altering the integrity and strength of the network and speculatively resulting in premature cell death. Another consideration that could be made is that the accumulation of PINK1 R98W observed *in vivo* is not exclusively localized to mitochondria but is present in the cytosol. A couple possible mechanisms of disease with this particular variant include: (1) it is not adequately translocated to the inner mitochondrial membrane for cleavage by PARL, (2)

retrograde transport into the cytoplasm is defective post-cleavage, likely resulting in clogging and outer mitochondrial membrane accumulation,

Previous cellular studies done report impaired cleavage of PINK1 I111S^{124,130}. In contrast to these reports, our *in vitro* assay demonstrated a comparable catalytic efficiency of PARL towards His-FRET-*Hs*PINK1[70-134] I111S and WT. Additionally, PARL's affinity for His-FRET-*Hs*PINK1[70-134] I111S was comparable to that for the wild-type. The k_{cat} was significantly lower for the PD-variant than for His-FRET-*Hs*PINK1[70-134] WT. Similar to wild-type PINK1, the I111S variant resulted in Parkin recruitment in the presence of CCCP, suggesting intact import to the outer mitochondrial membrane upon membrane potential disruption was not impaired¹²⁴. This point mutation results in a decreased overall hydrophobicity of the transmembrane segment of this protein¹⁸², therefore it is plausible that the reported decrease in PARL-mediated cleavage isn't necessarily due to PARL's inability to recognize the substrate or actively cleave the substrate, but the substrate's ability to localize to the inner mitochondrial membrane where it would be cleaved by the PARL protease. Taken together, these results from our *in vitro* kinetic assay neither confirm nor refute the notion that PINK1 I111S may have defects in its trafficking to the inner mitochondrial membrane or if reported accumulation is a result of defective PARL-mediated cleavage.

The extra-transmembrane PD-linked mutation at glutamine-126 to a proline was meant to serve as a control. Analysis of patient fibroblasts harbouring this mutation

revealed fragmented mitochondrial morphology¹⁸³. No reports of altered processing have been reported for this variant, though the reported functional implications of this variant were based on its inability to recruit Parkin. Confocal imaging studies, done in collaboration with Dr. Nicolas Touret, using mCherry-PINK1 transfected HeLa cells do not exhibit an alteration in the turnover of mCherry-*HsPINK1* Q126P. Similar to the transmembrane PD-linked variants assessed using the His-FRET-*HsPINK1*[70-134] construct, there was no statistical significant difference in K_M or k_{cat}/K_M between the wild-type and Q126P. Again, there was a significant decrease in His-FRET-*HsPINK1*[70-134] Q126P turnover. Together, these results question the precision of this assay with respect to the His-FRET-*HsPINK1*[70-134] substrates. We cannot confidently confirm whether there is a cleavage defect with this variant.

To put all this information into perspective, I have prepared a model shown in **Figure 4.9**. PINK1 is constitutively being turned over *in vivo*, such that amounts detected are in very low amounts^{122,184-186}. Normal turnover of PINK1 demonstrates that there is neither a mitochondrial trafficking defect nor an impairment in PARL-mediated cleavage, as is shown for the wild-type protein. According to our *in vitro* assay, PARL protease-mediated cleavage of PINK1 transmembrane variants C92F, I111S, and Q126P may be impaired as a result of their decreased turnover. In contrast to other reports^{124,130}, R98W appears to be efficiently turned over by the PARL protease though the catalytic efficiency between wild-type and the PD-variant are comparable. Taken together, I propose that these particular variants may experience a defect in PARL-mediated proteolysis or they may experience

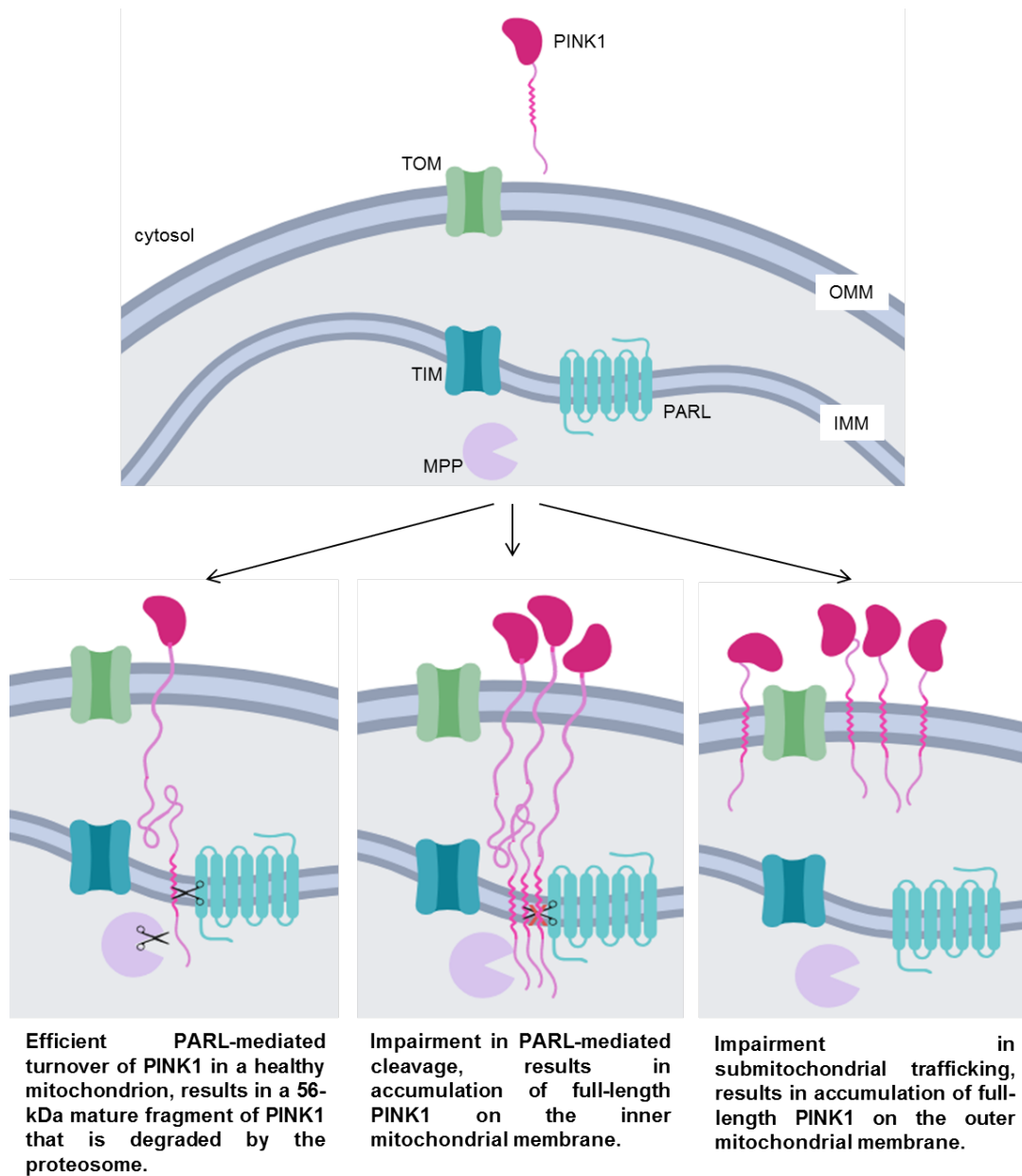


Figure 4.9. Proposed model for sub-mitochondrial localization of PINK1 variants demonstrating cleavage effects. Transmembrane variants C92F, R98W, I111S and extra-transmembrane variant Q126P demonstrated comparable catalytic efficiencies to the wild-type. Reported accumulation of PINK1 transmembrane variants C92F, R98W, and I111S may be due to a defect in PARL-mediated cleavage or an impairment in submitochondrial localization to the IMM.mitochondrial

trafficking defects, such that PINK1 is unable to localize to the inner mitochondrial membrane to meet and be proteolysed by the PARL protease.

Trafficking defects implicate other cellular proteins responsible for protein translocation. Molecular chaperones or heat shock proteins (*Hsp*) are produced by the cell in conditions of stress. Chaperones assist in folding of denatured proteins and sometimes degradation if the proteins are damaged¹⁸⁷. Weihofen *et al.* demonstrated *Hsp90* influences the subcellular distribution of PINK1 with co-chaperone *Cdc37*¹³¹. *Hsp90* accounts for localization and stability of some proteins in the cytosol, whereas the main mitochondrial chaperone is *Hsp70*. Along with *TIM44* and *Mge1*, they are responsible for the import and movement of pre-protein polypeptide domains within the mitochondrion. Submitochondrial localization of the PINK1 variants has not been studied in depth, but evidence provided for the association of PINK1 and *Hsp90* supports that speculation that it would also associate with chaperones in the mitochondrion. If mutations in PINK1 are influencing or inhibiting chaperone-mediated activity, this could account for accumulation of PINK1 observed with some PD-linked variants^{83,92,124}.

CHAPTER 5: Conclusions

5 Conclusions

This thesis sought to explore and uncover a mechanism behind the pathogenesis of PD-linked PINK1 transmembrane variants and their interaction with PARL protease. In order to assess functional implications of these variants, recombinant human PINK1 and human PARL protease were needed in adequate yield and purity. PINK1 is a very dynamic protein that functions as a cellular signal for removal of aged or damaged mitochondria. As a protein targeted to the mitochondrial membrane, PINK1 is considered a transient integral membrane protein. PARL protease, a true mitochondrial membrane resident contains a predicted 7 transmembrane segments. Neither human PINK1 or PARL have been recombinantly over-expressed, a major reason for this is that membrane proteins are very difficult to study. Their expression and purification require plenty of optimization, especially to result in a significant yield of stable protein. Membrane proteins studied *in vitro*, outside of their natural lipid environment, are prone to aggregation, misfolding, degradation, and a plethora of other protein fates. To mitigate these effects, several variables were optimized to ensure success of membrane protein purification. PARL protease and His-FRET-*Hs*PINK1[70-134] WT, C92F, I111S, and Q126P were successfully expressed and purified to a sufficient yield and purity for our *in vitro* FRET-based kinetic assay.

The rate of substrate turnover for the His-FRET-*Hs*PINK1[70-134] substrate is 1-2/hours, which indeed is quite slow however it is comparable to some findings with

kinetic studies using recombinant gamma-secretase in amyloid precursor protein cleavage¹⁸⁸. It is important to note that the kinetic results may not reflect the cleavage rates in physiologic conditions, but still may provide evidence toward defects in cleavage. Notably, some recombinant membrane proteins when extracted from the lipid bilayer can denature over time. For both recombinant PINK1 and PARL a small proportion of misfolded protein may be present in the purified protein sample. Despite the use of gel filtration, some proteins are particularly sensitive to further aggregation, especially since this step is known to further delipidate membrane protein samples¹⁸⁹. This would affect the ability of PARL to cleave the substrate by hindering access to the cleavage site. Presence of some misfolded PARL among the sample used for the assay could result in a lower presence of active PARL not accounted for in calculations, thereby negatively affecting the substrate turnover rate. Despite these potential shortcomings we demonstrate successful cleavage of recombinant human PINK1 by recombinant human PARL *in vitro*. Our kinetic results suggest PARL is a slow protease, particularly towards PINK1. Though this finding is not agreeable to the rapid turnover of PINK1 *in vivo*, together this information suggests that there are significant contributions from other proteases in the cleavage of PINK1¹⁹⁰. Regardless, our *in vitro* kinetic assay allowed us to assess the effects of the PD-linked mutations in the transmembrane domain of PINK1 on PARL-mediated cleavage.

Results from kinetic assays suggest PINK1 PD-linked variants C92F, I111S, R98W, and Q126P demonstrated comparable catalytic efficiencies to that of the wild-type.

Surprisingly, PD-linked variant R98W did not display a decrease but a significant increase in turnover rate compared to its wild-type match whereas the other PD-variants, C92F, I111S, and Q126P demonstrated significant decreases in k_{cat} though also had comparable k_{cat}/K_M values. Transitioning to a shorter synthetic construct, IQ-PINK1 peptides demonstrated comparable cleavage kinetics to the longer FRET-based substrate. Use of these IQ-*Hs*PINK1 peptides allowed for successful and relatively high confidence in the analysis of the PINK1 R98W variant. Taken together, these results allude towards a defect in some cellular processes. Whether the defect is in submitochondrial trafficking or the PARL-mediated cleavage is still unknown. Further kinetic analysis using IQ-*Hs*PINK1 peptides may provide more reliable results, and thus provide us with more confident conclusions regarding these PINK1 transmembrane PD-linked variants. Additionally, further study into the dynamics and structural implications of these point mutations will help reveal additional information about the mechanism of these PINK1 variants and how they contribute to the pathophysiology of Parkinson's disease.

Moving forward, this project will explore the mitochondrial accumulation of PINK1 in human cells. Similar to what has been done in the field, cellular studies of these particular transmembrane domain variants of PINK1 will look at cleavage defects *in vivo*. PINK1 has been cloned into the mCherry vector for confocal studies. This vector can be used to transfect HeLa cells, an immortal human cell line, for expression of PINK1. HeLa cells will be lysed and subject to SDS-PAGE for transblotting. mCherry-tagged PINK1 can be visualized using anti-mCherry

antibodies. Ideally, this assay would provide some cellular insight into physiologic cleavage events. Additionally, optimization of super-resolution microscopy of these variants would further support potential import and cleavage defect findings reported in this thesis.

Ultimately, this thesis presents *in vitro* analysis of the PARL-mediated intramembrane proteolysis of human PINK1. An established protocol to measure catalytic parameters such as the Michaelis constant, the substrate turnover rate, and the catalytic efficiency allowed us to characterize alterations in cleavage between different PINK1 PD-linked variants. This analysis, in conjunction with other *in vivo* assessments will help provide further understanding into the mechanism of PINK1-dependent mitophagy and how potential defects in PINK1 function, as a result of aberrant cleavage or trafficking, may affect health or alternately instigate disease.

References

References

- 1 Illis, L. S. Central nervous system regeneration does not occur. *Spinal Cord* **50**, 259-263, doi:10.1038/sc.2011.132 (2012).
- 2 DeLong, M. & Wichmann, T. Update on models of basal ganglia function and dysfunction. *Parkinsonism Relat Disord* **15 Suppl 3**, S237-240, doi:10.1016/S1353-8020(09)70822-3 (2009).
- 3 Hodge, G. K. & Butcher, L. L. Pars compacta of the substantia nigra modulates motor activity but is not involved importantly in regulating food and water intake. *Naunyn Schmiedebergs Arch Pharmacol* **313**, 51-67 (1980).
- 4 Lang, A. E. & Lozano, A. M. Parkinson's disease. First of two parts. *N Engl J Med* **339**, 1044-1053, doi:10.1056/NEJM199810083391506 (1998).
- 5 Calne, D. B., Stern, G. M., Laurence, D. R., Sharkey, J. & Armitage, P. L-dopa in postencephalitic parkinsonism. *Lancet* **1**, 744-746 (1969).
- 6 Calne, D. B., Stern, G. M., Spiers, A. S. & Laurence, D. R. L-dopa in idiopathic parkinsonism. *Lancet* **2**, 973-976 (1969).
- 7 Cotzias, G. C., Van Woert, M. H. & Schiffer, L. M. Aromatic amino acids and modification of parkinsonism. *N Engl J Med* **276**, 374-379, doi:10.1056/NEJM196702162760703 (1967).
- 8 Godwin-Austen, R. B., Tomlinson, E. B., Frears, C. C. & Kok, H. W. Effects of L-dopa in Parkinson's disease. *Lancet* **2**, 165-168 (1969).
- 9 Salat, D. & Tolosa, E. Levodopa in the treatment of Parkinson's disease: current status and new developments. *J Parkinsons Dis* **3**, 255-269, doi:10.3233/JPD-130186 (2013).
- 10 Deep-Brain Stimulation for Parkinson's Disease Study, G. *et al.* Deep-brain stimulation of the subthalamic nucleus or the pars interna of the globus pallidus in Parkinson's disease. *N Engl J Med* **345**, 956-963, doi:10.1056/NEJMoa000827 (2001).
- 11 Calne, D. B., Snow, B. J. & Lee, C. Criteria for diagnosing Parkinson's disease. *Ann Neurol* **32 Suppl**, S125-127 (1992).
- 12 Dick, F. D. *et al.* Environmental risk factors for Parkinson's disease and parkinsonism: the Geoparkinson study. *Occup Environ Med* **64**, 666-672, doi:10.1136/oem.2006.027003 (2007).
- 13 Jang, H., Boltz, D. A., Webster, R. G. & Smeyne, R. J. Viral parkinsonism. *Biochim Biophys Acta* **1792**, 714-721, doi:10.1016/j.bbadis.2008.08.001 (2009).
- 14 Shin, H. W. & Chung, S. J. Drug-induced parkinsonism. *J Clin Neurol* **8**, 15-21, doi:10.3988/jcn.2012.8.1.15 (2012).
- 15 Easterford, K., Clough, P., Kellett, M., Fallon, K. & Duncan, S. Reversible parkinsonism with normal beta-CIT-SPECT in patients exposed to sodium valproate. *Neurology* **62**, 1435-1437 (2004).
- 16 Jamora, D., Lim, S. H., Pan, A., Tan, L. & Tan, E. K. Valproate-induced Parkinsonism in epilepsy patients. *Mov Disord* **22**, 130-133, doi:10.1002/mds.21188 (2007).

- 17 Onofrj, M., Thomas, A. & Paci, C. Reversible parkinsonism induced by prolonged treatment with valproate. *J Neurol* **245**, 794-796 (1998).
- 18 Williams, D. R. & Litvan, I. Parkinsonian syndromes. *Continuum (Minneapolis)* **19**, 1189-1212, doi:10.1212/01.CON.0000436152.24038.e0 (2013).
- 19 Williams, D. R. *et al.* Characteristics of two distinct clinical phenotypes in pathologically proven progressive supranuclear palsy: Richardson's syndrome and PSP-parkinsonism. *Brain* **128**, 1247-1258, doi:10.1093/brain/awh488 (2005).
- 20 Gnanalingham, K. K., Byrne, E. J., Thornton, A., Sambrook, M. A. & Bannister, P. Motor and cognitive function in Lewy body dementia: comparison with Alzheimer's and Parkinson's diseases. *J Neurol Neurosurg Psychiatry* **62**, 243-252 (1997).
- 21 Barmore, R. *Diagnosis*, <<https://parkinson.org/Understanding-Parkinsons/Diagnosis>> (
- 22 McCann, H., Stevens, C. H., Cartwright, H. & Halliday, G. M. alpha-Synucleinopathy phenotypes. *Parkinsonism Relat Disord* **20 Suppl 1**, S62-67, doi:10.1016/S1353-8020(13)70017-8 (2014).
- 23 Murphy, D. D., Rueter, S. M., Trojanowski, J. Q. & Lee, V. M. Synucleins are developmentally expressed, and alpha-synuclein regulates the size of the presynaptic vesicular pool in primary hippocampal neurons. *J Neurosci* **20**, 3214-3220 (2000).
- 24 Chandra, S., Chen, X., Rizo, J., Jahn, R. & Sudhof, T. C. A broken alpha-helix in folded alpha-synuclein. *J Biol Chem* **278**, 15313-15318, doi:10.1074/jbc.M213128200 (2003).
- 25 Polymeropoulos, M. H. *et al.* Mutation in the alpha-synuclein gene identified in families with Parkinson's disease. *Science* **276**, 2045-2047 (1997).
- 26 Luk, K. C. *et al.* Pathological alpha-synuclein transmission initiates Parkinson-like neurodegeneration in nontransgenic mice. *Science* **338**, 949-953, doi:10.1126/science.1227157 (2012).
- 27 Stefanis, L. alpha-Synuclein in Parkinson's disease. *Cold Spring Harb Perspect Med* **2**, a009399, doi:10.1101/cshperspect.a009399 (2012).
- 28 Staff, H. *Parkinson's Disease: Classification*, <<https://www.umcvc.org/health-library/hw78534>> (2017).
- 29 Jankovic, J. Parkinson's disease: clinical features and diagnosis. *J Neurol Neurosurg Psychiatry* **79**, 368-376, doi:10.1136/jnnp.2007.131045 (2008).
- 30 Gelb, D. J., Oliver, E. & Gilman, S. Diagnostic criteria for Parkinson disease. *Arch Neurol* **56**, 33-39 (1999).
- 31 Yagi, S. *et al.* Progression from unilateral to bilateral parkinsonism in early Parkinson disease: implication of mesocortical dopamine dysfunction by PET. *J Nucl Med* **51**, 1250-1257, doi:10.2967/jnumed.110.076802 (2010).
- 32 Zach, H., Dirks, M., Bloem, B. R. & Helmich, R. C. The Clinical Evaluation of Parkinson's Tremor. *J Parkinsons Dis* **5**, 471-474, doi:10.3233/JPD-150650 (2015).
- 33 Morris, M. E. Movement disorders in people with Parkinson disease: a model for physical therapy. *Phys Ther* **80**, 578-597 (2000).

- 34 Thanvi, B. R., Munshi, S. K., Vijaykumar, N. & Lo, T. C. Neuropsychiatric non-
35 motor aspects of Parkinson's disease. *Postgrad Med J* **79**, 561-565 (2003).
- 36 Ma, S. Y., Roytta, M., Rinne, J. O., Collan, Y. & Rinne, U. K. Correlation between
37 neuromorphometry in the substantia nigra and clinical features in
38 Parkinson's disease using disector counts. *J Neurol Sci* **151**, 83-87 (1997).
- 39 Greffard, S. *et al.* Motor score of the Unified Parkinson Disease Rating Scale as
40 a good predictor of Lewy body-associated neuronal loss in the substantia
41 nigra. *Arch Neurol* **63**, 584-588, doi:10.1001/archneur.63.4.584 (2006).
- 42 Grosch, J., Winkler, J. & Kohl, Z. Early Degeneration of Both Dopaminergic and
43 Serotonergic Axons - A Common Mechanism in Parkinson's Disease. *Front
44 Cell Neurosci* **10**, 293, doi:10.3389/fncel.2016.00293 (2016).
- 45 Lang, A. E. & Lozano, A. M. Parkinson's disease. Second of two parts. *N Engl J
46 Med* **339**, 1130-1143, doi:10.1056/NEJM199810153391607 (1998).
- 47 Nandhagopal, R., McKeown, M. J. & Stoessl, A. J. Functional imaging in
48 Parkinson disease. *Neurology* **70**, 1478-1488,
49 doi:10.1212/01.wnl.0000310432.92489.90 (2008).
- 50 Parkinson, J. An essay on the shaking palsy. 1817. *J Neuropsychiatry Clin
51 Neurosci* **14**, 223-236; discussion 222, doi:10.1176/jnp.14.2.223 (2002).
- 52 Poewe, W. Non-motor symptoms in Parkinson's disease. *Eur J Neurol* **15
53 Suppl 1**, 14-20, doi:10.1111/j.1468-1331.2008.02056.x (2008).
- 54 Shulman, L. M., Taback, R. L., Rabinstein, A. A. & Weiner, W. J. Non-recognition
55 of depression and other non-motor symptoms in Parkinson's disease.
56 *Parkinsonism Relat Disord* **8**, 193-197 (2002).
- 57 Postuma, R. B. *et al.* Identifying prodromal Parkinson's disease: pre-motor
58 disorders in Parkinson's disease. *Mov Disord* **27**, 617-626,
59 doi:10.1002/mds.24996 (2012).
- 60 Davie, C. A. A review of Parkinson's disease. *Br Med Bull* **86**, 109-127,
61 doi:10.1093/bmb/ldn013 (2008).
- 62 Nambu, A. A new dynamic model of the cortico-basal ganglia loop. *Prog Brain
63 Res* **143**, 461-466, doi:10.1016/S0079-6123(03)43043-4 (2004).
- 64 Obeso, J. A. *et al.* Functional organization of the basal ganglia: therapeutic
65 implications for Parkinson's disease. *Mov Disord* **23 Suppl 3**, S548-559,
66 doi:10.1002/mds.22062 (2008).
- 67 Wolters, E. Non-motor extranigral signs and symptoms in Parkinson's
68 disease. *Parkinsonism Relat Disord* **15 Suppl 3**, S6-12, doi:10.1016/S1353-
69 8020(09)70770-9 (2009).
- 70 Obeso, J. A. *et al.* Missing pieces in the Parkinson's disease puzzle. *Nat Med*
71 **16**, 653-661, doi:10.1038/nm.2165 (2010).
- 72 Exner, N., Lutz, A. K., Haass, C. & Winklhofer, K. F. Mitochondrial dysfunction
73 in Parkinson's disease: molecular mechanisms and pathophysiological
74 consequences. *EMBO J* **31**, 3038-3062, doi:10.1038/emboj.2012.170 (2012).
- 75 Greenamyre, J. T., MacKenzie, G., Peng, T. I. & Stephans, S. E. Mitochondrial
76 dysfunction in Parkinson's disease. *Biochem Soc Symp* **66**, 85-97 (1999).
- 77 Hughes, A. J., Daniel, S. E., Kilford, L. & Lees, A. J. Accuracy of clinical diagnosis
78 of idiopathic Parkinson's disease: a clinico-pathological study of 100 cases. *J
79 Neurol Neurosurg Psychiatry* **55**, 181-184 (1992).

- 52 Wu, Y., Le, W. & Jankovic, J. Preclinical biomarkers of Parkinson disease. *Arch Neurol* **68**, 22-30, doi:10.1001/archneurol.2010.321 (2011).
- 53 Chung, S. J. *et al.* Common variants in PARK loci and related genes and Parkinson's disease. *Mov Disord* **26**, 280-288, doi:10.1002/mds.23376 (2011).
- 54 Giovannini, P. *et al.* Early-onset Parkinson's disease. *Mov Disord* **6**, 36-42, doi:10.1002/mds.870060107 (1991).
- 55 Pagano, G., Ferrara, N., Brooks, D. J. & Pavese, N. Age at onset and Parkinson disease phenotype. *Neurology* **86**, 1400-1407, doi:10.1212/WNL.0000000000002461 (2016).
- 56 Jankovic, J. & Kapadia, A. S. Functional decline in Parkinson disease. *Arch Neurol* **58**, 1611-1615 (2001).
- 57 Mehanna, R., Moore, S., Hou, J. G., Sarwar, A. I. & Lai, E. C. Comparing clinical features of young onset, middle onset and late onset Parkinson's disease. *Parkinsonism Relat Disord* **20**, 530-534, doi:10.1016/j.parkreldis.2014.02.013 (2014).
- 58 Kostic, V., Przedborski, S., Flaster, E. & Sternic, N. Early development of levodopa-induced dyskinesias and response fluctuations in young-onset Parkinson's disease. *Neurology* **41**, 202-205 (1991).
- 59 Stocchi, F., Vacca, L. & Radicati, F. G. How to optimize the treatment of early stage Parkinson's disease. *Transl Neurodegener* **4**, 4, doi:10.1186/2047-9158-4-4 (2015).
- 60 Morrison, J. H. & Hof, P. R. Life and death of neurons in the aging brain. *Science* **278**, 412-419 (1997).
- 61 Dupuis, L. *et al.* Mitochondria in amyotrophic lateral sclerosis: a trigger and a target. *Neurodegener Dis* **1**, 245-254, doi:10.1159/000085063 (2004).
- 62 Moreira, P. I., Carvalho, C., Zhu, X., Smith, M. A. & Perry, G. Mitochondrial dysfunction is a trigger of Alzheimer's disease pathophysiology. *Biochim Biophys Acta* **1802**, 2-10, doi:10.1016/j.bbadis.2009.10.006 (2010).
- 63 Quintanilla, R. A. & Johnson, G. V. Role of mitochondrial dysfunction in the pathogenesis of Huntington's disease. *Brain Res Bull* **80**, 242-247, doi:10.1016/j.brainresbull.2009.07.010 (2009).
- 64 Winklhofer, K. F. & Haass, C. Mitochondrial dysfunction in Parkinson's disease. *Biochim Biophys Acta* **1802**, 29-44, doi:10.1016/j.bbadis.2009.08.013 (2010).
- 65 Frank, S. *et al.* The role of dynamin-related protein 1, a mediator of mitochondrial fission, in apoptosis. *Dev Cell* **1**, 515-525 (2001).
- 66 Smirnova, E., Shurland, D. L., Ryazantsev, S. N. & van der Bliek, A. M. A human dynamin-related protein controls the distribution of mitochondria. *J Cell Biol* **143**, 351-358 (1998).
- 67 Chan, D. C. Mitochondria: dynamic organelles in disease, aging, and development. *Cell* **125**, 1241-1252, doi:10.1016/j.cell.2006.06.010 (2006).
- 68 Kim, I., Rodriguez-Enriquez, S. & Lemasters, J. J. Selective degradation of mitochondria by mitophagy. *Arch Biochem Biophys* **462**, 245-253, doi:10.1016/j.abb.2007.03.034 (2007).

- 69 Lemasters, J. J. Selective mitochondrial autophagy, or mitophagy, as a targeted defense against oxidative stress, mitochondrial dysfunction, and aging. *Rejuvenation Res* **8**, 3-5, doi:10.1089/rej.2005.8.3 (2005).
- 70 Cerveny, K. L., Studer, S. L., Jensen, R. E. & Sesaki, H. Yeast mitochondrial division and distribution require the cortical num1 protein. *Dev Cell* **12**, 363-375, doi:10.1016/j.devcel.2007.01.017 (2007).
- 71 Detmer, S. A. & Chan, D. C. Functions and dysfunctions of mitochondrial dynamics. *Nat Rev Mol Cell Biol* **8**, 870-879, doi:10.1038/nrm2275 (2007).
- 72 Hoppins, S., Lackner, L. & Nunnari, J. The machines that divide and fuse mitochondria. *Annu Rev Biochem* **76**, 751-780, doi:10.1146/annurev.biochem.76.071905.090048 (2007).
- 73 Tatsuta, T. & Langer, T. Quality control of mitochondria: protection against neurodegeneration and ageing. *EMBO J* **27**, 306-314, doi:10.1038/sj.emboj.7601972 (2008).
- 74 Ashrafi, G. & Schwarz, T. L. The pathways of mitophagy for quality control and clearance of mitochondria. *Cell Death Differ* **20**, 31-42, doi:10.1038/cdd.2012.81 (2013).
- 75 Strappazon, F. *et al.* AMBRA1 is able to induce mitophagy via LC3 binding, regardless of PARKIN and p62/SQSTM1. *Cell Death Differ* **22**, 517, doi:10.1038/cdd.2014.190 (2015).
- 76 Lackner, L. L. Shaping the dynamic mitochondrial network. *BMC Biol* **12**, 35, doi:10.1186/1741-7007-12-35 (2014).
- 77 Rodolfo, C., Campello, S. & Cecconi, F. Mitophagy in neurodegenerative diseases. *Neurochem Int* **117**, 156-166, doi:10.1016/j.neuint.2017.08.004 (2018).
- 78 Martinez-Vicente, M. Neuronal Mitophagy in Neurodegenerative Diseases. *Front Mol Neurosci* **10**, 64, doi:10.3389/fnmol.2017.00064 (2017).
- 79 Unoki, M. & Nakamura, Y. Growth-suppressive effects of BPOZ and EGR2, two genes involved in the PTEN signaling pathway. *Oncogene* **20**, 4457-4465, doi:10.1038/sj.onc.1204608 (2001).
- 80 Manning, G., Whyte, D. B., Martinez, R., Hunter, T. & Sudarsanam, S. The protein kinase complement of the human genome. *Science* **298**, 1912-1934, doi:10.1126/science.1075762 (2002).
- 81 Schubert, A. F. *et al.* Structure of PINK1 in complex with its substrate ubiquitin. *Nature* **552**, 51-56, doi:10.1038/nature24645 (2017).
- 82 Kumar, A. *et al.* Structure of PINK1 and mechanisms of Parkinson's disease-associated mutations. *Elife* **6**, doi:10.7554/eLife.29985 (2017).
- 83 Deas, E. *et al.* PINK1 cleavage at position A103 by the mitochondrial protease PARL. *Hum Mol Genet* **20**, 867-879, doi:10.1093/hmg/ddq526 (2011).
- 84 Ferrara, N. & Kerbel, R. S. Angiogenesis as a therapeutic target. *Nature* **438**, 967-974, doi:10.1038/nature04483 (2005).
- 85 Hannigan, G., Troussard, A. A. & Dedhar, S. Integrin-linked kinase: a cancer therapeutic target unique among its ILK. *Nat Rev Cancer* **5**, 51-63, doi:10.1038/nrc1524 (2005).
- 86 Herman, S. E. *et al.* Bruton tyrosine kinase represents a promising therapeutic target for treatment of chronic lymphocytic leukemia and is

- effectively targeted by PCI-32765. *Blood* **117**, 6287-6296, doi:10.1182/blood-2011-01-328484 (2011).
- 87 Shimokawa, H. & Takeshita, A. Rho-kinase is an important therapeutic target in cardiovascular medicine. *Arterioscler Thromb Vasc Biol* **25**, 1767-1775, doi:10.1161/01.ATV.0000176193.83629.c8 (2005).
- 88 Okatsu, K. *et al.* PINK1 autophosphorylation upon membrane potential dissipation is essential for Parkin recruitment to damaged mitochondria. *Nat Commun* **3**, 1016, doi:10.1038/ncomms2016 (2012).
- 89 Okatsu, K., Kimura, M., Oka, T., Tanaka, K. & Matsuda, N. Unconventional PINK1 localization to the outer membrane of depolarized mitochondria drives Parkin recruitment. *J Cell Sci* **128**, 964-978, doi:10.1242/jcs.161000 (2015).
- 90 Silvestri, L. *et al.* Mitochondrial import and enzymatic activity of PINK1 mutants associated to recessive parkinsonism. *Hum Mol Genet* **14**, 3477-3492, doi:10.1093/hmg/ddi377 (2005).
- 91 Takatori, S., Ito, G. & Iwatsubo, T. Cytoplasmic localization and proteasomal degradation of N-terminally cleaved form of PINK1. *Neurosci Lett* **430**, 13-17, doi:10.1016/j.neulet.2007.10.019 (2008).
- 92 Jin, S. M. *et al.* Mitochondrial membrane potential regulates PINK1 import and proteolytic destabilization by PARL. *J Cell Biol* **191**, 933-942, doi:10.1083/jcb.201008084 (2010).
- 93 Lin, W. & Kang, U. J. Structural determinants of PINK1 topology and dual subcellular distribution. *BMC Cell Biol* **11**, 90, doi:10.1186/1471-2121-11-90 (2010).
- 94 Shiba-Fukushima, K. *et al.* PINK1-mediated phosphorylation of the Parkin ubiquitin-like domain primes mitochondrial translocation of Parkin and regulates mitophagy. *Sci Rep* **2**, 1002, doi:10.1038/srep01002 (2012).
- 95 Zhou, C. *et al.* The kinase domain of mitochondrial PINK1 faces the cytoplasm. *Proc Natl Acad Sci U S A* **105**, 12022-12027, doi:10.1073/pnas.0802814105 (2008).
- 96 Becker, D., Richter, J., Tocilescu, M. A., Przedborski, S. & Voos, W. Pink1 kinase and its membrane potential ($\Delta\psi$)-dependent cleavage product both localize to outer mitochondrial membrane by unique targeting mode. *J Biol Chem* **287**, 22969-22987, doi:10.1074/jbc.M112.365700 (2012).
- 97 Jin, S. M. & Youle, R. J. PINK1- and Parkin-mediated mitophagy at a glance. *J Cell Sci* **125**, 795-799, doi:10.1242/jcs.093849 (2012).
- 98 Sekine, S. & Youle, R. J. PINK1 import regulation; a fine system to convey mitochondrial stress to the cytosol. *BMC Biol* **16**, 2, doi:10.1186/s12915-017-0470-7 (2018).
- 99 Ulmschneider, M. B., Sansom, M. S. & Di Nola, A. Properties of integral membrane protein structures: derivation of an implicit membrane potential. *Proteins* **59**, 252-265, doi:10.1002/prot.20334 (2005).
- 100 Ulmschneider, M. B. *et al.* Transmembrane helices containing a charged arginine are thermodynamically stable. *Eur Biophys J* **46**, 627-637, doi:10.1007/s00249-017-1206-x (2017).

- 101 Urban, S. & Freeman, M. Substrate specificity of rhomboid intramembrane proteases is governed by helix-breaking residues in the substrate transmembrane domain. *Mol Cell* **11**, 1425-1434 (2003).
- 102 Yuzuru Imai, N. H. in *Autophagy: Cancer, Other Pathologies, Inflammation, Immunity, Infection, and Aging* Vol. 4 (ed Elsevier) Ch. 15, 227-238 (2014).
- 103 Koonin, E. V. *et al.* The rhomboids: a nearly ubiquitous family of intramembrane serine proteases that probably evolved by multiple ancient horizontal gene transfers. *Genome Biol* **4**, R19 (2003).
- 104 Jeyaraju, D. V., McBride, H. M., Hill, R. B. & Pellegrini, L. Structural and mechanistic basis of Parl activity and regulation. *Cell Death Differ* **18**, 1531-1539, doi:10.1038/cdd.2011.22 (2011).
- 105 Pellegrini, L. & Scorrano, L. A cut short to death: Parl and Opa1 in the regulation of mitochondrial morphology and apoptosis. *Cell Death Differ* **14**, 1275-1284, doi:10.1038/sj.cdd.4402145 (2007).
- 106 Shi, G. *et al.* Functional alteration of PARL contributes to mitochondrial dysregulation in Parkinson's disease. *Hum Mol Genet* **20**, 1966-1974, doi:10.1093/hmg/ddr077 (2011).
- 107 Heinitz, S., Klein, C. & Djarmati, A. The p.S77N presenilin-associated rhomboid-like protein mutation is not a frequent cause of early-onset Parkinson's disease. *Mov Disord* **26**, 2441-2442, doi:10.1002/mds.23889 (2011).
- 108 Spinazzi, M. & De Strooper, B. PARL: The mitochondrial rhomboid protease. *Semin Cell Dev Biol* **60**, 19-28, doi:10.1016/j.semcdb.2016.07.034 (2016).
- 109 Saita, S. *et al.* PARL mediates Smac proteolytic maturation in mitochondria to promote apoptosis. *Nat Cell Biol* **19**, 318-328, doi:10.1038/ncb3488 (2017).
- 110 McQuibban, G. A., Saurya, S. & Freeman, M. Mitochondrial membrane remodelling regulated by a conserved rhomboid protease. *Nature* **423**, 537-541, doi:10.1038/nature01633 (2003).
- 111 McQuibban, G. A., Lee, J. R., Zheng, L., Juusola, M. & Freeman, M. Normal mitochondrial dynamics requires rhomboid-7 and affects Drosophila lifespan and neuronal function. *Curr Biol* **16**, 982-989, doi:10.1016/j.cub.2006.03.062 (2006).
- 112 Rahman, M. & Kylsten, P. Rhomboid-7 over-expression results in Opa1-like processing and malfunctioning mitochondria. *Biochem Biophys Res Commun* **414**, 315-320, doi:10.1016/j.bbrc.2011.09.047 (2011).
- 113 Noble, S., Ismail, A., Godoy, R., Xi, Y. & Ekker, M. Zebrafish Parla- and Parlb-deficiency affects dopaminergic neuron patterning and embryonic survival. *J Neurochem* **122**, 196-207, doi:10.1111/j.1471-4159.2012.07758.x (2012).
- 114 Cipolat, S. *et al.* Mitochondrial rhomboid PARL regulates cytochrome c release during apoptosis via OPA1-dependent cristae remodeling. *Cell* **126**, 163-175, doi:10.1016/j.cell.2006.06.021 (2006).
- 115 Wai, T. *et al.* The membrane scaffold SLP2 anchors a proteolytic hub in mitochondria containing PARL and the i-AAA protease YME1L. *EMBO Rep* **17**, 1844-1856, doi:10.15252/embr.201642698 (2016).
- 116 Gispert, S. *et al.* Parkinson phenotype in aged PINK1-deficient mice is accompanied by progressive mitochondrial dysfunction in absence of

- neurodegeneration. *PLoS One* **4**, e5777, doi:10.1371/journal.pone.0005777 (2009).
- 117 Lu, W. *et al.* Genetic deficiency of the mitochondrial protein PGAM5 causes a Parkinson's-like movement disorder. *Nat Commun* **5**, 4930, doi:10.1038/ncomms5930 (2014).
- 118 Okatsu, K. *et al.* A dimeric PINK1-containing complex on depolarized mitochondria stimulates Parkin recruitment. *J Biol Chem* **288**, 36372-36384, doi:10.1074/jbc.M113.509653 (2013).
- 119 Lazarou, M. *et al.* The ubiquitin kinase PINK1 recruits autophagy receptors to induce mitophagy. *Nature* **524**, 309-314, doi:10.1038/nature14893 (2015).
- 120 Klein, C. & Westenberger, A. Genetics of Parkinson's disease. *Cold Spring Harb Perspect Med* **2**, a008888, doi:10.1101/cshperspect.a008888 (2012).
- 121 Geisler, S. *et al.* The PINK1/Parkin-mediated mitophagy is compromised by PD-associated mutations. *Autophagy* **6**, 871-878 (2010).
- 122 Narendra, D. P. *et al.* PINK1 is selectively stabilized on impaired mitochondria to activate Parkin. *PLoS Biol* **8**, e1000298, doi:10.1371/journal.pbio.1000298 (2010).
- 123 Seibler, P. *et al.* Mitochondrial Parkin recruitment is impaired in neurons derived from mutant PINK1 induced pluripotent stem cells. *J Neurosci* **31**, 5970-5976, doi:10.1523/JNEUROSCI.4441-10.2011 (2011).
- 124 Meissner, C., Lorenz, H., Hehn, B. & Lemberg, M. K. Intramembrane protease PARL defines a negative regulator of PINK1- and PARK2/Parkin-dependent mitophagy. *Autophagy* **11**, 1484-1498, doi:10.1080/15548627.2015.1063763 (2015).
- 125 Bonifati, V. *et al.* Early-onset parkinsonism associated with PINK1 mutations: frequency, genotypes, and phenotypes. *Neurology* **65**, 87-95, doi:10.1212/01.wnl.0000167546.39375.82 (2005).
- 126 Ibanez, P. *et al.* Mutational analysis of the PINK1 gene in early-onset parkinsonism in Europe and North Africa. *Brain* **129**, 686-694, doi:10.1093/brain/awl005 (2006).
- 127 Valente, E. M. *et al.* Hereditary early-onset Parkinson's disease caused by mutations in PINK1. *Science* **304**, 1158-1160, doi:10.1126/science.1096284 (2004).
- 128 Song, S. *et al.* Characterization of PINK1 (PTEN-induced putative kinase 1) mutations associated with Parkinson disease in mammalian cells and *Drosophila*. *J Biol Chem* **288**, 5660-5672, doi:10.1074/jbc.M112.430801 (2013).
- 129 Fallaize, D., Chin, L. S. & Li, L. Differential submitochondrial localization of PINK1 as a molecular switch for mediating distinct mitochondrial signaling pathways. *Cell Signal* **27**, 2543-2554, doi:10.1016/j.cellsig.2015.09.020 (2015).
- 130 Meissner, C., Lorenz, H., Weihofen, A., Selkoe, D. J. & Lemberg, M. K. The mitochondrial intramembrane protease PARL cleaves human Pink1 to regulate Pink1 trafficking. *J Neurochem* **117**, 856-867, doi:10.1111/j.1471-4159.2011.07253.x (2011).

- 131 Weihofen, A., Ostaszewski, B., Minami, Y. & Selkoe, D. J. Pink1 Parkinson mutations, the Cdc37/Hsp90 chaperones and Parkin all influence the maturation or subcellular distribution of Pink1. *Hum Mol Genet* **17**, 602-616, doi:10.1093/hmg/ddm334 (2008).
- 132 Russ, W. P. & Engelman, D. M. The GxxxG motif: a framework for transmembrane helix-helix association. *J Mol Biol* **296**, 911-919, doi:10.1006/jmbi.1999.3489 (2000).
- 133 Marongiu, R. *et al.* Whole gene deletion and splicing mutations expand the PINK1 genotypic spectrum. *Hum Mutat* **28**, 98, doi:10.1002/humu.9472 (2007).
- 134 Sim, C. H. *Investigating the role of PINK1 in Parkinson's disease*, The University of Melbourne, (2011).
- 135 Dickey, S. W., Baker, R. P., Cho, S. & Urban, S. Proteolysis inside the membrane is a rate-governed reaction not driven by substrate affinity. *Cell* **155**, 1270-1281, doi:10.1016/j.cell.2013.10.053 (2013).
- 136 Dusterhoft, S., Kunzel, U. & Freeman, M. Rhomboid proteases in human disease: Mechanisms and future prospects. *Biochim Biophys Acta Mol Cell Res* **1864**, 2200-2209, doi:10.1016/j.bbamcr.2017.04.016 (2017).
- 137 Strisovsky, K., Sharpe, H. J. & Freeman, M. Sequence-specific intramembrane proteolysis: identification of a recognition motif in rhomboid substrates. *Mol Cell* **36**, 1048-1059, doi:10.1016/j.molcel.2009.11.006 (2009).
- 138 Prestel, J. *et al.* Clinical and molecular characterisation of a Parkinson family with a novel PINK1 mutation. *J Neurol* **255**, 643-648, doi:10.1007/s00415-008-0763-4 (2008).
- 139 Seddon, A. M., Curnow, P. & Booth, P. J. Membrane proteins, lipids and detergents: not just a soap opera. *Biochim Biophys Acta* **1666**, 105-117, doi:10.1016/j.bbamem.2004.04.011 (2004).
- 140 Passow, H. Molecular aspects of band 3 protein-mediated anion transport across the red blood cell membrane. *Rev Physiol Biochem Pharmacol* **103**, 61-203 (1986).
- 141 Brooks, C. L., Morrison, M. & Joanne Lemieux, M. Rapid expression screening of eukaryotic membrane proteins in *Pichia pastoris*. *Protein Sci* **22**, 425-433, doi:10.1002/pro.2223 (2013).
- 142 Korepanova, A. *et al.* Cloning and expression of multiple integral membrane proteins from *Mycobacterium tuberculosis* in *Escherichia coli*. *Protein Sci* **14**, 148-158, doi:10.1110/ps.041022305 (2005).
- 143 White, S. *Membrane Proteins of Known 3D Structures*, <<http://blanco.biomol.uci.edu/mpstruc/>> (1998).
- 144 Larsen, M. W., Bornscheuer, U. T. & Hult, K. Expression of *Candida antarctica* lipase B in *Pichia pastoris* and various *Escherichia coli* systems. *Protein Expr Purif* **62**, 90-97, doi:10.1016/j.pep.2008.07.012 (2008).
- 145 Alberts, B., Johnson, A. & Lewis, J. *Molecular Biology of the Cell: Membrane Proteins*. Vol. 4th (New York: Garland Science, 2002).
- 146 Arutyunova, E. *et al.* Allosteric regulation of rhomboid intramembrane proteolysis. *EMBO J* **33**, 1869-1881, doi:10.15252/embj.201488149 (2014).

- 147 Baba, T. *et al.* Construction of Escherichia coli K-12 in-frame, single-gene knockout mutants: the Keio collection. *Mol Syst Biol* **2**, 2006 0008, doi:10.1038/msb4100050 (2006).
- 148 Cereghino, J. L. & Cregg, J. M. Heterologous protein expression in the methylotrophic yeast *Pichia pastoris*. *FEMS Microbiol Rev* **24**, 45-66 (2000).
- 149 Cregg, J. M., Vedvick, T. S. & Raschke, W. C. Recent advances in the expression of foreign genes in *Pichia pastoris*. *Biotechnology (N Y)* **11**, 905-910 (1993).
- 150 Ahmad, M., Hirz, M., Pichler, H. & Schwab, H. Protein expression in *Pichia pastoris*: recent achievements and perspectives for heterologous protein production. *Appl Microbiol Biotechnol* **98**, 5301-5317, doi:10.1007/s00253-014-5732-5 (2014).
- 151 Inan, M. & Meagher, M. M. Non-repressing carbon sources for alcohol oxidase (AOX1) promoter of *Pichia pastoris*. *J Biosci Bioeng* **92**, 585-589 (2001).
- 152 Hasslacher, M. *et al.* High-level intracellular expression of hydroxynitrile lyase from the tropical rubber tree *Hevea brasiliensis* in microbial hosts. *Protein Expr Purif* **11**, 61-71, doi:10.1006/prep.1997.0765 (1997).
- 153 Hartmann, L., Kugler, V. & Wagner, R. Expression of Eukaryotic Membrane Proteins in *Pichia pastoris*. *Methods Mol Biol* **1432**, 143-162, doi:10.1007/978-1-4939-3637-3_10 (2016).
- 154 Rodriguez, F. *et al.* Structural model for the protein-translocating element of the twin-arginine transport system. *Proc Natl Acad Sci U S A* **110**, E1092-1101, doi:10.1073/pnas.1219486110 (2013).
- 155 McDowell, D. G., Burns, N. A. & Parkes, H. C. Localised sequence regions possessing high melting temperatures prevent the amplification of a DNA mimic in competitive PCR. *Nucleic Acids Res* **26**, 3340-3347 (1998).
- 156 Kumar, A. & Kaur, J. Primer Based Approach for PCR Amplification of High GC Content Gene: Mycobacterium Gene as a Model. *Mol Biol Int* **2014**, 937308, doi:10.1155/2014/937308 (2014).
- 157 Sahdev, S., Saini, S., Tiwari, P., Saxena, S. & Singh Saini, K. Amplification of GC-rich genes by following a combination strategy of primer design, enhancers and modified PCR cycle conditions. *Mol Cell Probes* **21**, 303-307, doi:10.1016/j.mcp.2007.03.004 (2007).
- 158 Chester, N. & Marshak, D. R. Dimethyl sulfoxide-mediated primer T_m reduction: a method for analyzing the role of renaturation temperature in the polymerase chain reaction. *Anal Biochem* **209**, 284-290, doi:10.1006/abio.1993.1121 (1993).
- 159 Delidow, B. C., Lynch, J. P., Peluso, J. J. & White, B. A. Polymerase chain reaction : basic protocols. *Methods Mol Biol* **15**, 1-29, doi:10.1385/0-89603-244-2:1 (1993).
- 160 Ho, S. N., Hunt, H. D., Horton, R. M., Pullen, J. K. & Pease, L. R. Site-directed mutagenesis by overlap extension using the polymerase chain reaction. *Gene* **77**, 51-59 (1989).
- 161 Shenoy, A. R. & Visweswariah, S. S. Site-directed mutagenesis using a single mutagenic oligonucleotide and DpnI digestion of template DNA. *Anal Biochem* **319**, 335-336 (2003).

- 162 Baneyx, F. Recombinant protein expression in *Escherichia coli*. *Curr Opin Biotechnol* **10**, 411-421 (1999).
- 163 Nilsson, J., Stahl, S., Lundeberg, J., Uhlen, M. & Nygren, P. A. Affinity fusion strategies for detection, purification, and immobilization of recombinant proteins. *Protein Expr Purif* **11**, 1-16, doi:10.1006/prep.1997.0767 (1997).
- 164 Arutyunova, E., Panigrahi, R., Strisovsky, K. & Lemieux, M. J. Production of Recombinant Rhomboid Proteases. *Methods Enzymol* **584**, 255-278, doi:10.1016/bs.mie.2016.10.031 (2017).
- 165 Structural Genomics, C. *et al.* Protein production and purification. *Nat Methods* **5**, 135-146, doi:10.1038/nmeth.f.202 (2008).
- 166 Francis, D. M. & Page, R. Strategies to optimize protein expression in *E. coli*. *Curr Protoc Protein Sci* **Chapter 5**, Unit 5 24 21-29, doi:10.1002/0471140864.ps0524s61 (2010).
- 167 Baldwin, R. L. Temperature dependence of the hydrophobic interaction in protein folding. *Proc Natl Acad Sci U S A* **83**, 8069-8072 (1986).
- 168 Spiess, C., Beil, A. & Ehrmann, M. A temperature-dependent switch from chaperone to protease in a widely conserved heat shock protein. *Cell* **97**, 339-347 (1999).
- 169 Guzman, L. M., Belin, D., Carson, M. J. & Beckwith, J. Tight regulation, modulation, and high-level expression by vectors containing the arabinose PBAD promoter. *J Bacteriol* **177**, 4121-4130 (1995).
- 170 Porath, J. Immobilized metal ion affinity chromatography. *Protein Expr Purif* **3**, 263-281 (1992).
- 171 Pellegrini, L. *et al.* PAMP and PARL, two novel putative metalloproteases interacting with the COOH-terminus of Presenilin-1 and -2. *J Alzheimers Dis* **3**, 181-190 (2001).
- 172 Arutyunova, E. *et al.* An internally quenched peptide as a new model substrate for rhomboid intramembrane proteases. *Biol Chem* **399**, 1389-1397, doi:10.1515/hsz-2018-0255 (2018).
- 173 Freeman, M. Rhomboid proteases and their biological functions. *Annu Rev Genet* **42**, 191-210, doi:10.1146/annurev.genet.42.110807.091628 (2008).
- 174 Hohenblum, H., Gasser, B., Maurer, M., Borth, N. & Mattanovich, D. Effects of gene dosage, promoters, and substrates on unfolded protein stress of recombinant *Pichia pastoris*. *Biotechnol Bioeng* **85**, 367-375, doi:10.1002/bit.10904 (2004).
- 175 Norden, K. *et al.* Increasing gene dosage greatly enhances recombinant expression of aquaporins in *Pichia pastoris*. *BMC Biotechnol* **11**, 47, doi:10.1186/1472-6750-11-47 (2011).
- 176 Bernales, S., McDonald, K. L. & Walter, P. Autophagy counterbalances endoplasmic reticulum expansion during the unfolded protein response. *PLoS Biol* **4**, e423, doi:10.1371/journal.pbio.0040423 (2006).
- 177 Liu, C. Y. & Kaufman, R. J. The unfolded protein response. *J Cell Sci* **116**, 1861-1862, doi:10.1242/jcs.00408 (2003).
- 178 Liu, Y., Song, Y., Madahar, V. & Liao, J. Quantitative Forster resonance energy transfer analysis for kinetic determinations of SUMO-specific protease. *Anal Biochem* **422**, 14-21, doi:10.1016/j.ab.2011.12.019 (2012).

- 179 Quiros, P. M., Langer, T. & Lopez-Otin, C. New roles for mitochondrial proteases in health, ageing and disease. *Nat Rev Mol Cell Biol* **16**, 345-359, doi:10.1038/nrm3984 (2015).
- 180 Ghezzi, D. *et al.* Mutations in TTC19 cause mitochondrial complex III deficiency and neurological impairment in humans and flies. *Nat Genet* **43**, 259-263, doi:10.1038/ng.761 (2011).
- 181 Saunders, C. *et al.* CLPB variants associated with autosomal-recessive mitochondrial disorder with cataract, neutropenia, epilepsy, and methylglutaconic aciduria. *Am J Hum Genet* **96**, 258-265, doi:10.1016/j.ajhg.2014.12.020 (2015).
- 182 Sim, C. H., Gabriel, K., Mills, R. D., Culvenor, J. G. & Cheng, H. C. Analysis of the regulatory and catalytic domains of PTEN-induced kinase-1 (PINK1). *Hum Mutat* **33**, 1408-1422, doi:10.1002/humu.22127 (2012).
- 183 Exner, N. *et al.* Loss-of-function of human PINK1 results in mitochondrial pathology and can be rescued by parkin. *J Neurosci* **27**, 12413-12418, doi:10.1523/JNEUROSCI.0719-07.2007 (2007).
- 184 Beinlich, F. R., Drees, C., Piehler, J. & Busch, K. B. Shuttling of PINK1 between Mitochondrial Microcompartments Resolved by Triple-Color Superresolution Microscopy. *ACS Chem Biol* **10**, 1970-1976, doi:10.1021/acscchembio.5b00295 (2015).
- 185 Matsuda, N. *et al.* PINK1 stabilized by mitochondrial depolarization recruits Parkin to damaged mitochondria and activates latent Parkin for mitophagy. *J Cell Biol* **189**, 211-221, doi:10.1083/jcb.200910140 (2010).
- 186 Yamano, K. & Youle, R. J. PINK1 is degraded through the N-end rule pathway. *Autophagy* **9**, 1758-1769, doi:10.4161/auto.24633 (2013).
- 187 Whitley, D., Goldberg, S. P. & Jordan, W. D. Heat shock proteins: a review of the molecular chaperones. *J Vasc Surg* **29**, 748-751 (1999).
- 188 Kamp, F. *et al.* Intramembrane proteolysis of beta-amyloid precursor protein by gamma-secretase is an unusually slow process. *Biophys J* **108**, 1229-1237, doi:10.1016/j.bpj.2014.12.045 (2015).
- 189 Lemieux, M. J., Reithmeier, R. A. & Wang, D. N. Importance of detergent and phospholipid in the crystallization of the human erythrocyte anion-exchanger membrane domain. *J Struct Biol* **137**, 322-332 (2002).
- 190 Greene, A. W. *et al.* Mitochondrial processing peptidase regulates PINK1 processing, import and Parkin recruitment. *EMBO Rep* **13**, 378-385, doi:10.1038/embor.2012.14 (2012).
- 191 Nair, S. S., Subba Reddy, N. & Hareesha, K. Motif mining: an assessment and perspective for amyloid fibril prediction tool. *Bioinformatics* **8**, 70-74 (2012).
- 192 Lopez de la Paz, M. & Serrano, L. Sequence determinants of amyloid fibril formation. *Proc Natl Acad Sci U S A* **101**, 87-92, doi:10.1073/pnas.2634884100 (2004).

Appendix

Appendix

Buffers

10X Potassium phosphate buffer

23 g K_2HPO_4

118.13 g KH_2PO_4

900 mL ddH₂O

pH to 6.0

Fill remaining volume to 1 L

10X Yeast Nitrogen Base buffer

34 g yeast nitrogen base without amino acids and without ammonium sulphate

100 g ammonium sulphate

Fill to 1 L with ddH₂O

10X TB salts

23.1 g KH_2PO_4

125.44 g K_2HPO_4

Fill to 1 L with ddH₂O

50X TAE

242 g Tris

18.61 g disodium EDTA

57.1 mL acetic acid

Fill to 1 L with ddH₂O

1X SDS

144 g glycine

30.2 g Tris

10 g SDS

Fill to 1 L with ddH₂O

Anode buffer

24.22 g Tris

500 mL ddH₂O

pH to 8.9

Fill remaining volume to 1 L

Cathode buffer

6.055 g Tris

8.96 g tricine

5 mL 10% SDS

Fill to 500 mL with ddH₂O

Media

LB (1 L)

25 g LB powder

Fill to 1 L ddH₂O

(For plates, add 20 g agar)

TB (1 L)

24 g yeast extract (2.4%)

12 g tryptone (1.2%)

5 g glycerol (0.5%)

Fill to 900 mL with ddH₂O

100 mL 10X TB salts

Low-salt LB (1 L)

5 g yeast extract

10 g tryptone

5 g NaCl

900 mL ddH₂O

pH to 7.5

Fill remaining volume to 1 L

(For plates, add 20 g agar)

YPD (1 L)

10 g yeast extract

20 g peptone

Fill to 900 mL with ddH₂O

100 mL 20% dextrose

(For plates, add 20 g agar)

YPDS (1 L)

10 g yeast extract

20 g peptone

182.17 g sorbitol

Fill to 900 mL with ddH₂O

100 mL 20% dextrose

(For plates, add 20 g agar)

BMGY (1 L)

10 g yeast extract

20 g peptone

Fill to 780 mL with ddH₂O

100 mL 10X Potassium Phosphate buffer

100 mL 10X YNB buffer

2 mL 500X biotin

20 mL 50% sterile glycerol

BMMY (1 L)

10 g yeast extract

20 g peptone

Fill to 790 mL with ddH₂O

100 mL 10X Potassium Phosphate buffer

100 mL 10X YNB buffer

2 mL 500X biotin

10 mL 100% methanol

Gels

SDS-PAGE gel

When making 14% resolving + 4% stacking gels, the resolving layer is always prepared first. To make two gels 3.9 mL of ddH₂O, 3.5 mL of 40% acrylamide, 2.5 mL 1.5 M Tris-HCl pH 8.8, and 100 µL 10% SDS were combined and thoroughly mixed. 100 µL 10% APS and 15 µL TEMED were then added, quickly mixed, and poured between two plates where the reaction mixture polymerized forming an evenly cast resolving layer for the gel. Preparation of the stacking layer required 6.4 mL ddH₂O, 1 mL 40% acrylamide, 2.5 mL 0.5 M Tris-HCl pH 6.8, 100 µL 10% SDS, 10 µL 10% APS and 15 µL TEMED before being poured on top of the formed resolving layer. A 10-well forming comb was inserted into the solution between the plates. Upon complete polymerization, the comb was removed and the gel was ready to be used for electrophoresis.

SDS-PAGE electrophoresis requires a single buffer, 1X SDS running buffer, to fill both the inner and outer chambers of the gel electrophoresis apparatus.

Tricine gel

Similar to the preparation of an SDS-PAGE gel, tricine gels have both a resolving layer and a stacking layer. The 13% resolving layer is made of 3.9 mL 40% acrylamide, 4 mL 3X tricine gel buffer, 1.5 g glycerol, 2.9 mL ddH₂O, 60 µL APS, and 6 µL TEMED. Once formed, the 4% stacking gel is made and poured on top. The stacking layer is made of 0.6 mL 40% acrylamide, 1.5 mL 3X tricine gel buffer, 3.85 mL ddH₂O, 90 µL APS, and 6 µL TEMED.

Running of a tricine gel requires two different buffers, a cathode buffer and an anode buffer. The cathode buffer is used to fill the inner chamber, whereas the anode buffer is used to fill the outer chamber.

2% Agarose gel

For a gel thickness of about 1 cm, 1.4 g of agarose was dissolved in 70 mL of 1X TAE buffer in an Erlenmeyer flask. The solution was microwaved to aid the dissolving of agarose. Following complete homogeneity of the solution, the solution was left at room temperature to cool to a temperature of approximately 50 °C before adding 7 µL of ethidium bromide. The solution was then poured into a gel caster and left to polymerize as the temperature reached room temperature.

0.5% Agarose gel

The protocol to make a 0.5% agarose gel is identical to that explained in section 2.3.3, with the exception of the amount of agarose. Instead of using 1.4 g of agarose, 0.35 g of agarose was dissolved in 70 mL of 1X TAE buffer.

PINK1 fibril formation studies

Protein aggregation is a common theme between many neurodegenerative diseases. This aggregation is typically a result of protein misfolding. Oftentimes, the misfolding of protein is a mechanism of quality control within the cell in response to cellular stress or damage. When there is aberrant accumulation or aggregation of proteins in healthy cells, normal, healthy functions begin to go awry. The formation of amyloid fibrils is characteristic of many protein misfolding-linked diseases. Benchmark examples are amyloid- β 42 (A β 42) peptide in Alzheimer's disease (AD) or huntingtin (HTT) in Huntington's disease (HD). Recently, the idea of amyloid fibril formation in Parkinson's disease has been explored. The presence and aggregation of alpha-synuclein protein in PD has been identified as a main component of the lewy bodies found in the brains of PD patients. Similarly to alpha-synuclein, other proteins, such as PINK1, may demonstrate similar mechanisms of protein misfolding - contributing to the pathogenesis of PD.

Computational predictions of PINK1 propensity to aggregate

We question whether regions near the TMD of PINK1 contribute to its association (dimerization) (Okatsu 2013) or aggregation, and subsequent PD pathologies. The formation of PINK1-stabilized aggresomes has been reported in mammalian cells (Um 2009; Um 2010). Additionally, histologic studies have demonstrated increases in both soluble and insoluble forms of PINK1 in various rat models of PD (6-hydroxydopamine-, rotenone-, or MG132-induced PD) (Um 2010). Our structural analysis of PINK1 using *in silico* methods revealed some regions of disorder, particularly in the group-named juxtamembrane region, found between the transmembrane domain and the kinase domain. To determine if this region and surrounding areas result in aggregation, intrinsic properties of PINK1 have been explored using AGGRESCAN. Analysis of these properties may give insight into the proclivity of PINK1 aggregation *in vivo*. Furthermore, insight is provided towards the likelihood of PINK1 to form amyloidogenic fibrils.

The propensity for proteins to aggregate is primarily governed by the polypeptide sequence. Intrinsic properties have been identified and thoroughly studied. This has allowed for the development of several algorithms and programs, such as AGGRESCAN, with the power to predict aggregation prone regions and overall aggregation propensity in a protein based on its sequence. The following aggregation properties of PINK1 were computed using AGGRESCAN:

1. Amino acid aggregation-propensity value average (a^4v) over a sliding window.

2. Normalized amino acid aggregation-propensity value average for 100 residues (Na^4vSS).
3. Normalized number of Hot Spots for 100 residues ($NnHS$).
4. Total Hot Spot Area per residue ($THSAr$).
5. Hot Spot Area (HSA).
6. Area of the Aggregation Profile above the Hot Spot threshold divided by the number of residues in the input amino acid sequence ($AATr$).

Figure A1 shows a truncated aggregation profile for PINK1-FL. The calculated average aggregation propensity Na^4vSS by AGGRESCAN was positive, suggesting an innate propensity of PINK1 to aggregate.

Na^4vSS was determined for 4 PD-linked variants of PINK1. In each case, there was an increase in aggregation propensity with the exception of I111S. Na^4vSS of PINK1-FL WT was 0.7; for PD variants C92F, R98W, I111S, and Q126P these values were 0.9, 1.1, 0.3, 0.5, and 0.8, respectively. In attempt to determine a differential in aggregation propensity between PINK1 WT and the variants, Na^4vSS of the variant was subtracted by that of the WT (**Figure A2**).

The number of total hot spots per residue, total aggregation peaks was assessed. For all 6 PD-linked variants assessed, this value remained the same value of 3.3 (**Figure A3.A**). This is not surprising, as the total number of hot spots should not be affected by single point mutations. In contrast, a single point mutation may have an effect on

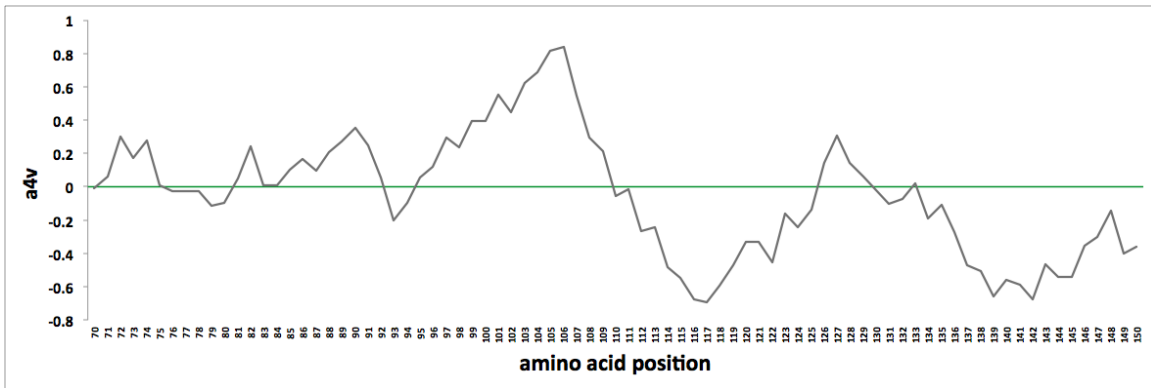


Figure A1. Aggregation profile for PINK1 residues 70-150. a4v is a value for the aggregation propensity of individual amino acids in a polypeptides chain. Points above the green line demonstrate regions of the protein with a high propensity to aggregate based on the residues present.

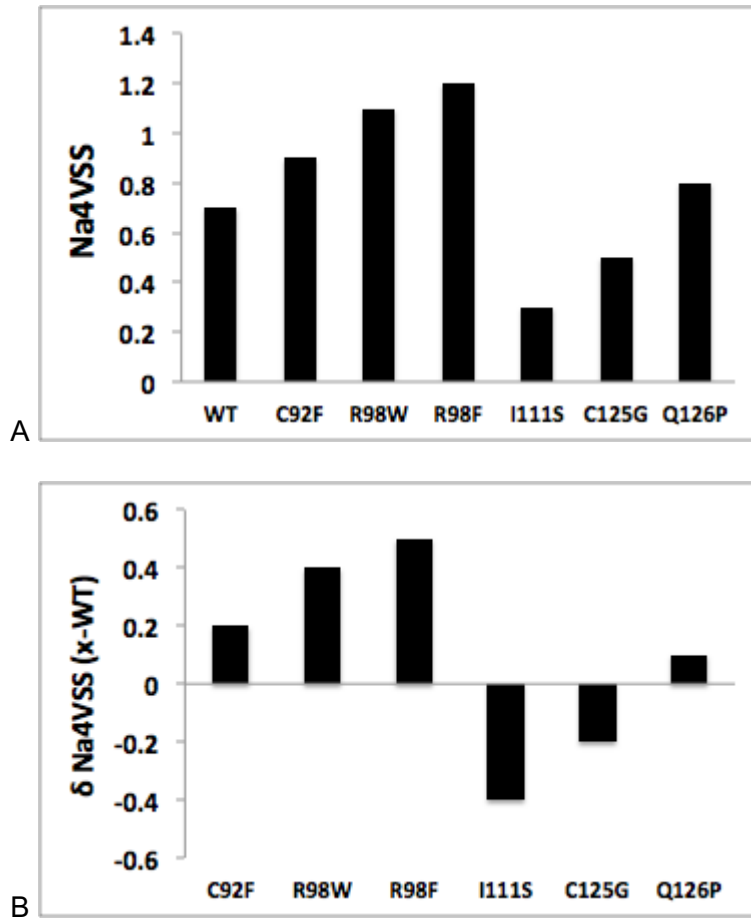


Figure A2. Average aggregation propensities for PD-linked transmembrane PINK1 variants. Na4vSS is a measure of the average propensity for a protein or polypeptide sequence input to aggregate.

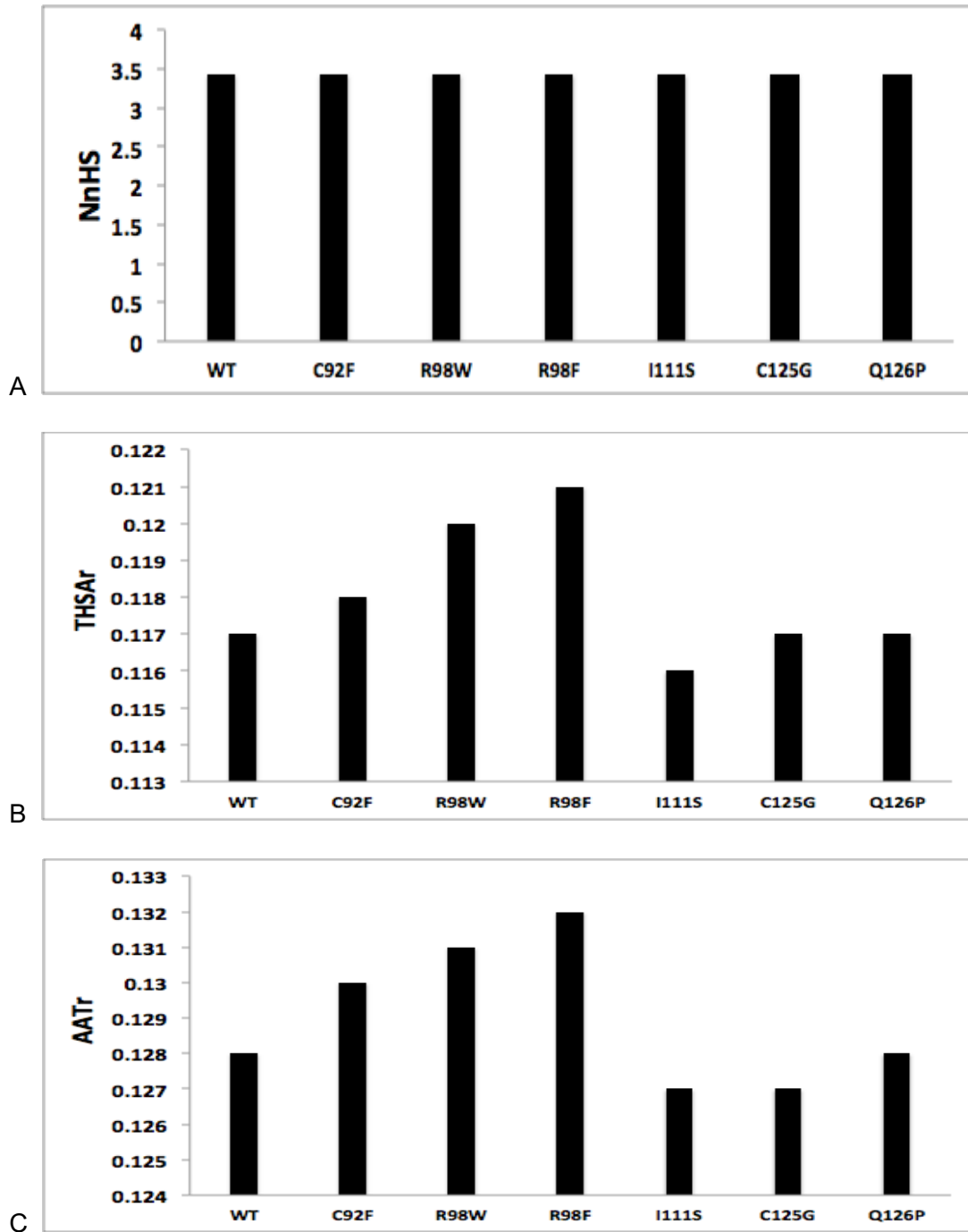


Figure A3. Aggregation parameters of PINK1. (A) Number of hot spots for each PD-linked transmembrane variant. (B) A measure of the potency of the aggregation peaks based on amino acid aggregation values found in each hot spot. (C) Average aggregating potency of residues above detection threshold.

the total Hot Spot Area per residue - a measure of the potency of the aggregation peaks (**Figure A3.B**). This result suggests that the aggregation potency of PINK1 is dependent on the point mutation present. 2 out of 3 transmembrane variants, C92F and R98W, demonstrate an increase in aggregation potency, whereas I111S shows a decrease in this parameter along with the extra-transmembrane mutation Q126P. Similarly, the average aggregating potency of residues above detection threshold (AATr) shares this mutation dependent trend (**Figure A3.C**).

Hot Spot Area (*HSA*) is the Area of the Aggregation Profile above the Hot Spot threshold in a given Hot Spot. Large densities of aggregating peaks, *HSAs*, throughout the entire span of the protein, particularly throughout the transmembrane domain and the kinase domain are seen (**Figure A4**).

To determine the potential effect of having an intrinsically disordered or an unfolding tendency on PINK1's aggregation propensity, analysis was performed using FoldIndex. The output of this was a graphical representation of PINK1 intrinsic folding (**Figure A5**). This result suggests that overall PINK1 is properly folded, according to its amino acid sequence.

Amyloidogenic patterns (hexa-peptides) were cross-referenced with PINK1 using ScanProsite (**Figure A6**). 5 regions within PINK1 were found to have a sequence

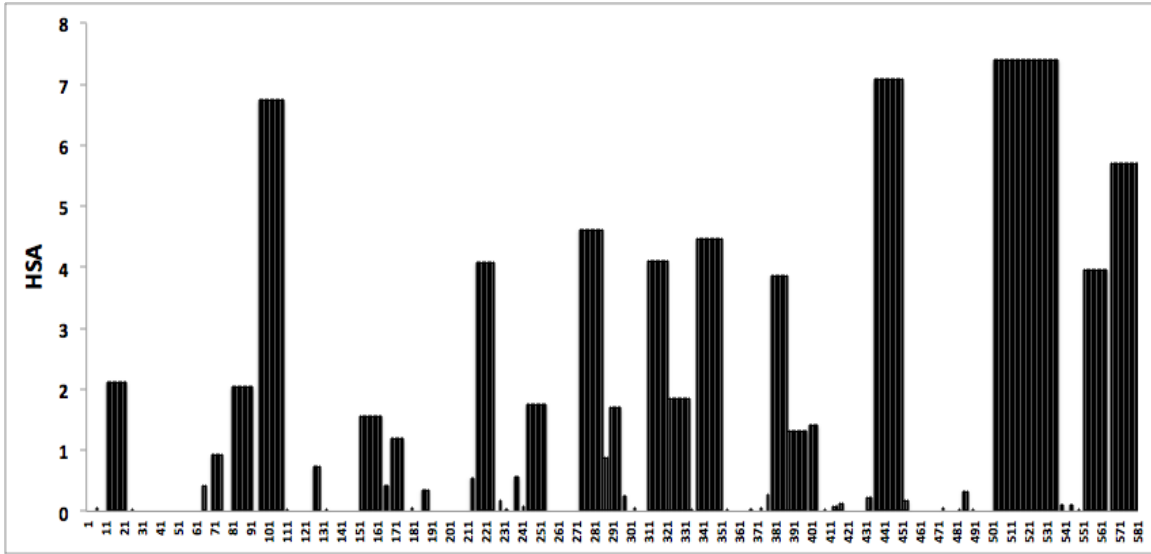


Figure A4. Aggregation Hot Spot Areas (*HSA*) in PINK1. *HSA* is a measure for the area of the aggregation profile above the Hot Spot threshold. Large areas or densities of aggregating areas make up these hot spots span the entire length of PINK1.

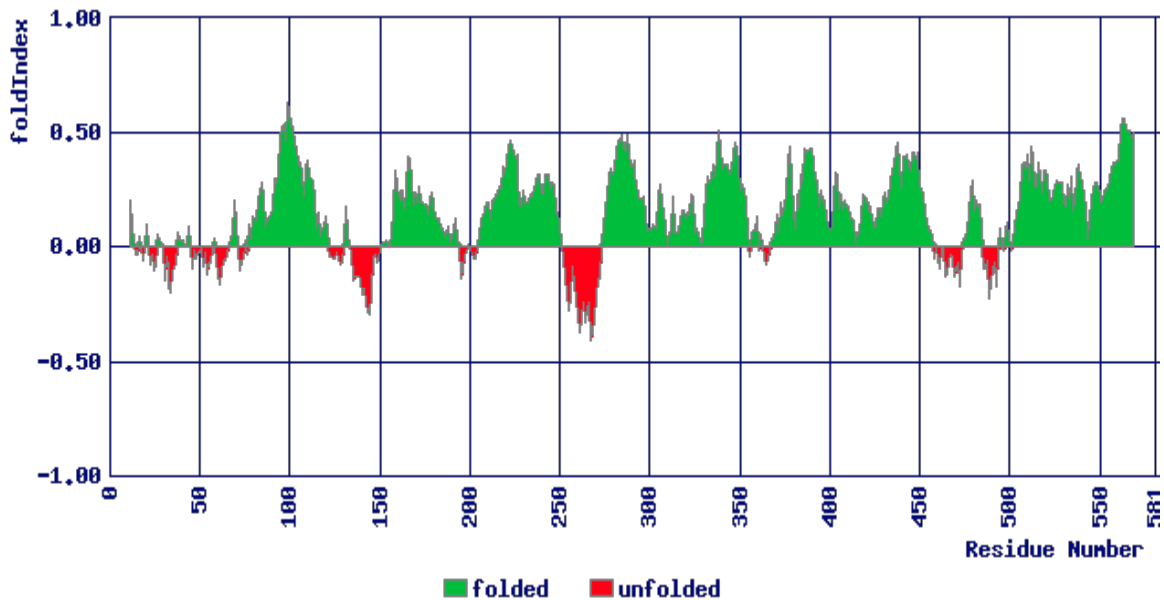


Figure A5. Computational assessment of PINK1 intrinsic folding. According to the residues of PINK1 input into the server, overall PINK1 appears to be properly folded with few exceptions. One particular exception is in the region between the transmembrane domain and the kinase domain where mutations of interest, particularly Q126P, reside.



Figure A6. Location of detected amyloidogenic patterns on PINK1-FL via ScanProsite. Red bars denoting residues that match amyloid fibril pattern motif. Amino acids 124-129, 152-157, 220-225, 400-405, 443-448, respectively^{191,192}.

match with proposed amyloidogenic properties (P-{PKRHW}-[VLS(C)WFNQ]-[ILTYWFN]-[FIY]-{PKRH})¹⁹¹. Amino acids within {} brackets denote the amino acid that may not be in this residue position; amino acids within [] brackets denote the possible amino acids that may be present within the amyloidogenic protein/peptide sequence. Residues in PINK1 that match amyloid fibril pattern motif are found at positions 124-129, 152-157, 220-225, 400-405, 443-448. Interestingly, the mutation at position 126 from a glutamine to a proline diminishes the amyloidogenic property of residues 124-129.

Though entirely based on computational analysis, programs such as AGGRESCAN and ScanProsite are powerful tools to preliminarily assess the propensity of proteins to aggregate *in vivo* and to identify potential sites of fibrillation given a protein sequence, respectively. Given these results, further assessment can be done to explore PINK1 dynamics with regards to self-interaction and assembly.

Cryo-EM

Cryo-electron microscopy is a technique that has been gaining power and trust in the field of structural biology. This technique begins with a rapid cooling of the sample, a process known as vitrification. The rapid nature of vitrification results in a solid, amorphous sample with the sample integrity intact due to the inability of water in the sample to form crystals – interfering or disrupting the protein structure. Following this step, the solid sample is screened and then imaged using an electron microscope. 2D information is extracted from these images and

processed via reconstruction software yielding 3D models of the sample's content, such as protein structure or protein interactions.

Cryo-EM has been recently used to study the fibril structure of A β 42, the main component of plaques found in the brains of AD patients and to discover the formation of amyloid fibril structure of α -synuclein, a major component of the Lewy bodies that are a physiologic hallmark of PD patients. Li *et al.* provided high-resolution structures of recombinant full-length α -synuclein fibrils. Incubation of N-acetylated full-length α -synuclein in buffer allowed for spontaneous fibril formation. Interestingly, in a dose-dependent manner these fibrils induced cytotoxicity in HEK 293T cells. In rat primary neurons, fibril introduction led to the aggregation of endogenous phosphorylated α -synuclein. Together, these results suggest a mechanism of fibril transmission and propagation. Specific PD-linked α -synuclein variants were reported to play a role in fibril structure. There are familial PD mutations that are found in the dimer interface, changes in these residues interrupt the interactions that help stabilize the proper, or WT, folding of the fibril structure. Despite this, these particular familial mutations were still able to form amyloid fibrils, though these fibril structures were distinctive from that of WT α -synuclein fibrils. Recognition of these structural changes may provide insight into altered fibril dynamics and aggregation kinetics that may play a significant role in the pathophysiology of PD in these familial cases.

To assess whether PINK1 may also be plagued to a fate of fibrillation, a synthetic peptide was ordered from Peptide2go for analysis by way of cryo-EM. 5-FAM-*HsPINK1* was ordered including the boundaries 86-120 (VVRAWGCAGPCGRAVFLAFGLGLGLIEEKQAESRR) led by an N-terminal 5-carboxyfluorescein (5-FAM) label. 5-FAM-*HsPINK1*⁸⁶⁻¹²⁰ was incubated with ddH₂O in one trial and 50 mM Tris-HCl pH 7.0 in a subsequent trial. Upon screening, aggregates were observed. These aggregates looked similar to prion-infected cow brain homogenates, extended “tree-branch” like in appearance. Suggesting fibril bundle formation. Though this result is preliminary, it is both possible and plausible that PINK1 has fibril forming properties similar to that of α -synuclein. Similar to α -synuclein, PINK1 is known to dimerize. Unlike α -synuclein, the residues in PINK1 responsible for this phenomenon are unknown. The PINK1 dimer-containing complex forms on the outer mitochondrial membrane, it is likely that there are dimer-supporting interactions found within or around the transmembrane domain. Further assessment of this peptide by cryo-EM could uncover fibrillation within this region of PINK1, providing additional insight into the pathogenesis of these PD-linked variants.

Cloning, expression and purification of MBP-hPINK1 WT and PD-linked variants

Previous work in the lab had explored the expression and purification of an MBP-*HsPINK1*⁸⁹⁻¹¹¹ fusion protein to obtain an organically extracted PINK1 TM peptide. I sought out to express an MBP-*HsPINK1* fusion encompassing the transmembrane domain and surrounding regions as such in the His-*HsPINK1* construct. Residues 70-

134 were cloned from the pBAD:His-FRET-*HsPINK1*[70-134] vector and inserted into the pMAL vector. Following a similar protocol to that explained in 3.2.1, *Pink1*[70-134] WT, C92F, and R98W were successfully cloned into the pMAL vector.

Expression and purification of MBP-*HsPINK1*[70-134] followed an established protocol in the lab without any hitches. A freshly transformed *E. coli* DH5 α colony was selected and used to inoculate a starter culture of 125 mL LB supplemented with 0.4% glucose + 100 μ g/mL. This starter culture was incubated overnight at 37 $^{\circ}$ C with shaking (220 RPM). The following morning 20 mL of the overnight culture was used to subinoculate 1 L LB + 0.4% glucose + 100 μ g/mL ampicillin (x6) and grown at 37 $^{\circ}$ C, 220 RPM. Once the OD600 reached 0.6, the cells were induced with 0.5 mM IPTG and the incubation temperature was decreased to 24 $^{\circ}$ C for an induction time of 72 hours. Cells were then harvested using the JLA8.1 rotor at 8000 $\times g$ for 20 minutes. Supernatant was poured out and cells were either stored at -20 $^{\circ}$ C until subsequent use for protein isolation and purification or used immediately.

Cells were resuspended in 5 times the pellet weight in buffer (20 mM KPO₄ buffer pH 8.0, 120 mM NaCl, 5% glycerol, 1 mM EDTA, 1 mM PMSF, 1 mM DTT, 10 μ g/mL DNase + protease inhibitor tablets). Upon homogenous resuspension, cells were passed through the Emulsiflex C3 homogenizer three times for cell lysis. Following lysis, cell lysate was incubated with 0.5% Triton X-100 on ice for 10 minutes. Triton X-100-treated lysate was subjected to an ultracentrifugation spin at 25 000 $\times g$ for 30 minutes using the TI45 rotor. This centrifugation step pellets cellular debris and

unbroken cells. Similarly to the appended fluorescent proteins on His-FRET-*HsPINK1*[70-134], MBP increases the solubility of the PINK1 segment expressed; therefore the protein of interest is found in the soluble fraction of any centrifugation spin.

Again, similarly to the purification of His-FRET-*HsPINK1*[70-134], MBP-*HsPINK1*[70-134] was subjected to affinity chromatography. Though unlike that experienced by the purified His-FRET-*HsPINK1*[70-134] product, MBP-*HsPINK1*[70-134] is much cleaner due to a higher specificity of the amylose column to the maltose binding protein fused to *HsPINK1*. 2 mL of amylose resin was equilibrated with 10 CV 1X PSE buffer. Supernatant and equilibrated resin was mixed and incubated at 4 °C on nutator for 2 hours. Following this batch-binding step, the sample-resin slurry was poured through a gravity flow column. The resin collected and packed at the bottom of the column for remainder of the purification process. Column was washed with 1X PSE buffer until the OD₂₈₀ of the washes reached less than 0.05. MBP-*HsPINK1*[70-134] was eluted off the column with 40 mM maltose in 1X PSE buffer. Elutions were collected in 1 mL fractions and the OD₂₈₀ was measured to track when protein was no longer coming off the column. All fractions containing protein were pooled and then concentrated using a 30 kDa Amicon concentrator. Instead of incubating MBP-*HsPINK1*[70-134] with TEV protease to separate *HsPINK1*[70-134] from MBP, concentrated protein was then distributed into 30 µL aliquots, flash frozen with liquid nitrogen, and stored at -80 °C for subsequent use.

MBP-*Hs*PINK1[70-134] WT, C92F, R98W, and Q126P were all successfully cloned, expressed, and purified. With the successful purification of the R98W variant, I anticipated I would be able to use this construct to assess cleavage by the PARL protease in a gel-shift-based assay. Due to the slow nature of this protease, cleavage was not detected on a gel of either WT PINK1 or any of the variants. Despite this shortcoming, MBP-*Hs*PINK1[70-134] could be useful to assess other aspects of this region of PINK1. For example, circular dichroism (CD) could be used to assess secondary structure, elucidating any effects the point mutations may be having on the structure of PINK1. *In vitro* assays, such as the thioflavin T assay, could be used to study formation of PINK1 aggregates with these PD-linked variants. Further processing of the protein to isolate the peptide from MBP could allow for recombinant protein to be sent for cryo-EM to look at fibril formation of this particular region human PINK1.